

# **Laser assisted modification of optical and structural properties of composite glass with silver nanoparticles**

## **Dissertation**

Zur Erlangung des Doktorgrades  
des Fachbereichs Physik  
der Martin-Luther Universität Halle-Wittenberg

Vorgelegt von  
Alexander V. Podlipensky  
aus Minsk, Weißrussland

Gutachter:

1. Professor Dr. Heinrich Graener (Martin Luther Universität Halle Wittenberg)
2. Professor Dr. Gero von Plessen (Physikalisches Institut, RWTH Aachen)

verteidigt am 26.04.2005

**urn:nbn:de:gbv:3-000008361**

[<http://nbn-resolving.de/urn/resolver.pl?urn=nbn%3Ade%3Agbv%3A3-000008361>]

# Contents

---

<b>Introduction</b>	<b>1-2</b>
<b>Chapter 1. Propagation of optical beams in composite medium containing metal nanoparticles.</b>	<b>3-19</b>
1.1. The Basics of the Linear and Nonlinear Wave Interactions.....	3
1.2. Propagation of a plain electromagnetic wave in a linear isotropic medium. The dispersion, absorption and reflection of light.....	5
1.3. Nonlinear propagation of electromagnetic wave.....	7
1.3.1. Second order susceptibility. Second Harmonic generation (SHG).....	7
1.3.2. Third-order nonlinearities.....	10
1.4. Nonlinear ionization.....	12
1.4.1. Photoionization.....	12
1.4.2. Avalanche ionization.....	13
1.5. Optical properties of nanocomposites containing metal nanoparticles.....	14
<b>Chapter 2. Technique of the experiment.</b>	<b>20-30</b>
2.1. Laser system used for photomodifications of Ag nanoparticles.....	20
2.2. Irradiation technique using laser Gaussian beams.....	21
2.3. Spectroscopic technique.....	25
2.4. Relaxation dynamics measurements.....	27
2.5 Preparation and characterization of glass samples containing Ag nanoparticles.....	27
<b>Chapter 3. Photomodification of single Ag nanoparticles embedded in soda-lime glass.</b>	<b>31-63</b>
3.1 Transformation of the spherical shape of Ag nanoparticles: effect of the laser polarization, pulse intensity and wavelength.....	32
3.1.1. The laser induced dichroism: effect of the laser pulse intensity and writing density on the anisotropic shape modifications.....	32
3.1.2. Angular dependences of the laser induced dichroism.....	36
3.1.3. Subsequent modifications by multicolour irradiation. ....	37
3.1.4. Modifications induced by fs laser pulses at 267 nm (interband effect).....	38
3.1.4. Femtosecond laser induced dichroism in composite glass with spherical Ag nanoparticles: first summary.....	39
3.2. Modification of soda-lime glass by 150 fs laser pulses at 400 nm. Colour centres in the glass.....	41

3.3. Effect of the temperature on the laser induced modifications of Ag nanoparticles.....	45
3.3.1. SP bands modification by temperature treatment.....	45
3.3.2. Luminescence study of the temperature induced modifications.....	46
3.3.3. Effect of the temperature on the laser assisted modifications.....	50
3.3.4. Interpretation and discussion of the temperature assisted effects.....	50
3.4. Dynamic of the laser induced modifications of Ag nanoparticles in soda-lime glass.....	54
3.5. Mecanism of the anisotropic shape modifications of spherical Ag nanoparticles in soda-lime glass upon fs laser irradiation.....	58
3.5.1. Surface Plasmon assisted photoemission from metal nanoparticles.....	58
3.5.2. Dipole-dipole interactions of the SP with induced free electron carrier in the surrounding glass matrix.....	61
3.5.3. Ionization assisted anisotropic shape transformation of spherical Ag nanoparticles in soda lime glass.....	62

**Chapter 4. Laser assisted structural modifications of strongly aggregated Ag nanoparticles in soda-lime glass 64-75**

4.1. Anisotropic nanostructures created by fs laser irradiation in glass containing aggregated Ag nanoparticles.....	65
4.2. Modification of optical and structural properties of aggregated Ag nanoparticles in glass by exposure to ns laser pulses near to the SP resonance.....	69

**Chapter 5. First steps towards application of the fs laser induced dichroism in composite glass with spherical Ag nanoparticles. 76-88**

5.1. 3D anisotropic structuring in the glass with filling factor gradient of Ag nanoparticles in the depth.....	77
5.2. Composite glass with Ag nanoparticles as a promising media for 3D optical data storage by spectral coding.....	81
5.2.1. Effect of the peak pulse intensity on the spot size of the modified area in composite glass with Ag nanoparticles.....	82
5.2.2. Spectral data coding in composite glass with Ag nanoparticles exposed to fs laser pulses.....	84
5.3. Preparation of high contrast structural polarizer in composite glass with Ag nanoparticle by multicolor fs laser irradiation.....	86

**Chapter 6. Summary and outlook 89**

**References 91**

## **Introduction**

From the Middle Ages coloration of glass or solutions containing colloids of noble metals stirred attention of many researches. It's well known that silver particles typically demonstrate yellow color while gold and copper colloids are responsible for the red coloration of stained glass windows. The first explanation of extinction spectra and coloration of metal particles was carried out by Mie in 1908 [1.8]. Since then optical properties of metal nanoparticles have extensively been studied in different fields of science and technology.

The linear and nonlinear optical properties of metallic nanoparticles in dielectrics are dominated by the strong surface plasmon resonances (SPR). Since spectral position and shape of these SPR can be designed within a wide spectral range throughout the visible and near infrared by choice of the metal and the dielectric matrix, or manipulation of size, shape and spatial arrangement of the metal clusters, these composite materials are very promising candidates for a great number of applications in the field of photonics. In this context, laser-based techniques to modify shape and arrangement of the metal clusters are of great interest since they provide a very powerful and flexible tool to control and optimize the linear and nonlinear optical properties of these materials.

Recently, it has been shown [3.14] that the excitation of the single spherical Ag nanoparticles by fs laser pulses near to the SPR evokes a laser induced dichroism in the composite glass indicating shape modification of the metal clusters. However, the mechanism of the shape transformations seems to be very complicated and still needs additional investigations. This thesis considers some aspects of interactions of intense fs laser pulses with silver nanoparticles incorporated in soda-lime glass. Presented here investigations of the fs laser assisted modifications of Ag nanoparticles in dependence on the laser pulse intensity, excitation wavelength, temperature as well as performed luminescence and relaxation dynamic studies reveal new information concerning the processes arising by excitation of the silver cluster near to the SPR and leading to structural alterations.

Additionally, effects of the fs and ns laser pulses on the system of aggregated Ag nanospheres are shown here. For instance, exposure of the compact packed metal clusters to intense fs laser pulses demonstrates anisotropic structural modifications in the sample, which in turn strongly dependent on excitation wavelength and affected

by collective interactions. On the other hand, the thermal instabilities produced in the samples by ns second laser pulses result in ripening of periodically distributed in the glass chain-like silver structures. The possible mechanisms responsible for the observed effects are discussed.

The last chapter of this thesis refers to the possible applications of the fs laser induced dichroism in the glass containing spherical clusters. In turn, an opportunity of the 3D anisotropic structuring as well as 3D data storage in these materials is demonstrated and discussed. Moreover, proposed technique could find many additional applications in development of different 3D polarization and wavelength selective microdevices such as polarizers, filters, gratings, RGB and DWDM devices, optical and plasmonic embedded circuits.

## Chapter 1.

# Propagation of optical beams in composite medium containing metal nanoparticles

In this chapter I review some of the basic linear and nonlinear optics govern the interaction of the intense laser radiation with a medium. The linear and nonlinear response of the medium strongly effects on the propagation of electromagnetic wave in the optical material and can even result in the permanent modification of its physical properties. In turn, the linear and nonlinear optical features of composite materials with metal nanostructures are dominated by surface plasma oscillations. The fact that the surface plasmon (SP) strongly depends on size, shape, distribution of metal nanoparticles as well as on surrounding dielectric matrix offers an opportunity for manufacturing of new promising nonlinear materials, nanodevices and optical elements.

## 1.1. The Basics of the Linear and Nonlinear Wave Interactions.

The starting point of the electromagnetic theory of propagation of electromagnetic radiation in material media is the Maxwell's equations for the macroscopic electromagnetic field, which may be written (SI system)

$$\nabla \times \vec{H} = \vec{i} + \frac{\partial \vec{D}}{\partial t}, \quad 1.1$$

$$\nabla \times \vec{E} = -\frac{\partial \vec{B}}{\partial t}, \quad 1.2$$

$$\nabla \cdot \vec{D} = \rho_F, \quad 1.3$$

$$\nabla \cdot \vec{B} = 0, \quad 1.4$$

where  $\vec{E}$  is the electric field and  $\vec{B}$  the magnetic induction. The electric displacement  $\vec{D}$ , magnetic field  $\vec{H}$  and the current density  $\vec{i}$  are defined by constitutive equations

$$\vec{D} = \epsilon_0 \vec{E} + \vec{P} = \epsilon_0 \epsilon \vec{E}, \quad 1.5$$

$$\vec{H} = \frac{1}{\mu_0} \vec{B} - \vec{M}, \quad 1.6$$

$$\vec{i} = \sigma \vec{E} \quad 1.7$$

where  $\vec{P}$  and  $\vec{M}$  are the electric and magnetic polarizations,  $\sigma$  is the conductivity of the medium,  $\rho_F$  is the density of external charges; and  $\epsilon_0$  and  $\mu_0$  are the electric and magnetic permittivity in vacuum, respectively;  $\epsilon$  is the relative dielectric permittivity of the medium. For the sake of simplicity, we shall limit ourselves to the non-magnetic media ( $\vec{M} = 0$ ). Thus, after substitution of Eqs.1.5-1.7 in Eqs.1.1-1.4 the electromagnetic wave equation can be derived

$$\nabla \times \nabla \times \vec{E} + \mu_0 \sigma \frac{\partial \vec{E}}{\partial t} + \epsilon_0 \mu_0 \frac{\partial^2 \vec{E}}{\partial t^2} + \mu_0 \frac{\partial^2 \vec{P}}{\partial t^2} = 0 \quad 1.8$$

Moreover, the optical polarization  $\vec{P}$  in Eq.1.8 induced in the medium by propagating electromagnetic wave can be expressed by a Taylor series:

$$\vec{P} = \epsilon_0 \chi^{(1)} \cdot \vec{E} + \epsilon_0 \chi^{(2)} \cdot \vec{E} \vec{E} + \epsilon_0 \chi^{(3)} \cdot \vec{E} \vec{E} \vec{E} + \dots, \quad 1.9$$

where  $\chi^{(n)}$  is a susceptibility tensor of (n+1) rank and  $\vec{E}$  is the propagating electric field. The first term in Eq.1.9 describes linear polarization component while higher terms are responsible for nonlinear contribution. Thus, the wave equation Eq.1.8 can be modified:

$$\nabla \times \nabla \times \vec{E} + \mu_0 \sigma \frac{\partial \vec{E}}{\partial t} + \epsilon_0 \mu_0 (1 + \chi^{(1)}) \frac{\partial^2 \vec{E}}{\partial t^2} + \mu_0 \frac{\partial^2 \vec{P}_{NL}}{\partial t^2} = 0, \quad 1.10$$

where  $\vec{P}_{NL} = \epsilon_0 \chi^{(2)} \cdot \vec{E} \vec{E} + \epsilon_0 \chi^{(3)} \cdot \vec{E} \vec{E} \vec{E} + \dots$ . The typical values of  $\chi^{(2)}$  and  $\chi^{(3)}$  for the usual kind of crystals are  $\chi^{(2)} \sim 10^{-9}$  esu and  $\chi^{(3)} \sim 10^{-14}$  esu. Therefore, for the weak incident optical field the nonlinear contribution in polarization can be neglected ( $\vec{P}_{NL} \rightarrow 0$ ) and Eq.1.10 becomes the well known ordinary wave equation:

$$\nabla \times \nabla \times \vec{E} + \mu_0 \sigma \frac{\partial \vec{E}}{\partial t} + \epsilon_0 \mu_0 (1 + \chi^{(1)}) \frac{\partial^2 \vec{E}}{\partial t^2} = 0 \quad 1.11$$

In this case, the polarization response of a medium to a given monochromatic component  $\vec{E}(\omega, \vec{r})$  of applied field is limited only by the electric permittivity  $\epsilon$ ; the other frequency components of the field do not effect on  $\vec{P}_L(\omega, \vec{r})$  or  $\vec{E}(\omega, \vec{r})$ . If the

applied field is an intense laser field, the second- and/or third-order polarization components expressed by Eq.1.9 may no longer be neglected. Then the nonlinear term containing  $\vec{P}_{NL}$  in Eq.1.10 can be recognized as a source that can emit coherent radiation at a new frequency. Thus, nonlinear polarization induced in the media by propagating monochromatic electromagnetic wave is responsible for optical harmonic generation.

## **1.2. Propagation of a plain electromagnetic wave in a linear isotropic medium. The dispersion, absorption and reflection of light.**

Let us consider propagation of a plain electromagnetic wave with frequency  $\omega$  in a medium with linear susceptibility  $\chi^{(1)}$ . Here the intensity of the light is assumed to be low enough to exclude the nonlinear interactions. Thus, only the first linear term of the Eq.1.9 was taken into account. Denoting the arbitrary direction of propagation as  $z$  and specializing the problem to one dimension by taking  $\partial/\partial x = \partial/\partial y = 0$ , a solution of the wave equation Eq.1.11 can be presented as a plain electromagnetic wave, which is propagating in the medium with the electric field strength expressed as

$$\vec{E}(z,t) = \vec{E}_0 \exp(i\vec{k}\vec{r} - i\omega t) = \vec{E}_0 \exp(ikz - i\omega t), \quad 1.12$$

where  $\vec{E}_0$  is an electric field amplitude of oscillating electromagnetic wave and wave vector  $k$ , which in general case can be given as

$$\vec{k} = \vec{k}' + i\vec{k}'', \quad 1.13$$

where  $\vec{k}'$  and  $\vec{k}''$  are real and imaginary part of the wave vector. Taking in to account Eq.1.13 we can rewrite Eq.1.12 as follow

$$\vec{E}(z,t) = \vec{E}_0 \exp(-k''z) \exp(ik'z - i\omega t), \quad 1.14$$

In turn, the Eq.1.14 clarifies the physical sense of real and imaginary part of the wave vector. Thus,  $k''$  is responsible for the damping of the electromagnetic wave in the medium and defines the amplitude, while the real part  $k'$  is combined with the phase of the electromagnetic wave. Moreover, from the Eq.1.14 the absorption coefficient can be expressed via imaginary part of the wave vector as

$$\alpha = 2k'' \quad 1.15$$

Substituting the electric vector Eq.1.12 in the wave equation Eq.1.11 and taking in to account  $\nabla \times \nabla \times \vec{E} = \nabla \nabla \cdot \vec{E} - \nabla^2 \vec{E} = -\nabla^2 \vec{E}$  ( $\nabla \cdot \vec{E} = 0$  in homogeneous with no external charges ( $\rho_f = 0$ )) we obtain

$$k^2 = \omega^2 \mu_0 \varepsilon_0 \varepsilon(\omega) = \frac{\omega^2}{c^2} \varepsilon(\omega), \quad 1.16$$

where

$$\varepsilon(\omega) = \varepsilon' + i\varepsilon'' = (1 + \chi^{(1)}(\omega)) + i \frac{\sigma(\omega)}{\varepsilon_0 \omega} = (1 + \chi'(\omega)) + i(\chi''(\omega) + \frac{\sigma(\omega)}{\varepsilon_0 \omega}) \quad 1.17$$

is a relative complex dielectric permittivity of the medium and  $c = 1/\sqrt{\mu_0 \varepsilon_0}$  is the light velocity in the vacuum,  $\chi^{(1)}(\omega) = \chi'(\omega) + i\chi''(\omega)$  is the complex linear susceptibility of the medium. Using the anharmonic oscillator model to the electronic response of the medium in a oscillating electric field [1.1] the linear susceptibility can be expressed via Lorenz function:

$$\chi^{(1)}(\omega) = \frac{Ne^2}{m\varepsilon_0[(\omega_0^2 - \omega^2) + i\omega\gamma]}, \quad 1.18$$

where N is the concentration of electrons, e – charge of the electron, m – masse of the electron,  $\omega_0$  is frequency of the electron motion,  $\gamma$  is the damping term. Moreover, real and the imaginary parts of the linear susceptibility (Eq.1.18) are connected via Kramers-Kronig relation:

$$\chi'(\omega) = \frac{1}{\pi} \int_{-\infty}^{+\infty} \frac{\chi''(\Omega)}{\Omega - \omega} d\Omega. \quad 1.19$$

By analogy with the complex wave vector (Eq.1.13) and using the Eq.1.16, *complex index of refraction* of a medium can be defined as

$$n(\omega) = n' + in'' = \sqrt{\varepsilon(\omega)}, \quad 1.20$$

where  $k' = \frac{\omega}{c} n'$  and  $k'' = \frac{\omega}{c} n''$ . Hence, using the Eqs.1.15,1.16 and 1.20 one can determine the absorption coefficient and refractive index of the medium as

$$\alpha(\omega) = \frac{2\omega}{c} \text{Im} \sqrt{\varepsilon(\omega)}, \quad 1.21$$

$$n'(\omega) = \text{Re} \sqrt{\varepsilon(\omega)}. \quad 1.22$$

At the same time, the Eq.1.16 testifies connection between wave vector and the imaginary part of dielectric permittivity in Eq.1.17:

$$2k'k'' = \frac{\omega^2}{c^2} \varepsilon'' \quad 1.23$$

Thus, using the Eq.1.15 and expression for real part of refractive index it is possible to derive the following expression for the absorption coefficient:

$$\alpha = \frac{\omega}{cn'} \varepsilon'' . \quad 1.24$$

The Eq.1.24 indicates that imaginary part of the dielectric permittivity is responsible for the damping of the electromagnetic wave in the medium. Moreover, as it was shown in the Eq.1.17,  $\varepsilon''$  consists of two components: conduction electrons in the medium define the first one; the second one is associated with electron transitions in atomic system described by the Lorenz model (Eq.1.18).

Therefore, the absorption coefficient and refractive index are defined by the dielectric properties of the medium. Furthermore, the absorption is responsible for the attenuation of the amplitude of the electromagnetic wave propagating in the medium and refractive index defines the phase of this electromagnetic wave. Moreover, effects observed on the boundary of two media (refraction and reflection) are also caused by linear optical response of the media. In turn, the energy reflection coefficient by normal incidence can be expressed using the complex refractive index (Eq.1.20):

$$R(\omega) = \frac{|n_1(\omega) - n_2(\omega)|^2}{|n_1(\omega) + n_2(\omega)|^2} , \quad 1.25$$

where  $n_1$  and  $n_2$  are the complex refractive indexes of the two media forming a separating boundary.

### 1.3. Nonlinear propagation of electromagnetic wave.

If the laser intensity is high, the wave equation Eq.1.11 is not valid any more. Instead, one has to use the nonlinear wave equation (Eq.1.10) and to take into account higher polarization orders (Eq.1.9). In this case, the nonlinear interactions results in polarization components with new frequencies, which can be recognized as a source emitting additional harmonics.

#### 1.3.1 Second order susceptibility. Second Harmonic generation (SHG).

Second order nonlinearity is the most important phenomenon responsible for optical Second Harmonic Generation (SHG), what actually is the first nonlinear effect discovered after invention of the laser, implicating conversion of the energy of propagating in the nonlinear media electromagnetic wave with frequency  $\omega$  to that of a wave at  $2\omega$ ; parametric generation, where strong pump radiation at frequency  $\omega_3$  induces in the nonlinear media two waves at  $\omega_1$  and  $\omega_2$  to be satisfied the condition  $\omega_3 = \omega_1 + \omega_2$ ; frequency up-conversion (sum frequency) of wave with low frequency  $\omega_1$  to a signal of a higher frequency  $\omega_3$  by mixing with a strong laser field at  $\omega_2$ , where  $\omega_3 = \omega_1 + \omega_2$ .

The nonlinear interaction of two optical fields of frequencies at  $\omega_1$  and  $\omega_2$ , respectively, in second order nonlinear media induces the nonlinear polarization component at  $\omega_3$  to be expressed according to the Eq.1.9 as:

$$\begin{aligned} P_i^{\omega_3=\omega_1+\omega_2} &= \epsilon_0 \chi_{ijl}^{\omega_3=\omega_1+\omega_2} E_j^{\omega_1} E_l^{\omega_2}, \\ P_i^{\omega_3=\omega_1-\omega_2} &= \epsilon_0 \chi_{ijl}^{\omega_3=\omega_1-\omega_2} E_j^{\omega_1} E_l^{\omega_2*}, \end{aligned} \quad 1.26$$

where  $\chi_{ijl}^{\omega_3}$  is the second order susceptibility tensor,  $E_j^{\omega_1}$  and  $E_k^{\omega_2}$  are the amplitudes of two interacting fields given by

$$\begin{aligned} E_j^{(\omega_1)}(z,t) &= \frac{1}{2}[E_{1j}(z)e^{i(\omega_1 t - k_1 z)} + c.c.] \\ E_k^{(\omega_2)}(z,t) &= \frac{1}{2}[E_{2k}(z)e^{i(\omega_2 t - k_2 z)} + c.c.] \end{aligned} \quad 1.27$$

According to the Eq.(1.26) only media with lack of center of symmetry can possess a nonvanishing  $\chi_{ijl}$  tensor. This follows from the requirement that in a centrosymmetric crystal a reversal of the signs of  $E_j^{\omega_1}$  and  $E_k^{\omega_2}$  must cause a reversal in the sign of  $P_i^{\omega_3=\omega_1+\omega_2}$  and not affect the amplitude:

$$\chi_{ijl}^{\omega_3=\omega_1+\omega_2} E_j^{\omega_1} E_k^{\omega_2} = -\chi_{ijl}^{\omega_3=\omega_1+\omega_2} (-E_j^{\omega_1})(-E_k^{\omega_2}). \quad 1.28$$

This means  $\chi_{ijl}^{\omega_3}=0$ . Additionally, the fact that an order of electric field components don't play any role in Eq.1.26 testifies that  $\chi_{ijl} = \chi_{ijj}$ . Thus, according to the Kleinman's conjecture [1.1] the second order susceptibility tensor  $\chi_{ijl}$  of third rank come to second rank tensor with 10 independent coefficients. In turn, the tensor  $\chi_{ij}$  is determined by the poin-group of symmetry of nonlinear medium.

According to the model of the anharmonic oscillator in a cubic potential [1.1] the second order nonlinear optical susceptibility can be derived as

$$\chi^{(2)}(\omega, \omega, 2\omega) = \frac{-DNe^3}{2m^2 [(\omega_0^2 - \omega^2) + i\omega\gamma]^2 ((\omega_0^2 - 4\omega^2) + i2\omega\gamma)}, \quad 1.29$$

where N is the concentration of electrons, e – charge of the electron, m – masse of the electron, D is a constant,  $\omega_0$  is frequency of the electron motion,  $\gamma$  is the damping term. From Eqs.1.18 and 1.29 the second order susceptibility can be expressed via linear susceptibility by the well known Miller's rule:

$$\chi_{ijk}^{(2)}(\omega, \omega, 2\omega) = \chi_{ii}^{(1)}(\omega) \chi_{jj}^{(1)}(\omega) \chi_{kk}^{(1)}(2\omega) \delta_{ijk}, \quad 1.30$$

Here,  $\chi_{ii, jj}^{(1)}(\omega)$  and  $\chi_{kk}^{(1)}(2\omega)$  are the linear susceptibilities at fundamental and SH wavelengths, respectively,  $\delta_{ijk}$  is a universal tensor defined by the symmetry of the nonlinear media. Expression Eq.1.30 proves the fact that second order nonlinearity is strongly dependent on linear susceptibilities of nonlinear material at fundamental wavelength and SH. Moreover, as it follows from Eq.1.29 verging of excitation frequency  $\omega$  and/or SH  $2\omega$  towards an absorption resonance evokes an enhancement of second order nonlinear coefficient in several orders of magnitudes. According to the Eq.1.26 the nonlinear polarization at  $\omega_3 = \omega_1 + \omega_2$  can be written as

$$P_k^{\omega_3}(z,t) = \epsilon_0 \chi_{kij}^{(2)}(\omega_1, \omega_2, \omega_3) E_{1i}(z) E_{2j}(z) e^{i[(\omega_1 + \omega_2)t - (k_1 + k_2)z]} + c.c. \quad 1.31$$

Lets consider the case of SH generation, when  $\omega_1 = \omega_2 = \omega$  and  $\omega_3 = 2\omega$ . Substituting Eq.1.31 and Eq.1.25 in Eq.1.10 after simple mathematical derivations and assuming non-conducting media ( $\sigma = 0$ ), we obtain coupled wave equation for SHG:

$$\frac{dE_{3k}}{dz} = -\frac{i\omega}{cn} \chi_{kij}^{(2)}(\omega, \omega, 2\omega) E_{1i} E_{2j} e^{i\Delta k z}, \quad 1.32$$

where wave vector mismatch  $\Delta k = k_3 - 2k_1$ . This equation describes the evolution of the electric field amplitude of SH in the depth of nonlinear crystal. Similar equations can be arrived for cases of sum and difference frequencies. Integration of Eq.1.32 trough the crystal length L and taking in to account the boundary condition  $E_3(z=0)=0$  one can obtain:

$$E_{3k}(L) = 2 \frac{\omega}{cn} \chi_{kij}^{(2)}(\omega, \omega, 2\omega) E_{1i} E_{2j} \frac{1 - e^{i\Delta k L}}{\Delta k} \quad 1.33$$

Using a relation for the intensity

$$I = \frac{1}{2} \sqrt{\frac{\epsilon_0 \mathcal{E}'}{\mu_0}} E_k E_k^* = \frac{c \epsilon_0 n}{2} |E|^2 \quad 1.34$$

the Eq.1.33 gives the output intensity for SH

$$I^{(2\omega)} = 8 \frac{\omega^2}{c^3 n^3 \epsilon_0} (\chi_{kij}^{(2)})^2(\omega, \omega, 2\omega) I^{(\omega)^2} L^2 \frac{\sin^2(\Delta k L / 2)}{(\Delta k L / 2)^2}, \quad 1.35$$

where  $I^{(\omega)}$  is the intensity for fundamental frequency radiation. According to the Eq.1.35 the efficient SHG requires *the phase-matching* conditions

$$\Delta k = k^{2\omega} - 2k^\omega = \frac{2\omega}{c} (n^{2\omega} - n^\omega) = 0, \quad 1.36$$

where  $n^\omega$  and  $n^{2\omega}$  are the refractive indexes at fundamental and SH frequencies in nonlinear media. However, the nonlinear frequency conversion is continually limited by the availability of suitable nonlinear materials. The phase-matching is the most restrictive requirement placed on a crystal and reduces the number of potential crystals to only a few hundred out of over 13000 known crystals. The method of quasi phase matching in materials with special periodical modulation of refractive indexes  $n^\omega$  and  $n^{2\omega}$  and/or nonlinear coefficient is important for overcoming the restriction of satisfying the conventional phase matching requirement and extending the range of utility of existing crystals.

### 1.3.2 Third-order nonlinearities.

In this part, I briefly consider optical phenomena caused by the third term of the material polarization in Eq.1.9. The third order nonlinearities are responsible for such processes as the optical and dc Kerr effect, dc electric field assisted SHG, self focusing, third-harmonic generation, stimulated Brillouin and Raman scattering, optical phase conjugation and two photon absorption. Some of them definitely are playing significant role by interaction of intense fs laser pulses with composite glass.

For the sake of simplicity, lets consider a centrosymmetric medium, where second order nonlinear susceptibility  $\chi^{(2)} = 0$ . Thus, the material polarization becomes:

$$\vec{P} = \epsilon_0 \chi^{(1)} + P_{NL}^{(3)} = \epsilon_0 (\chi^{(1)} + \chi^{(3)} \cdot \vec{E} \vec{E}) \vec{E} \quad 1.37$$

where  $\chi^{(1)}$  and  $\chi^{(3)}$  are linear and cubic nonlinear susceptibilities of a medium,  $\vec{E}$  is the electric field strength of the incident electromagnetic wave . Using the Eq.1.5 we can define the relative dielectric permittivity as

$$\epsilon = \frac{\epsilon_0 \vec{E} + \vec{P}}{\epsilon_0 \vec{E}} = 1 + \chi^{(1)} + \chi^{(3)} |E|^2 . \quad 1.38$$

According to Eq.1.22 for the refractive index and assuming that the nonlinear term is relatively small the Eq.1.38 follows to:

$$n = n_0 + \frac{\chi^{(3)} |E|^2}{2n_0} = n_0 + n_2 I , \quad 1.39$$

where  $n_0$  is the linear refractive index,  $n_2 = \frac{\chi^{(3)}}{\epsilon_0 c n_0^2}$  is the nonlinear refractive index, I

is the electromagnetic wave intensity given by Eq.1.34. Thus, the Eq.1.39 indicates that the medium with cubic nonlinearity demonstrates dependence of the refractive index on the light intensity. In general, the third-order nonlinear susceptibility  $\chi^{(3)}$  can be presented by analogy with  $\chi^{(1)}$  as a complex parameter

$$\chi^{(3)}(\omega_1, \omega_2, \omega_3) = \chi^{(3)'}(\omega_1, \omega_2, \omega_3) + i \chi^{(3)''}(\omega_1, \omega_2, \omega_3) . \quad 1.40$$

Moreover, the real and the complex parts are connected via nonlinear Kramer-Kronig relation [1.2]:

$$\chi^{(3)'}(\omega_1, \omega_2, \omega_3) = \frac{2}{\pi} \int_0^{+\infty} \frac{\Omega \chi^{(3)''}(\Omega, \omega_2, \omega_3)}{\Omega^2 - \omega_1^2} d\Omega . \quad 1.41$$

In analogy with linear case, it can be shown [1.2, 1.3] that imaginary part of the cubic nonlinear susceptibility is responsible for the damping of the electromagnetic wave due to two-photon absorption in the medium:

$$\alpha(\omega_1) = \alpha^{(2)}(\omega_1)I = \frac{2\omega_1}{c^2 \epsilon_0} \chi^{(3)''}(\omega_1, \omega_2, -\omega_2)I, \quad 1.42$$

where  $\alpha^{(2)}(\omega_1)$  is the nonlinear absorption coefficient,  $I$  is intensity of light given by Eq.1.34. According to Eq.1.42, increase of the laser intensity can evoke nonlinear absorption in the medium with cubic nonlinearity caused by two-photon absorption. Therefore, the nonlinear refractive index as well as absorption coefficient linearly depends on the laser intensity.

On the other hand, the optical Kerr effect expressed by the Eq.1.39 is responsible for such phenomena as self-focusing of an laser beam, self-phase modulation of an laser pulse, optical bistability of the nonlinear medium.

The self-focusing of the intense laser beam arises from a variation of the intensity in the beam profile. Thus, if the laser beam profile is characterized by the Gaussian function and  $n_2$  is positive (most materials), the refractive index in the center of the beam is considerably higher compared to the wings. These alterations create a positive acting lens, which focuses the beam. The self-focusing results in beam size decrease and following rise of the intensity in the beam center. If the beam size finally achieves a diffractive limit, a filament is formed. On the other hand, if the intensity is high enough, the electron plasma can be induced acting as a negative lens, which prevents following focusing of the beam.

In contrast to the self-focusing, where the intensity beam profile leads to special variation of the refractive index, the self-phase modulation arises due to temporal intensity modulation resulting in the refractive index varying with time. This produces, in turn, a time dependent phase shift of the laser pulse [1.4]. The laser pulse in slowly-varying envelope approximation can be given as

$$E(z, t) = \frac{1}{2} [E_0(z, t) \exp(ikz - i\omega_0 t) + c.c.], \quad 1.43$$

where  $E_0(z, t)$  describes the envelope of the laser pulse. Thus, taking into account Eq.1.39 the phase of the laser pulse (Eq.1.43) can be written as

$$\phi(z, t) = kz - \omega_0 t = \frac{\omega_0}{c} z(n_0 + n_2 I(z, t)) - \omega_0 t, \quad 1.44$$

where the laser pulse intensity according to Eq.1.34 is given by  $I(z, t) = \frac{c\epsilon_0 n_0}{2} |E_0(z, t)|^2$ . Thus, the high laser pulse intensity can result in additional phase shift caused by nonlinear refractive index. Since the frequency of the wave is  $\omega = -\frac{\partial \phi}{\partial t}$ , the phase modulation Eq.1.44 leads to a frequency modulation

$$\omega(t) = \omega_0 - \frac{n_2 \omega_0 z}{c} \frac{\partial}{\partial t} I(z, t). \quad 1.45$$

According to the Eq.1.45, the spectrum of the self-phase modulated field is broadened leading to supercontinuum generation [1.4].

The supercontinuum generation opens wide opportunities for ultrafast laser spectroscopy. In turn, we applied this technique in pump-probe experiments, where white light created by 150 fs laser pulses in sapphire plate was used as a probe pulse for modification dynamics measurements in nanocomposite glass (Chapter 3, Section 3.4). Moreover, the supercontinuum generation in the glass could result in induced ionization and colour center formation caused by single photon absorption of the blue wing of the broadened pulses [1.5].

## 1.4 Nonlinear ionization.

In previous section I have considered nonlinear phenomena induced in a medium by intense laser radiation. However, under some circumstances the nonlinear interactions of the electromagnetic wave with matter can lead to permanent structural modifications in it. This, results in considerable changes of the linear and nonlinear optical properties of the exposed material. As used here, the most important mechanism responsible for the permanent modification of matter is the laser assisted ionization.

Ionization of dielectrics requires transition of electrons from valence band to conduction band. Thus, if the photon energy of excitation wave is less than the energy gap between valence and conduction bands, the ionization due to single photon absorption is excluded. As it was shown above, increase of the light intensity leads to enhancement of two-photon absorption in the medium with cubic nonlinearity. Thus, ionization of the dielectric can be induced even by intense laser excitation at wavelengths far away from the fundamental absorption edge due to two-photon (multi-photon) absorption caused by nonlinear processes in the material.

One has to distinguish two classes of nonlinear ionization mechanisms: photoionization and avalanche ionization [1.6], which results in plasma formation responsible for nonlinear phenomena and structural modifications in dielectrics.

### 1.4.1 Photoionization.

Photoionization refers to direct excitation of the electrons by the laser field. Moreover, the ionization caused by nonlinear absorption of several photons is describing as *the multi-photon ionization* (Fig.1.1A). On the other hand, according to Eq.1.34 increase of the laser intensity refers to grows of the electric field strength of the electro-magnetic wave. In turn, strong electric fields can suppress the Coulomb well of the electron bonded with an atom. If the deformation of the electron potential energy is high enough (1.1B), the valence electron tunnels through the short potential

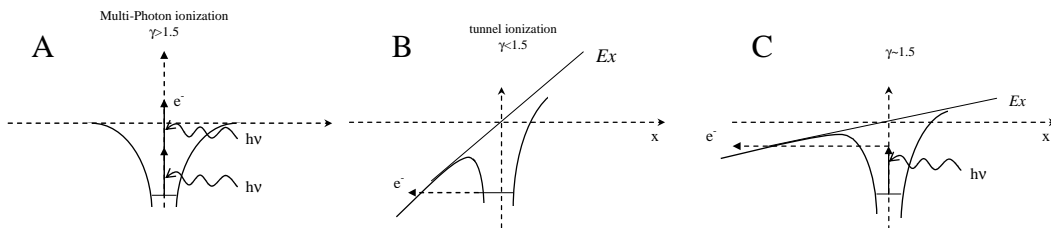


Fig.1.1 Photoionization of the electron placed in coulomb well: A – two-photon ionization; B – tunnelling ionization, C – intermediate state.

*Chapter 1. Propagation of optical beams in composite medium containing metal nanoparticles*

barrier and becomes free. This mechanism of photoionization is called *the tunnel ionization*. As a fact, the both types of the photoionization depend on material, laser frequency and intensity. Moreover, the probability of the one or another ionization mechanism is predicted by the Keldysh parameter [1.7]:

$$\gamma = \frac{\omega}{e} \left[ \frac{mcn\epsilon_0 E_g}{I} \right]^{\frac{1}{2}}, \quad 1.46$$

where  $\omega$  is the laser frequency,  $I$  is the laser intensity,  $m$  and  $e$  are the reduced mass and charge of the electron,  $c$  is the light velocity,  $n$  is the refractive index of material,  $E_g$  is the energy gap between valence and conduction band in the material. Thus, if the Keldysh parameter is higher than 1.5, then photoionization is caused predominantly by multi-photon processes (Fig.1.1A). Otherwise, by Keldysh parameter below of 1.5 the tunnel ionization is most important. If the Keldysh parameter near to 1.5 results apparently in a mixture of the both mechanisms (Fig.1.1C).

The Eq.1.46 testifies that multi-photon ionization is more favourable at higher laser frequencies. On the other hand, high laser intensity and low laser frequency lead to the tunnel ionization.

*1.4.2. Avalanche ionization.*

The free electrons induced by photoionization result in a broad absorption band and the laser radiation can be absorbed linearly if the plasma density becomes high enough. Indeed, according the Drude model the electric permittivity of the free electron carrier can be given as

$$\epsilon(\omega) = 1 - \frac{\omega_p^2}{\omega^2 + i\gamma\omega}, \quad 1.47$$

where  $\omega_p = \sqrt{\frac{Ne^2}{m\epsilon_0}}$  is the plasma frequency,  $N$  – is the free electron density,  $e$  and  $m$  are the charge and reduced mass of the electron,  $\gamma$  is a damping parameter associated with Drude scattering time. According the Eq.1.24 the absorption of a medium depends on imaginary part of the complex electric permittivity and for the free electron plasma we obtain

$$\epsilon''(\omega) = \frac{\omega_p^2 \gamma}{\omega(\omega^2 + \gamma^2)}. \quad 1.48$$

It is obvious that absorption of the free carrier increases with growth of the free electron density, which in turn depends on the laser intensity and ionization rate. Following absorption of the laser radiation by the free electrons leads to rapid plasma heating moving the conduction electrons to higher energy states. If resulting electrons energy exceeds the bottom of the conduction band by more than the band gap energy between valence and conduction band, the hot free electron can transfer saved energy to an electron in valence band via non-elastic collisions. As an outcome, we receive two electrons in the bottom of conduction band, each of which can be involved in the collisional ionization again. Thus, the electron plasma density

grows in this case quickly proportional to exponential function of time [1.6]. This mechanism of ionization is called *the avalanche ionization*. As it can be seen from the discussion, the avalanche ionization requires some seed electrons in the conduction band, which can be produced by photoionization of impurities and defects in the matrix.

Following plasma relaxation leads to the energy transfer from the electrons to the lattice. It has to be pointed out that the energy transfer occurs in time scales much shorter as the thermal diffusion time. Nevertheless, for the laser pulses with duration longer than several tens ps the energy transfer occurs on time scale of the pulse duration. Then the energy is transported out of the exposed area by thermal diffusion. If the temperature of the irradiate region overcomes the melting or fraction temperature, the damage of the surface can be achieved. In the case of intense fs laser pulses the avalanche ionization leads to the extremely high electron density and energy of the laser pulse effectively deposited in plasma. Only after laser pulse is gone the plasma energy is transferred to the lattice. Since the energy transfer is much faster than the thermal diffusion time, induced ablation by ultra-short laser pulses occurs with minor thermal defects.

## **1.5 Optical properties of nanocomposites containing metal nanoparticles.**

The theoretical discussion and derivations performed above for a homogeneous medium are valid also for the nanocomposite materials. However, interaction of an electromagnetic wave with nanostructures reveals novel optical phenomena indicating unrivalled optical properties of these materials caused by different intrinsic and extrinsic size effects in the clusters with size less than the wavelength. For instance, in this section I will consider interaction of the metal clusters with external electromagnetic wave.

It is well known that the linear and nonlinear optical response of metal nanoparticles are specified by oscillations of the surface electrons in Coulomb well formed by the positively charged ionic core. This type of excitations is called the surface plasmon (SP). In 1908 Mie [1.8] proposed a solution of Maxwell's equations, which explains the origin of the SP resonance in extinction spectra and coloration of the metal colloids. During the last century optical properties of metal nanoparticles has extensively been studied and metalo-dielectric nanocomposites found various applications in different fields of science and technology [1.9-1.11]. Strong effect of the size, shape, distribution of the nanoparticles as well as of the environment on the SP resonances offers an opportunity for development of very promising novel nonlinear materials, nanodevices and optical elements by manipulation of the nanostructural properties of the metal particles.

### *1.5.1. Surface plasmon resonance of metal nanoparticles: effect of size, shape and surrounding matrix.*

Propagating electromagnetic wave in the medium with incorporated spherical metal nanoparticle causes displacement of conduction electrons relative to the positively charger ionic core (Fig.1.2), which evokes induced dipole oscillating with frequency of the incident wave. If the radius of the sphere is much smaller than the

*Chapter 1. Propagation of optical beams in composite medium containing metal nanoparticles*

wavelength of the electromagnetic wave, electrostatic approximation [1.12] is valid and the dipole moment of the embedded in dielectric sphere can be given as:

$$\vec{p}(\omega) = \alpha \epsilon_0 \vec{E}_0(\omega) = 4\pi \epsilon_0 R^3 \frac{\epsilon_i(\omega) - \epsilon_h}{\epsilon_i(\omega) + 2\epsilon_h} \vec{E}_0(\omega), \quad 1.49$$

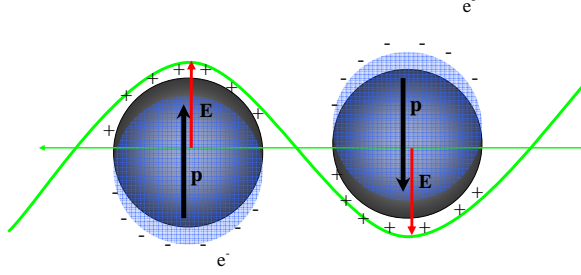


*Fig.1.2 Plasmon oscillations in metal sphere induced by electromagnetic wave.*

where  $\alpha$  is the polarisability of the sphere,  $R$  is the radius of the nanoparticle,  $E_0$  the electric field strength of an incident electromagnetic wave,  $\epsilon_0$  the electric permittivity of vacuum,  $\epsilon_i(\omega)$  and  $\epsilon_h$  are the relative complex electric permittivity of metal and host matrix, respectively. If the metal inclusion is placed in a transparent dielectric

matrix owing the electric permittivity with predominant real part ( $\text{Im}[\epsilon_h] \rightarrow 0$ ), then using the Eq.1.24 the absorption cross section of the spherical nanoparticle can be derived from 1.49 and written as

$$\sigma(\omega) = \frac{\omega}{c\sqrt{\epsilon_h}} \text{Im}[\alpha(\omega)] = 12\pi R^3 \frac{\omega\sqrt{\epsilon_h}}{c} \frac{\epsilon_i''(\omega)}{[\epsilon_i'(\omega) + 2\epsilon_h]^2 + \epsilon_i''(\omega)^2}, \quad 1.50$$

where  $\epsilon_i'(\omega)$  and  $\epsilon_i''(\omega)$  are real and imaginary part of the electric permittivity of the metal, which in turn can be described by the Drude-Sommerfeld formula:

$$\epsilon_i(\omega) = \epsilon_b + 1 - \frac{\omega_p^2}{\omega^2 + i\gamma\omega}, \quad 1.51$$

where  $\gamma$  is a damping constant of the electron oscillations and  $\epsilon_b$  is the complex electric permittivity associated with interband transitions of the core electrons in atom. The free electron plasma frequency is given by  $\omega_p = \sqrt{\frac{Ne^2}{m\epsilon_0}}$ , where  $N$  is the

density of the free electrons and  $m$  is the effective mass of an electron. Moreover, for the noble metals (Cu, Ag, Au) calculated plasma frequency is about of 9eV. As it can be seen from the Eqs.1.49 and 1.50, the well known Mie resonance occurs at the SP frequency  $\omega_{SP}$  under the following condition:

$$[\epsilon_i'(\omega_{SP}) + 2\epsilon_h]^2 + \epsilon_i''(\omega_{SP})^2 \rightarrow \text{Minimum}. \quad 1.52$$

If the imaginary part of the metal electric permittivity is small in comparison with  $\epsilon_i'(\omega)$  or has small frequency dependence, then condition Eq.1.52 can be written:

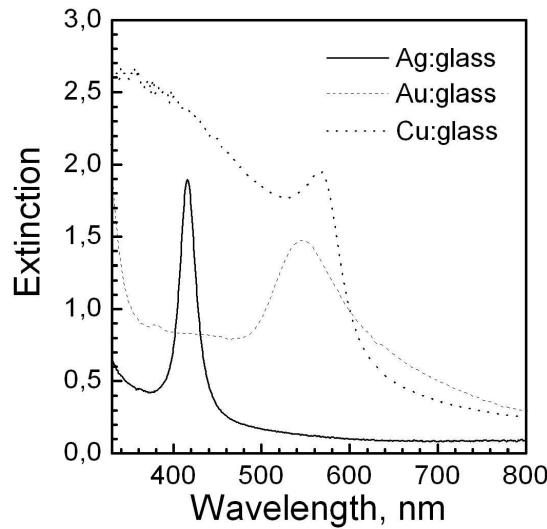


Fig.1.3 Extinction spectra of glass samples containing spherical Ag, Au and Cu nanoparticles.

Thus, if the condition Eq.1.53 is complied, the dipole moment and local electric field in vicinity of the nanosphere grow resonantly and can achieve magnitudes in many orders overcoming the field of the incident wave. This phenomenon is responsible for the SP enhanced nonlinearities of the metal colloids. On the other hand, in extinction spectra the SP absorption band occurs (Fig.1.3), which is specified by the type of the metal. For instance, silver nanoparticles embedded in glass matrix own the SP band peaked at about of 417 nm, while SP for Au and Cu nanoparticles is shifted in red spectral range and centered at 548 nm and 570 nm, respectively. A broad absorption bands below of 500 nm in the gold and copper containing nanocomposite glass are associated with interband (from d- to s-shell) transitions of the core electrons in metal atom. For the silver the interband resonance is peaked at 4 eV (310 nm) far away from the SP resonance [1.13].

In turn, position of the SP resonance can be derived from the Eq.1.53 substituting the real part of the metal electric permittivity given by the Eq.1.51:

$$\omega_{SP}^2 = \frac{\omega_p^2}{\text{Re}(\epsilon_b) + 1 + 2\epsilon_h} - \gamma^2. \quad 1.54$$

As it can be seen in the Eq.1.54, the core electrons have a significant influence on the surface plasmon and define obviously position of the SP resonance in extinction spectra (the Fig.1.3) for different noble metals. On the other hand, the Eq.1.54 qualitatively describes a dependence of the SP resonance on the dielectric properties of the host matrix, which the metal cluster is incorporated in: increase of

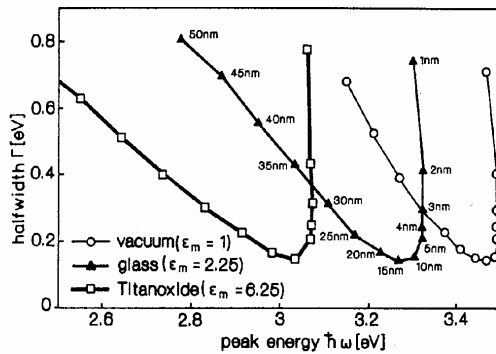


Fig.1.4 Dependence of the SP resonance of Ag nanoparticles on size and dielectric matrix. The figure is adopted from the Ref.[1.9].

the dielectric constant (refractive index) evokes shift of the absorption maximum towards long wavelengths (the Fig.1.4) [1.9, 1.14, 1.15].

The Fig.1.4 demonstrates also dependence of the SP resonance on the radius of the metal nanoparticle. Thus, as it is shown in the Fig.1.4, position of the SP resonance remains quasi constant for the Ag nanoparticles with radius smaller than 15 nm, while band halfwidth differs for these clusters by factor 4. In turn,

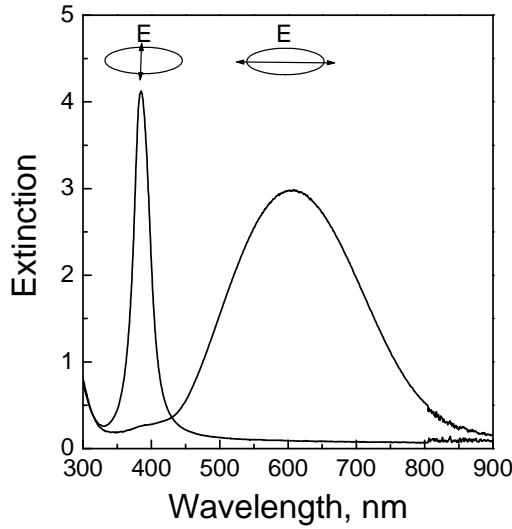


Fig.1.5 Polarized extinction spectra of the spheroidal Ag nanoparticle in soda-lime glass.

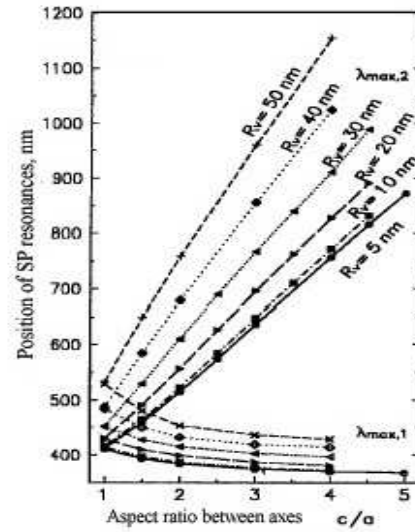


Fig.1.6 Dependence of the spectral gap between SP resonance modes of spheroidal Ag nanoparticle on aspect ratio between axes. The figure is adopted from the Ref.[1.16].

increase in the radius of the nanosphere larger than 15 nm leads to the shift of the SP resonance towards long wavelengths with simultaneous increase in the band halfwidth. According to the mean free-path model [1.9], such behaviour of the SP maximum can be explained by an influence of the cluster radius on the damping constant and consequently on the electric permittivity of the metal inclusion (the Eq.1.51).

On the other hand, from the size dependence of the SP it's quite obvious that metal nanoparticle with nonspherical shape will show several SP resonances in the spectra. For instance, the ellipsoidal clusters with axes  $a \neq b \neq c$  own three SP modes corresponding to polarizabilities along principal axes given as:

$$\alpha_k(\omega) = \frac{4\pi}{3} abc \frac{\epsilon_i(\omega) - \epsilon_h}{\epsilon_h + [\epsilon_i(\omega) + \epsilon_h]L_k}, \quad 1.55$$

where  $L_k$  is the geometrical depolarization factor for each axis ( $\sum L_k = 1$ ). Moreover, increase in the axis length leads to the minimization of the depolarization factor. For the spherical particle  $L_a = L_b = L_c = \frac{1}{3}$ .

Thus, if the propagation direction and polarization of the electromagnetic wave do not coincide with the axes of the ellipsoid, the extinction spectra can demonstrate three separate SP bands [1.9]. For spheroids  $a \neq b = c$  the spectra demonstrate two SP resonances. However, in polarized light parallel to the one of the axes the spectra demonstrate single SP band corresponding to appropriate axis (Fig.1.5). Moreover, the band in the red side is referred to the long axis, while the small axis demonstrate resonance in UV. The spectral gap between the SP modes, as it was shown in the Ref.[1.16], rises with increase of the aspect ratio between axes of the spheroid (Fig.1.6).

The dichroic properties of oblong metal nanoparticles are efficiently used by CORNING and CODIXX AG for manufacturing of broad band high contrast ( $\sim 10^5$ ) polarizers on the basis of glass containing Ag nanoparticles. Moreover, the position of the absorption band maximum can be shifted in very broad spectral range by appropriate aspect ratio between axes of the cluster driven in this case by the glass stretching parameters.

### 1.5.2 Optical properties of aggregated Ag nanoparticles.

Increasing fraction of metal clusters in a medium leads to decrease of the average particle distances. Thus, enhancement of the dipole moment of spherical metal cluster by excitation near to the SP resonance results in strong collective dipolar interactions between nanoparticles, which affect the linear and nonlinear optical properties of a nanocomposite material. For the purpose of this work it is sufficient to describe this effect in the approximation of the well known Maxwell-Garnett theory, which is widely applied to describe the optical properties of metal grains in dielectric matrices [1.9, 1.10, 1.17, 1.18]. Although it does not correctly take into account the multipolar interactions between nanoparticles considered in

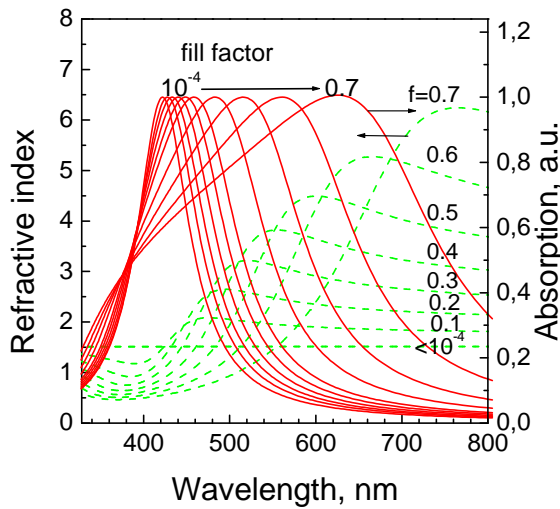


Fig.1.7 Absorption spectra and dispersion of metal-composite glass with Ag nanoparticles calculated by Maxwell-Garnett theory.

other work [1.19-1.21], the Maxwell-Garnett theory can be used in the following because it describes quite well the position and shape of the surface plasmon resonance and its dependence on the metal fill factor [1.22]. Moreover, propagation of the optical beams can be considered as in the homogeneous medium with an effective electric permittivity.

In turn, the effective dielectric constant  $\epsilon_{eff}(\omega)$  of a composite material with spherical metal inclusions having a fill factor  $f$  is given by the expression:

$$\epsilon_{eff}(\omega) = \epsilon_h \frac{(\epsilon_i(\omega) + 2\epsilon_h) + 2f(\epsilon_i(\omega) - \epsilon_h)}{(\epsilon_i(\omega) + 2\epsilon_h) - f(\epsilon_i(\omega) - \epsilon_h)}, \quad 1.56$$

where  $\epsilon_i(\omega)$  is  $\epsilon_h$  are complex electric permittivities of the metal (given by the Eq.1.51) and host matrix. Substituting the Eq.1.51 to Eq.1.55 and using Eqs.1.21 and 1.22 the absorption spectra and dispersion for spherical Ag nanoparticles can be calculated as a function of the volume fill factor of metal inclusions in the glass matrix ( $\epsilon_h=2.3$ ,  $\omega_p=9.2$  eV,  $\gamma=1 \times 10^{14} \text{s}^{-1}$  [1.9],  $\epsilon_b=4.2$  [1.18]). The (normalized) absorption spectra shown in Fig.1.7 demonstrate that the collective dipolar interactions between nanoparticles cause a significant broadening and red shift of the absorption band with increasing fill factor of silver inclusions in the glass matrix. At

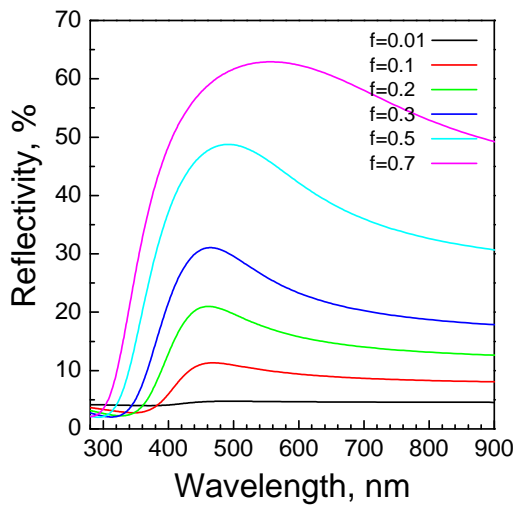


Fig.1.8 Calculated reflection spectra of metalo-composite glass with Ag nanoparticles calculated by Maxwell-Garnett theory.

the reflection spectra according to the Eq.1.25 clearly indicate increase in the reflectivity of the composite medium with Ag spherical nanoparticles by growth of the metal content (Fig.1.8).

In conclusion, the SP resonance defines the linear and nonlinear optical properties of composite materials containing metal nanoparticles. The SP assisted local field enhancement in vicinity to the surface of nanoparticle is responsible for high optical nonlinearity in plasmonic materials. In turn, the SP can be affected by the size, shape, distribution of metal clusters as well as by the dielectric properties of the host matrix. This offers an opportunity for creation of novel promising materials with special physical properties.

the same time, fill factor strongly effects on effective refractive index of composite glass. As it can be seen on the Fig.1.7, at low content of the silver inclusions in the glass ( $f=10^{-4}$ ) the refractive index is about of 1.54 corresponding to clear glass. On the other hand, higher fill factor results in significant modifications of dispersion dependences of composite glass and the refractive index varies from 0.5 up to 6 in whole visible spectral range. Demonstrated alterations of the absorption spectra and dispersion cause obviously a variation of reflection properties as function of the filling factor. Calculations of

Chapter 2.

## Technique of the experiment

### 2.1 Laser system used for photomodifications of Ag nanoparticles.

The experiments presented in this work were carried out using a commercial system of mode-locked Ti-sapphire laser with regenerative amplification produced by “Spectra Physics”. The laser system is schematically shown in Fig.2.1. The main part of the system consists of the Kerr lens mode-locked *Ti:sapphire oscillator* (“*Tsunami*”) pumped by 5W cw diode-pumped Nd:YVO<sub>4</sub> laser with intercavity doubling at 532 nm. The Ti<sup>3+</sup>: Al<sub>2</sub>O<sub>3</sub> (sapphire) has been known as an active media since 80<sup>th</sup> when Moulton demonstrated for the first time the pulse [2.1,2.2] and cw laser generation [2.3] on the Ti:sapphire. Absorption band centred at 520 nm and broad luminescence band in the spectral range of 670-1100 nm are associated with electron transition between ground state <sup>2</sup>T<sub>2</sub> and excited state <sup>2</sup>E of octahedrally coordinated Ti<sup>3+</sup> ions in Al<sub>2</sub>O<sub>3</sub> crystal (see Fig.2.1). Extremely broad luminescence band defines tuning range of Ti:sapphire laser from 670nm till 1100 nm [2.4]. Moreover, the broad amplification band allows to achieve in mode-locked operation

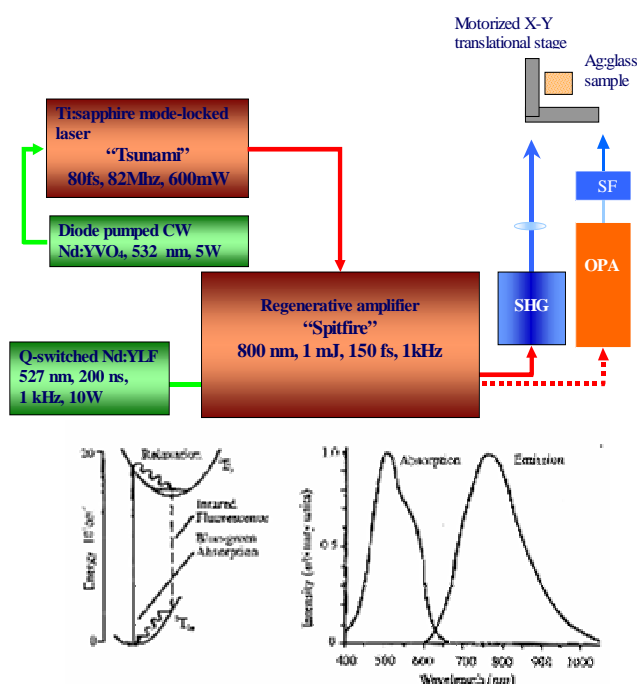


Fig.2.1 Set up of the “Spectra Physics” *Ti:sapphire* laser system. Scheme of electron transitions between laser energy levels of octahedrally coordinated Ti<sup>3+</sup> ion in Al<sub>2</sub>O<sub>3</sub> crystal, absorption and emission spectra.

pulses as short as ~5 fs [2.5-2.8]. To date, Ti<sup>3+</sup>:sapphire is the most common and commercially available tunable solid-state laser. Here, mode-locked Ti:sapphire laser with pulse duration of 80 fs and energy of up to 12 nJ, repetition rate of 82 MHz, tuning range of 720-840 nm was used. The tuning range was only restricted due to set of selective dielectric mirrors used in the laser cavity.

In order to increase the pulse energy from oscillator up to 1 mJ we used the *regenerative amplifier “Spitfire”* on the basis of Ti:sapphire crystal. The principle of the amplification lies as follows. An intense pump pulse produces the high population inversion in the laser crystal. Then a seed pulse coming in the system stimulates the electron transitions from the upper laser level, takes off the population inversion and induces stimulated emission. Therefore, whole energy emerged by electron transitions is deposited in the seed pulse. In “Spitfire” in order to enhance the amplification efficiency the seed pulse makes approximately 20 passes through the Ti:sapphire crystal placed in the cavity. In turn, amplifier was pumped at 527 nm by Q-switched Nd:YLF intercavity doubled laser with pulse energy of 10 mJ, pulse width about of 200 ns and repetition rate 1kHz. In other hand, to prevent a damage of the laser crystal, the chirped seed pulse from oscillator have to be stretched formally in order to decrease the peak pulse intensity on the crystal. After amplification pulse is compressed again. Splitting and compression was performed using system of two gratings and mirrors. Such technique allows to receive the pulses with duration about of 150 fs, energy up to 1 mJ (peak power ~6 GW) and pulse repetition rate of 1 kHz.

Using *the nonlinear frequency conversion* of intense laser pulses derived from Ti:sapphire system the radiation with wavelengths in the spectral range from UV to IR can be achieved. First, using second harmonic generation (SHG) in KDP crystal with 1 mm thickness the pulses with wavelengths of 380-420 nm were achieved. Following sum frequency (SF) of the SH and fundamental radiation in KDP crystal gives the wavelengths 250-280 nm. On other hand, using optical parametric generation in BBO crystal by pumping with pulses at 800 nm from Ti:sapphire system the radiation in the spectral range 1.2-1.6  $\mu\text{m}$  (signal) and 1.6-2.4  $\mu\text{m}$  (idler) was received. Following SF of signal and fundamental frequencies results in radiation in 490-700 nm spectral range. Thus, the whole UV and visible spectral range can be used for the study of Ag nanoparticles embedded in glass.

## 2.2 Irradiation technique using laser Gaussian beams.

To study the laser-induced modifications of Ag nanoparticles embedded in soda-lime glass the laser beam was focused by the lens or objective on the sample placed on the X-Y translation stage driven by computer. The focus of the lens, beam width, writing density (actually pulse number per spot area), as well as wavelength and intensity of the laser pulses have been chosen according to the goals of the experiments. Since the modifications in the composite glass described in this work were induced by focused laser beam with Gaussian intensity distribution, it is quite reasonable to introduce here the basic terms and equations of the Gaussian optics.

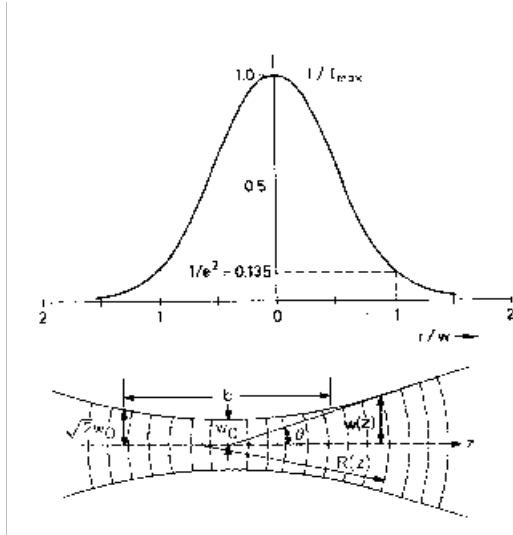


Fig. 2.2 Gaussian beam: (top) the intensity profile; (bottom) the mode size distribution along the propagation direction.

In general, the Gaussian beam is a result of the solution of the three dimensional wave equation and characterises the transversal electromagnetic modes (TEM) generated in the laser cavity. For the TEM<sub>00</sub> mode (the one from an infinite set of solutions), the intensity profile of the beam is expressed by the Gauss function:

$$I(r) = I_0 \exp\left(-\frac{2r^2}{\omega^2}\right), \quad 2.1$$

where  $I_0$  is a peak intensity,  $r$  is the distance from the beam center and  $\omega$  is a spot size of the laser beam. The peak intensity of the Gaussian beam is defined as:

$$I_0 = \frac{2P}{\pi\omega^2}, \quad 2.2$$

where  $P$  is the laser pulse power or output power (for the CW laser). According to the Eq.2.1 the intensity distribution across to the laser beam has a Gaussian form (Fig.2.2 top). Moreover, the beam spot size  $\omega$  corresponds to the distance from the center of the laser spot to the point, where the intensity drops down by factor  $e^2$  (see the top of the Fig.2.2). At the same time, the spot size is not invariant in direction of the wave propagation (bottom of the Fig.2.2) and is described by:

$$\omega(z) = \omega_0 \left[ 1 + \left( \frac{\lambda z}{\pi\omega_0^2 n} \right)^2 \right]^{\frac{1}{2}}, \quad 2.3$$

where  $\lambda$  is the laser wavelength,  $z$  is the coordinates along to the propagation direction,  $\omega_0$  is the beam waist,  $n$  refractive index of the medium, which the radiation is propagating in. According to the Eq.2.3, the range, where the laser spot size does not exceed the value of  $\sqrt{\omega_0}$ , is called the confocal parameter,  $b$ , which is given as:

$$b = \frac{2\pi\omega_0^2 n}{\lambda}. \quad 2.4$$

The radius of the curvature of wave front of the Gaussian beam can be determined as:

$$R(z) = z \left[ 1 + \left( \frac{\pi\omega_0^2 n}{\lambda z} \right)^2 \right]. \quad 2.5$$

The divergence of the beam at large values of  $z$  can be written as:

$$\theta \approx \frac{\omega}{z} \approx \frac{\lambda}{\pi\omega_0}. \quad 2.6$$

As it can be seen, the Eq.2.6 characterises the diffraction limited divergence of the laser beam. However, one has to notice that all equations presented above are valid only in the case of the TEM<sub>00</sub> mode. Generation of the high order modes and distortion of the wave front due to lens aberrations, thermal effects, nonlinear interactions in the matter lead to the degradation of the laser beam quality. In order to describe the mode structure of the ordinary laser beam the M<sup>2</sup> parameter is introduced [2.9, 2.10]. The M<sup>2</sup> factor is generally accepted as a figure of merit for estimation of the beam “quality”. Thus, using the M<sup>2</sup> factor the beam waist of the multimode Gaussian laser beam can be expressed as:

$$W_0 = M\omega_0, \quad 2.7$$

where  $\omega_0$  is the TEM<sub>00</sub> mode waist. Substituting the Eq.2.7 in Eqs.2.1-2.6 we receive the basic equations for characterization of ordinary laser beam:

$$I(r) = I_0 \exp\left(-\frac{2r^2}{W^2}\right), \quad 2.8$$

$$W(z) = W_0 \left[ 1 + \left( \frac{M^2 \lambda z}{\pi W_0^2 n} \right)^2 \right]^{\frac{1}{2}}, \quad 2.9$$

$$b = \frac{2\pi W_0^2 n}{M^2 \lambda}, \quad 2.10$$

$$\theta = M^2 \frac{\lambda}{\pi W_0}. \quad 2.11$$

The last equation indicates that the M<sup>2</sup> factor characterizes the deviation of the laser beam divergence from the diffraction limit. On the other hand, according to the Eq.2.11 the M<sup>2</sup> of the laser beam can be significantly improved by minimization of the laser beam size for example using the beam shapers [2.11] or even pinholes.

Thus, using Eq.2.9-2.11 we can determine the parameters of the ordinary laser beams propagating in the lens like medium. For instance, the spot waist  $\omega_0$  (see the Fig.2.3) of the laser beam produced by a lens with focus length  $f$  is given as:

$$\omega_0 = \frac{\frac{f\lambda}{\pi\omega_{01}n} M^2}{\sqrt{1 + \left( \frac{f\lambda}{\pi\omega_{01}n} M^2 \right)^2}} \approx M^2 \frac{\lambda f}{\pi\omega_{01}n} = M^2 \frac{\lambda}{\pi \cdot N.A.}, \quad 2.12$$

where  $\lambda$  is the laser wavelength,  $\omega_{01}$  is the spot size of the laser beam on the lens (see the Fig.2.3),  $n$  is the refractive index of the medium. N.A. is the numerical aperture of the lens. According to the Eq.2.12, in the case of the single mode laser, when the  $M^2=1$ , we obtain a diffraction limited laser beam spot waist. Degradation of the beam quality (which is characterized by increase of the divergence) leads to the increase of the spot size in the focus by the factor  $M^2$ .

In experiment,  $M^2$  can be easily estimated by measurement of the beam waist produced by a lens and comparison with the diffraction limited one. In our case, the laser radiation at 400 nm used for modification of the composite glass was focused by the 300 mm focus length lens yielding the waist in the focus not less as 60  $\mu\text{m}$ . At

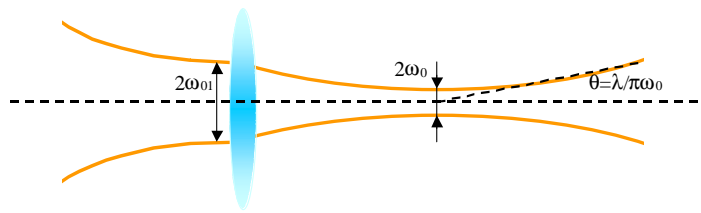


Fig.2.3. Focusing of the Gaussian beam.

the same time, the diffraction limited beam waist according to Eq.2.12 (with  $M^2=1$ ) give the magnitude about of 12  $\mu\text{m}$ . This testifies that the beam quality factor in our case was not less than 5.

In experiments related to the study of **intensity dependences of laser induced modifications**, the sample was placed before the focus and the laser spot size on the sample was about of 125  $\mu\text{m}$ . Irradiation of single spots on the samples was performed with various parameters (pulse energy, pulse frequency, pulse number, laser polarization) and modified region was investigated (Fig. 2.4).

For creation of the fine dichroitic structures demonstrated in the Chapter 4,

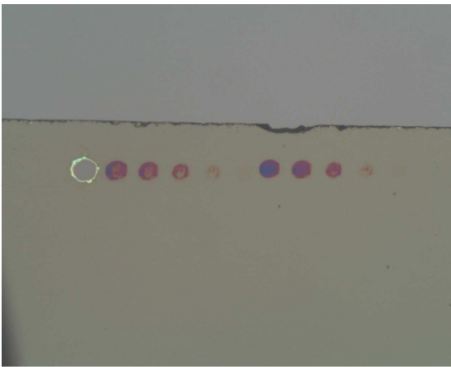


Fig. 2.4 Irradiated spots on the glass sample containing Ag nanoparticles.

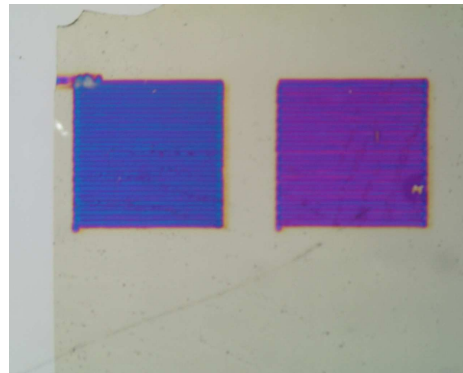


Fig. 2.5 Irradiated by fs laser homogenous fields on the glass sample containing spherical Ag nanoparticles

we used a mirror objective with N.A.=0.28. According to estimated  $M^2$  factor to be not less as 5 the resulted beam wais in the focus can not be less as 2  $\mu\text{m}$ . This restricts the minimal size of created structures. At the same time, the nonlinear dependence of the induced modifications on the laser pulse intensity allows to

achieve the smaller modification spot than the diffraction limit of the laser spot size predicted by Eq.2.12.

In experiments concerned with the study of wavelength dependences of the laser induced modifications the irradiation with fs laser was performed in multishot regime. Using X-Y translational stage the sample was moving in the plane, which is perpendicular to direction of the laser beam. Following this technique, the homogeneous fields usually of size 3x3 mm were irradiated (Fig.2.5). Moreover, writing density by irradiation of homogeneous fields can be varied by appropriated choice of the laser beam width, scan speed of the sample and laser pulse repetition rate.

### 2.3 Spectroscopic technique.

As it will be shown in the next chapters, irradiation of glass samples containing Ag nanoparticles by laser pulses with wavelength near to the SP band leads to the modifications of the shape and arrangement of the metal nanoparticles as well as surrounding matrix. These permanent laser induced modifications result in changes of spectral properties of the composite glass with silver nanoparticles. Thus, in our experiments we used experimental data obtained from transmission, reflection, and luminescence spectra in order to characterise the transformations occurring in the sample.

As it has been shown in the Chapter 1, the metal nanoparticles demonstrate strong absorption as well as strong scattering in the spectral range near to the surface plasmon resonance. Increase of fill factor of metal clusters in glass sample results additionally in growth of reflection coefficient. Therefore, transmission optical spectra include all three components. In turn, for data analysis transmission spectra were recalculated in extinction coefficients defined as natural logarithm from transmission.

In this work, we used two techniques for *transmission spectra measurements*. In order to study the wavelength dependences of laser induced

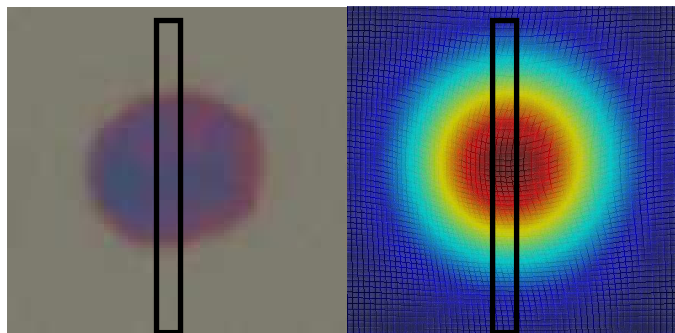


*Fig.2.6 Projection of the image of modified spot on the slit of spectrograph (left image) allows to measure intensity dependent transmission spectra across of the spot. Intensity calibration was performed by intensity profile measurements of the Gaussian laser beam (right).*

modifications transmission spectra of the samples containing Ag nanoparticles were measured in spectral range 200-1500 nm using two beams transmission spectrometer Shimadzu UV-3100. Using a Glan prism placed in the spectrometer the polarized spectra were measured from the sample area with size of 3x3mm<sup>2</sup>.

On the other hand, to study intensity dependences of Ag nanoparticle modifications a set-up for *position resolved transmission spectra measurements* has

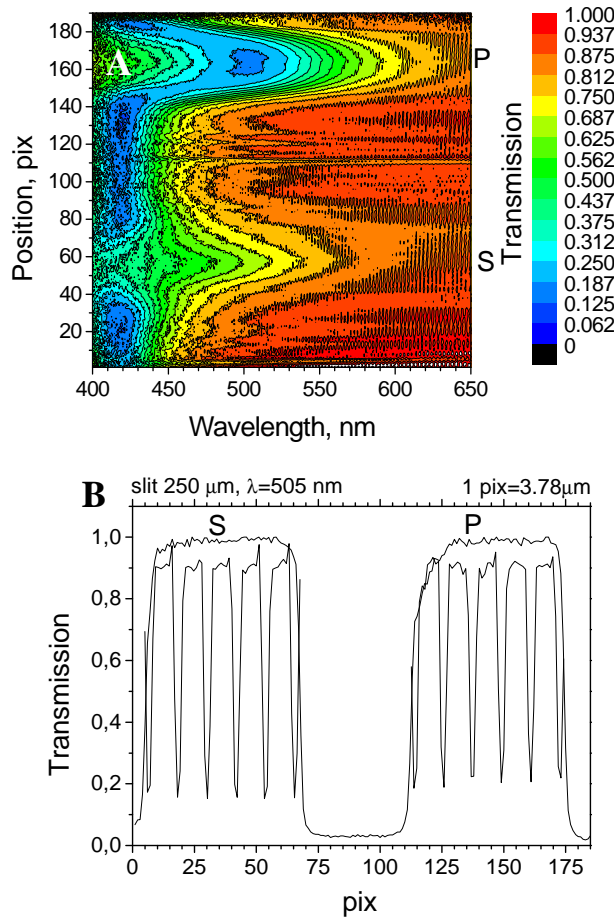


Fig.2.7. A: Position resolved polarized transmission spectra. B: Calibration of spectrometer for position resolved transmission spectra measurements.

modified area image (Fig.2.6 left). In such case, we cut only the thin central region of the spot image where spectral changes perpendicular to the slit are negligible while the spectra along to the slit are defined by Gaussian profile of the laser beam (Fig.2.6 right). Thus, we specialize the problem to one dimension. In order to split the image in two polarisations a polarize prism was placed in front of the spectrograph deriving o- and e- images separated on the slit of spectrograph. Thus, on the CCD we receive transmission spectra like (Fig.2.7a) simultaneously for both polarizations. In order to calibrate the image in real sizes the micro scale with scaling factor of  $50\ \mu\text{m}$  and/or the slit with size of  $250\ \mu\text{m}$  were used (Fig.2.7b). Thus, 1 pixel on the CCD in vertical direction corresponds approximately to the  $3.8\ \mu\text{m}$  on the sample. For wavelength calibration of spectrometer a Hg-Cd spectral lamp was used.

The *reflection spectra* of the composite glass studied in this thesis were measured using a “Carl Zeiss” Axioplan2 imaging microscope coupled with “J&M TIDAS” spectrometer in spectral range of 400-800 nm. By variation of the slit size and geometry in the spectrometer it is possible to measure spectra from the area on the sample with size down to  $10 \times 10\ \mu\text{m}^2$ .

The *luminescence spectra* were measured within the range of 400-780 nm using the same spectrograph coupled with CCD as for detection of position resolved transmission spectra. The photoluminescence of the samples were excited at 266 nm or 400 nm (third and second harmonic wavelength from the Ti:sapphire laser) and focused by system of lenses on the slit of the spectrograph.

been built. Samples were irradiated by laser beam with Gaussian intensity distribution. Using experimental data of the laser beam profile and measurements of the transmission spectra across the modified spot (Fig.2.6) we obtain a dependence of the spectra on the laser intensity.

The spectrometer was formed by a Jobin Yvon imaging spectrograph CP140 coupled with a CCD (TE/CCD-1024-EM/EEV30-11/UV from Roper Scientific). The measurements were performed in visible spectral range 400-800nm, where the quantum efficiency of this CCD varies only by 6% owing to the low temperature of the detector ( $-20^\circ\text{C}$ ) and a UV/AR coating to enhance ultraviolet sensitivity. Modified area on the sample was illuminated by broadband light source and focused on the slit of spectrograph by objective. The position of objective is chose so that the slit size of  $100\ \mu\text{m}$  is much less than the size of the

## 2.4 Relaxation dynamics measurements.

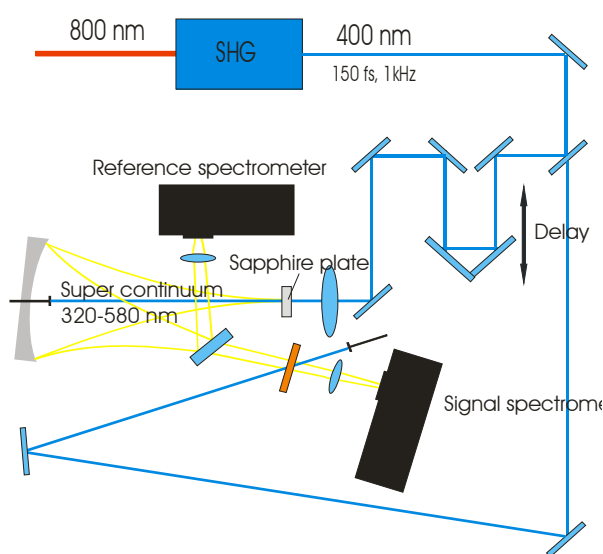


Fig.2.8 Set up for supercontinuum pump-probe experiments.

To study dynamic of the laser assisted modifications in composite glass a series of pump-probe experiments has been performed. The experimental set up is shown on the Fig.2.8. SH radiation at 400 nm with temporal pulse width typically of 150 fs derived from Ti:sapphire laser system was divided in two parts. First one was used as pump. The second part was passed through a fourfold delay line and then focused onto the sapphire plate for supercontinuum generation [2.12] in spectral range between 300 and 600 nm. In turn, achieved broadband radiation was used as a probe pulse. By the help of an appropriate dye solution (DASPI and Coumarin

152 in methanol) as a filter, the initial radiation at 400 nm is suppressed in order to smooth the spectrum of supercontinuum. Finally the supercontinuum is split into two equal parts. One part passes the sample at the sample at the excited spot, the other one serves as a reference. Both parts are then monitored by Si photodiode arrays after identical polychromators providing for each laser shot the complete spectrum of transient changes of the sample's optical density at the chosen delay time. The chirp of supercontinuum is determined by reference measurements on fused silica; the obtained information is then used to correct the data for delay time zero at each frequency position of the obtained transient data [2.13].

Using system of  $\lambda/2$  wave plate at 400 nm and polarizer energy of the pump pulses was changed. In the case of high pulse energy inducing permanent modifications the sample in experiment was moving between each two laser shorts.

## 2.5 Preparation and characterization of glass samples containing Ag nanoparticles.

In this work we studied Ag nanoparticles embedded in soda-lime glass matrix. In turn, samples containing silver clusters were prepared by Ag-Na ion exchange method with following annealing in reduction atmosphere. Modification of ion exchange and reduction conditions (annealing time, temperature and etc.) strongly affects size and distribution of silver nanoparticles in the glass substrate. Transmission Electron Microscopy (TEM) and Scanning Electron Microscopy (SEM) of original and modified samples was performed by Dr. H. Hofmeister (Max-Planck-Institute of Microstructure Physics, Halle) and Mr. F.Syrowotka (IWZ Materialwissenschaft, Halle).

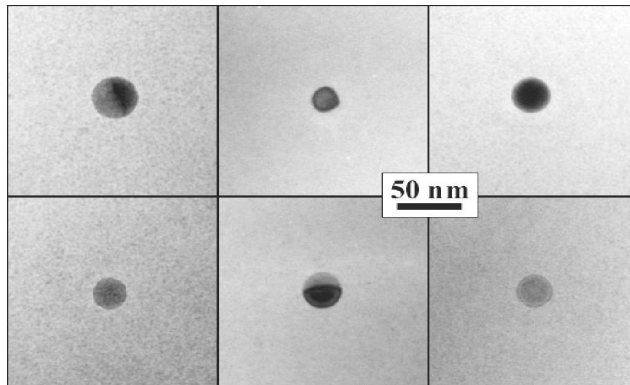


Fig. 2.9 Transmission electron microscopy of Ag nanoparticles in monodisperse glass samples

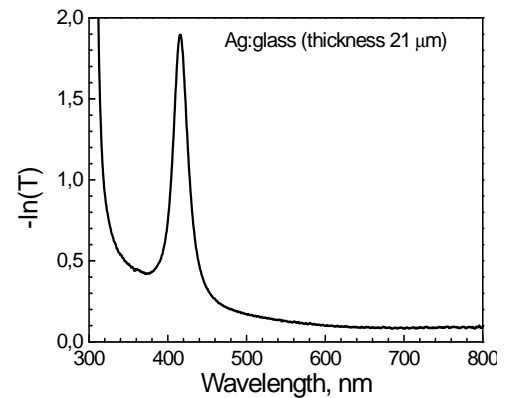


Fig. 2.10 Extinction spectra of monodisperse glass samples with Ag nanoparticles

For sample preparation soda lime glass (72.47 SiO<sub>2</sub>, 14.36 Na<sub>2</sub>O, 0.7 K<sub>2</sub>O, 6.1 CaO, 4.05 MgO, 1.49 Al<sub>2</sub>O<sub>3</sub>, 0.133 Fe<sub>2</sub>O<sub>3</sub>, 0.131 MnO, 0.37 SO<sub>3</sub>, weight %) was used as substrate. For Ag-Na ion exchange a glass plate is placed at 400 °C in a mixed melt of AgNO<sub>3</sub> and KNO<sub>3</sub> [2.14, 2.15]. Moreover, thickness of the glass substrate, time of ion exchange and weight concentration of AgNO<sub>3</sub> in the melt determine the concentration and distribution of Ag<sup>+</sup> ions in the glass sample. Following annealing of ion exchanged glass with high Ag<sup>+</sup> ion concentration in H<sub>2</sub> reduction atmosphere at 400-450°C leads to formation of spherical nanoparticles [2.14]. In experiments we used two different sorts of samples prepared in different ion-exchange conditions: monodisperse and polydisperse.

The *monodisperse* samples were prepared by the group of Dr. K.-J. Berg using ion exchange for a long time yielding homogeneous distribution of silver cations in the glass substrate. Following silver reduction results in formation of nanoparticles with mean diameter about of 30 nm (Fig.2.9) and distributed in the sample with filling factor about of 10<sup>-4</sup>. In turn, the fill factor of silver clusters is defined as a volume of inclusions in unit volume of composite material. An extinction spectrum of silver containing glass sample with thickness of 21 μm demonstrates an absorption band peaked at 413 nm and associated with localised surface oscillation of free electrons in Ag nanoparticles called surface plasmon (SP) (Fig. 2.10). As it can be seen in the spectra, silver nanoparticles demonstrate extremely high extinction cross section about of 1.3x10<sup>-10</sup> cm<sup>2</sup>, which exceeds the geometrical cross section of silver clusters almost in three orders of magnitude.

The *polydisperse* samples were provided for experiments by CODIXX AG prepared as intermediate product for manufacturing of broadband polarizers. The samples were prepared from a float soda-lime glass also using the Ag-Na ion exchange method. The spherical Ag nanoparticles of 30-40 nm mean diameter were distributed in thin surface layers of approximately 6 μm thickness. In particular, the fill factor of Ag nanoparticles near to the surface of some samples prepared by CODIXX AG was up to 0.7 and strongly decreased in the depth, as shown in the Fig. 2.11.

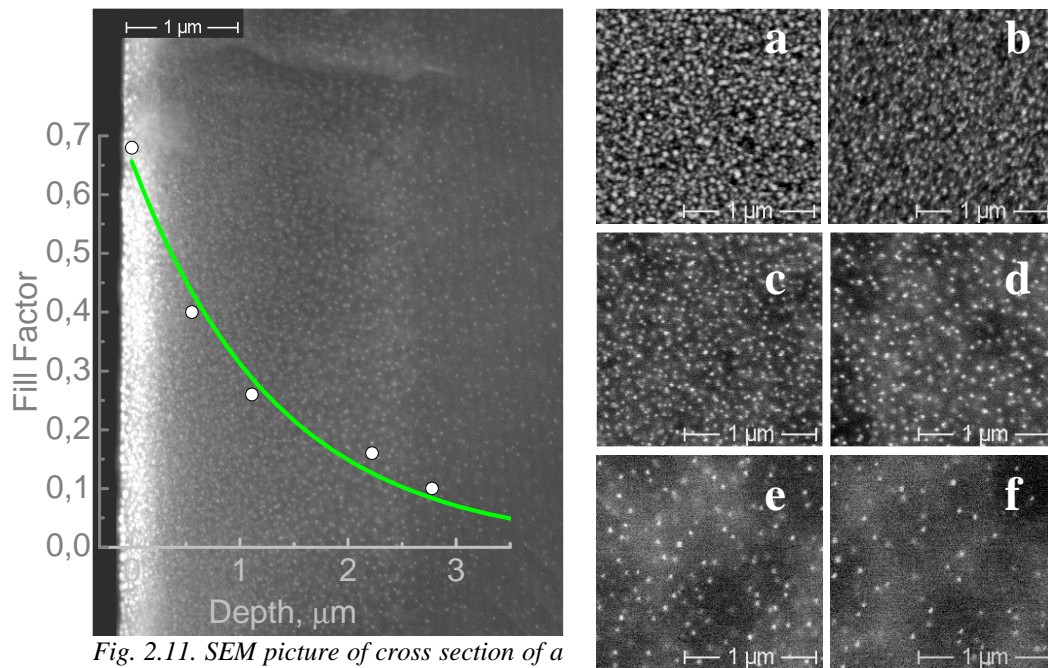


Fig. 2.11. SEM picture of cross section of a polydisperse glass sample with spherical Ag nanoparticles. Fill factor gradient in the depth.

In order to determine the fill factor gradient of Ag nanoparticles in the depth, the samples were etched in 12% HF acid with different detention time. Then thickness, Scanning Electron Microscopy (SEM) and extinction spectra of the samples were measured. For instance, the Fig.2.12 presents SEM images and extinction spectra of the sample used for 3D structuring presented in the Chapter 5. As is clearly seen in the SEM pictures of Fig. 2.12 (increasing etching time from (a) to (f)) and in the graph in the inset of Fig. 2.12

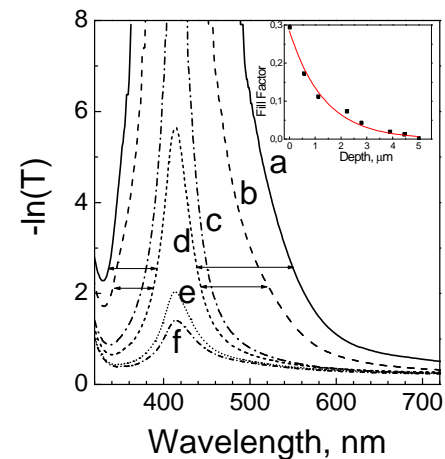


Fig. 2.12. SEM pictures of etched in 12% HF samples with Ag nanoparticles and corresponding extinction spectra (a – the fill factor 0.3; b – 0.25; c – 0.18; d – 0.08; e – 0.02; f–0.006. )

giving the pertinent fill factors estimated, the silver content has its highest value of  $f = 0.29$  directly below the glass surface, and then decreases strongly within a distance of a few microns. In Fig. 2.12 the corresponding extinction spectra are presented, with the same lettering ((a) to (f)) as in SEM images. As can be seen, the original samples show a strong and broad SP band corresponding to the spherical Ag nanoparticles incorporated in the glass matrix with high fill factor up to 0.29. Etching of the sample in HF acid results in fading of the absorption band caused by the decrease of thickness of the silver-containing layer, as well as by the decreasing fill factor of nanoparticles in the sample. Moreover, the extinction spectra indicate that the uppermost metal-rich layer (thickness  $< 1 \mu\text{m}$ ,  $f > 0.15$ ) is responsible for a shift of the red wing of the SP band towards longer wavelengths. This is well compatible with the predictions of Maxwell-Garnett theory (Chapter 1, Section 1.5), which predicts a shift of the peak position of the SP band from  $\approx 410 \text{ nm}$  ( $f \ll 1$ ) to  $\approx 460 \text{ nm}$  for the highest fill factor ( $f \approx 0.3$ ) observed experimentally. However, a

detailed analysis of the original sample's SP band is not possible due to its very large extinction. This observation can only be taken as a first hint to an inhomogeneous broadening caused by the spatial gradient of the silver fill factor in the sample. Moreover, the broadening and shift of the SP resonance towards long wavelength by increasing fill factor of Ag nanoparticles reflects rise of contribution of collective interactions between metal clusters in glass matrix.

Additionally, decrease in the fill factor in the depth of the glass substrate allows us to use the etching technique to prepare samples with low fill factor of silver nanoparticles (SEM on the Fig.2.12), which in turn were used to study photomodification of single nanoparticles presented in the Chapter 3.

## Chapter 3.

# **Photomodification of single Ag nanoparticles embedded in soda-lime glass**

In the last two decades growth of the interest to research on synthesis of composite materials containing metal nanoparticles is motivated by the rise of various potential applications in different fields of science and technology [3.1-3.3]. For instance, linear and nonlinear optical properties of such materials driven by surface plasma (SP) oscillations of the metal clusters offer the metalodielectric composites as promising media for development of novel nonlinear materials, nanodevices and optical elements. The SP resonance is very specific for different metals and strongly depends on size, shape, distribution and concentration of the nanoparticles as well as on the surrounding dielectric matrix. Thus, the laser-based techniques to modify shape and arrangement of the metal clusters [3.4-3.15] are of great interest since they provide a very powerful and flexible tool to control and optimize the linear and nonlinear optical properties of metalodielectric composites. Recently, it was discovered that a permanent transformation of initially spherical metal nanoparticles embedded in soda-lime glass into ellipsoidal (or more general, non-spherical) shapes can be made by irradiation with intense fs laser pulses near to the SP resonance [3.12-3.16]. Moreover, the dichroism in the spectra was strongly connected to the laser polarisation and inversely changed by irradiation in single-short and multi-short regimes [3.14]. However, the mechanism responsible for the anisotropic shape transformations of the spherical Ag nanoparticles seems to be very complicated and still needs detailed investigations.

In this chapter your attention will be focused on study of processes arising by interactions of intense fs laser pulses with single spherical Ag nanoparticles in soda-lime glass. Under “single nanoparticles” we consider a situation, when a volume concentration of silver inclusions is low enough and the collective interactions between nanoparticles can be neglected. The experimental results presented here include studies of intensity dependences of laser induced shape transformations of the silver nanoparticles, effect of the excitation wavelength, writing density and the temperature on the laser induced dichroism, dynamics of the laser induced modifications and luminescence study of modified composite glass. Interaction of intense fs laser pulses with host glass matrix resulting in ionization and colour center formation was also studied in this chapter.

### 3.1 Transformation of the spherical shape of Ag nanoparticles: effect of the laser polarization, pulse intensity and wavelength.

As it was mentioned above, the recent investigations performed by M. Kaempfe et al. [3.12-3.16] demonstrate a dichroism in composite glass with initially spherical Ag nanoparticles induced by irradiation with intense fs laser pulses at wavelengths near to the SP resonance. Moreover, single-shot and multi-shot irradiation resulted in an inversion of the dichroism in extinction spectra. However, fs laser induced modifications of spherical Ag nanoparticles can be effected by various factors such as the laser pulse intensity, number of shots per spot, laser wavelength, temperature as well as size, distribution of silver clusters and glass matrix composition. In this part, we will consider effect of the laser pulse intensity, pulse writing density and excitation wavelength on the laser-induced dichroism in soda-lime glass containing spherical Ag nanoparticles.

For measurements of the intensity dependences we used a technique of space resolved transmission spectra described in details in the Chapter 2. In combination with laser beam profile measurements the space resolved spectra were correlated with local laser pulse intensities (see Chapter 2). Effect of the excitation wavelength on the induced modifications was studied using exposure of the broad fields on the samples described also in the Chapter 2. Irradiation was performed using Ti:sapphire mode-locking laser with regenerative amplification by 150 fs laser pulses in a spectral range of 267-800 nm. Furthermore, it has to be mentioned that the laser pulse intensity used in experiments was much below the damage threshold of soda-lime glass to be about of  $1.5 \times 10^{14} \text{ W/cm}^2$  [3.17-3.18].

#### 3.1.1. The laser induced dichroism: effect of the laser pulse intensity and writing density on the anisotropic shape modifications.

In order to study the intensity dependences of the laser induced modifications in composite glass with spherical Ag nanoparticles the irradiation was carried out by

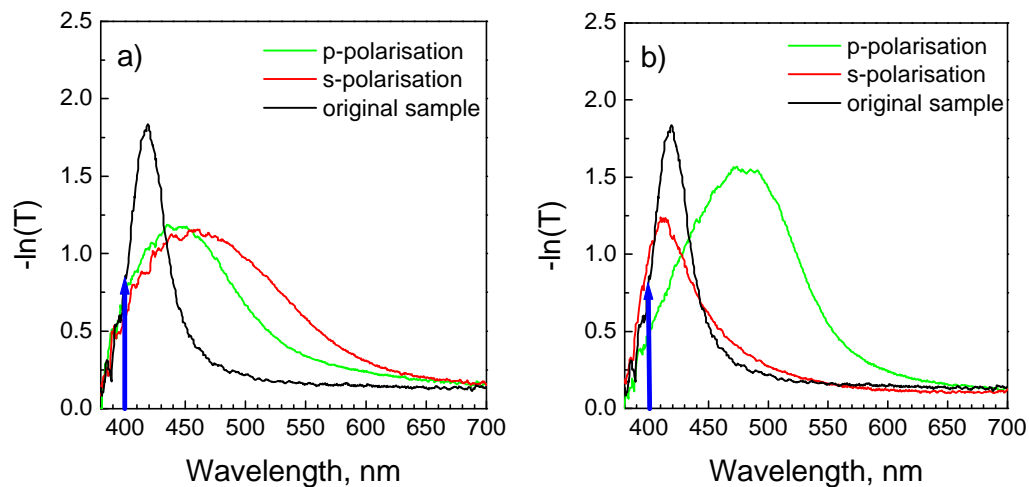


Fig.3.1. Polarised extinction spectra of samples with Ag nanoparticles: original sample and irradiated at 400 nm: a) in single shot regime, peak pulse intensity was  $2.4 \text{ TW/cm}^2$  (peak fluency  $360 \text{ mJ/cm}^2$ ); b) in multi-shot regime (100 pulses in single spot), peak pulse intensity was  $0.42 \text{ TW/cm}^2$  (peak fluency  $63 \text{ mJ/cm}^2$ )

### Chapter 3. Photomodification of single Ag nanoparticles embedded in soda-lime glass

150 fs laser pulses at 400 nm near to the SP resonance in single-shot as well as in the multi-shot mode. As it can be seen in Fig.3.1a, exposure in single-shot mode results in a splitting of the SP band of spherical Ag nanoparticles peaked at 418 nm in two polarization dependent bands slightly shifted toward long wavelengths: at 445 nm for p-polarisation (parallel to the laser polarisation); at 460 nm for s-polarisation (perpendicular to the laser polarisation). However, in order to induce visible dichroism we used the peak pulse intensity as high as  $2.4 \text{ TW/cm}^2$  (spectra measured in the centre of a modified spot on the sample). For the sake of simplicity let us call such type of dichroism as “blue-side dichroism” (p-polarised SP band is shifted in blue side of the spectra relative to the s- polarised one).

At the same time, the multi-shot irradiation (a number of pulses usually  $>100$  per spot) allows us significantly to reduce the laser pulse intensity to observe the anisotropy in the sample. Moreover, in multi-shot irradiation, as it's shown in the Fig.3.1b, the SP band for p-polarisation is shifted towards long wavelengths up to 500 nm while s-polarised SP band is peaked at 400 nm, demonstrating inversion of the dichroism in comparison with the single-shot mode. Such type of dichroism we will call below as “red-side dichroism”.

Observed fs laser induced dichroism in nanocomposite glass with spherical Ag nanoparticles (red-side and blue-side as well) can be explained by anisotropic modifications of the shape of the silver clusters. Moreover, as it was shown in Chapter 1, the spectral gap between SB peaks in p- an s-polarizations is defined by the aspect ratio (length to width) of the prolong metal clusters. In fact, the Transmission Electron Microscopy (TEM) (Fig.3.2) explicitly testifies formation of

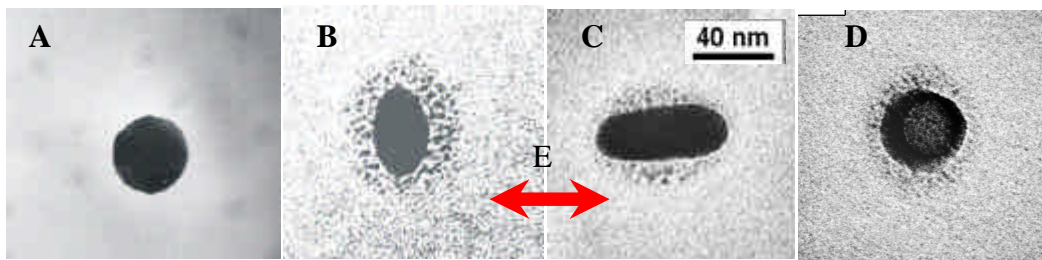


Fig.3.2. Transmission Electron Microscopy of Ag nanoparticles in soda-lime glass: A – original sample with spherical nanoparticles; B – irradiated sample in single pulse mode ( $I \sim 2 \text{ TW/cm}^2$ ); C and D – irradiated sample in multi-shot mode ( $I \sim 0.5 \text{ TW/cm}^2$ ). The laser polarisation shown as arrow is valid for all demonstrated cases.

oblong uniformly oriented Ag nanoparticles in irradiated samples. Moreover, by single shot irradiation Ag nanoparticles have been aligned perpendicular to the laser polarisation (Fig.3.2B), while multi-shot mode resulted in elongation of silver clusters parallel to the electric field vector (Fig.3.2C). At the same time, in the single-shot as well as in the multi-shot irradiation a part of particles, as it can be seen in the fig.3.2D, did not change the form demonstrating only formation of aggregated small metal clusters in the surrounding and define the isotropic contribution in extinction spectra.

An interesting phenomenon of orientation rotation of the silver clusters by single-shot and multi-shot irradiation obviously represents the different polarisation dependent mechanisms resulting in anisotropic shape modifications of spherical Ag nanoparticles. Moreover, as it has already been mentioned, the pulse intensity in single-shot and multi-shot modes differs by factor of 6 and can apparently play a key role in generation of blue-side and red-side dichroism.

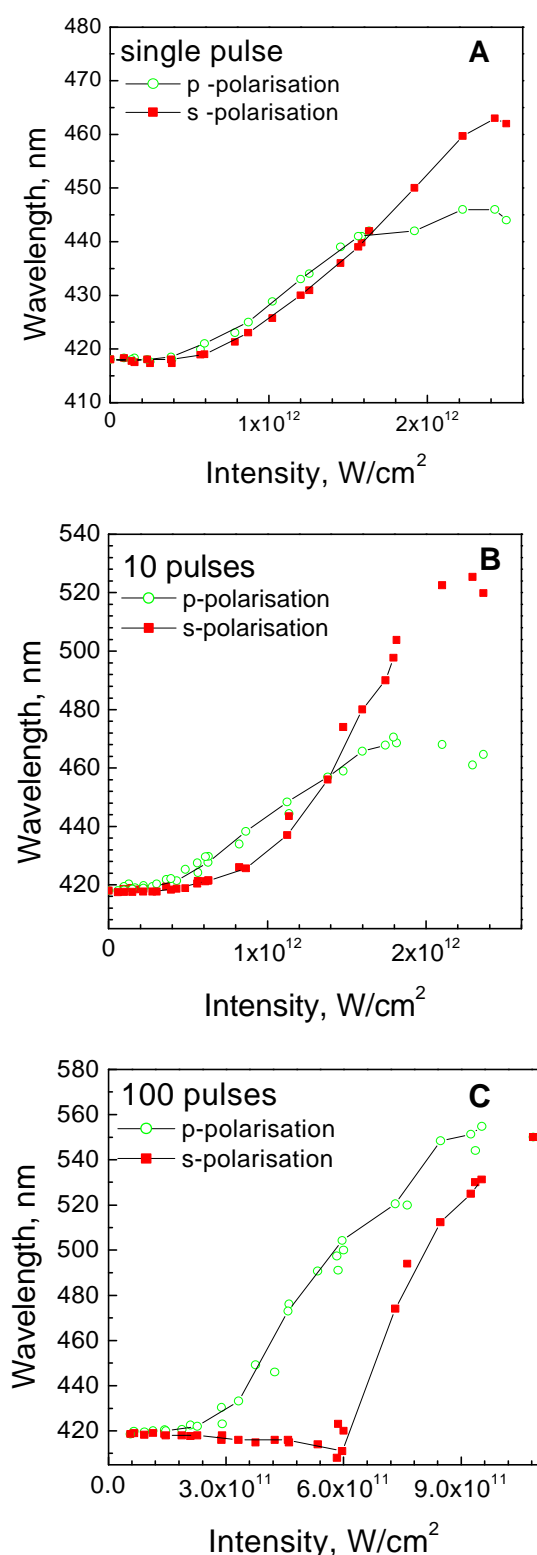


Fig.3.3. Dependence of SP maximum position in polarized extinction spectra of soda-lime glass with spherical Ag nanoparticles on laser pulse intensity by irradiation at 400 nm: A – single-shot irradiation; B – 10 pulses per spot; 100 – pulses per spot.

Indeed, a dependence of the SP maxima in polarised extinction spectra of modified samples on the laser pulse intensity presented in Fig.3.3 completely testifies our assumption. As it can be seen in the fig.3.3A, the laser induced changes in the extinction spectra by single-shot irradiation were detected only by overshoot of the intensity threshold of approximately 0.2 TW/cm<sup>2</sup>. Following increase of the pulse intensity leads to the shift of both p- and s- polarised bands towards long wavelength. Moreover, pulse intensities in the range of ~0.3-1.5 TW/cm<sup>2</sup> induce the weak red-side dichroism observed in multi-shot irradiation: p-polarised SP band is shifted a little bit farther towards long wavelengths relative to the SP peak for s-polarization. Near to the 1.5 TW/cm<sup>2</sup> extinction spectra are isotropic and only higher intensities extinction spectra indicate the blue-side dichroism of the SP resonance. By intensity of about 2.4 TW/cm<sup>2</sup> we reach the maximal spectral gap between p- and s-polarised SP bands peaked at 445 nm and 460 nm, respectively (Fig.3.1a). Following rise of the pulse intensity led to the blue shift of both SP resonances with simultaneous bleaching and broadening of SP bands in the spectra indicating obviously destruction of the silver nanoparticles (Fig.3.4).

The multi-shot irradiation with writing density of 10 pulses per spot doesn't change the intensity dependence of the induced dichroism (Fig.3.3B). As well as in the case of single-shot mode it can be characterised by two intensity ranges leading to the red-side (0.2-1.4 TW/cm<sup>2</sup>) and blue-side (1.4-2.4 TW/cm<sup>2</sup>) dichroism. However, in contrast to the single shot irradiation, increase of the number of laser pulses significantly improves the laser induced dichroism in glass with Ag

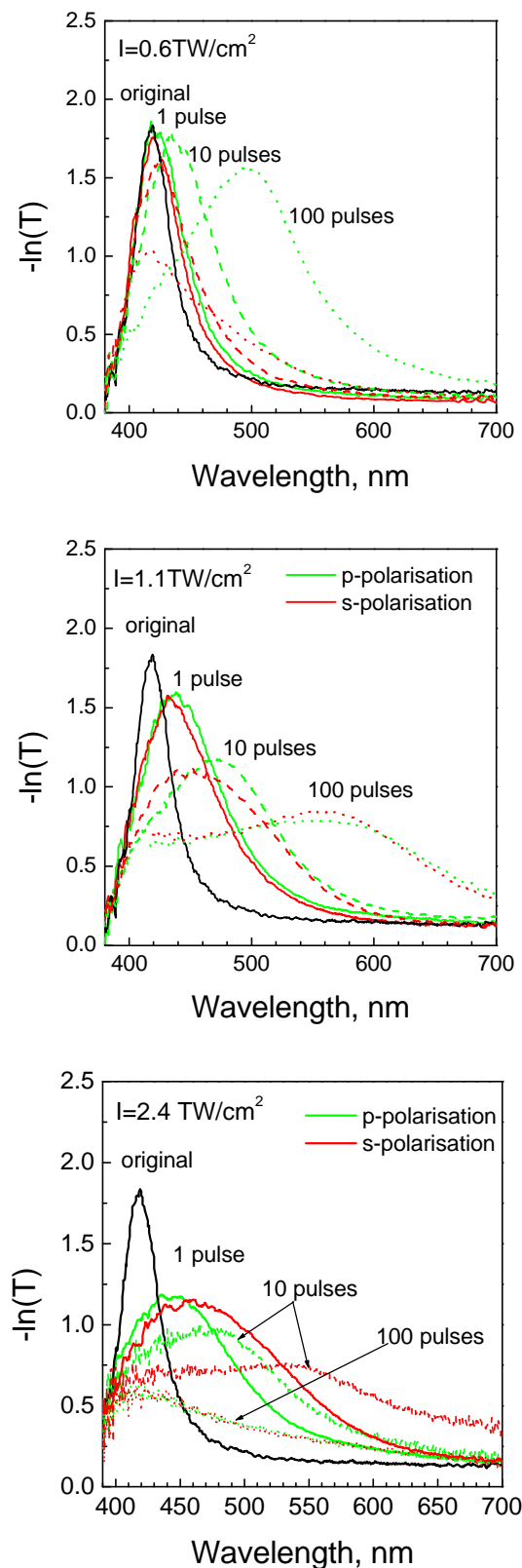


Fig.3.4 Extinction spectra of spherical Ag nanoparticles in soda-lime glass irradiated by 150 fs laser pulses at 400 nm with various peak pulse intensities.

nanoparticles.

Irradiation of the samples with 100 pulses (Fig.3.3C) doesn't indicate any changes in extinction spectra for intensities below of 0.2 TW/cm<sup>2</sup>, which is in the good agreement with single-shot and 10 shots irradiation. However, in contrast to the both previous cases, increase of the pulse intensity leads to a shift of s-polarised SP band in opposite directions relative to the original SP peak at 418 nm, while SP in p-polarisation moves towards long wavelengths. When the laser pulse intensity exceeds 0.6 TW/cm<sup>2</sup>, the s-polarised SP band moves in the red spectral range leading to decrease in dichroic contrast (Fig.3.4).

Furthermore, intensity dependence of the extinction spectra demonstrates destruction of the Ag nanoparticles upon exposure to intense fs laser pulses near to the SP resonance. As it can be seen from Fig.3.4 laser induced dichroism in the composite glass is accompanied by broadening and bleaching of the SP bands in extinction spectra especially for high pulse intensities. The rise of the pulse number accelerates these processes. For instance, by irradiation with intensity of 2.4 TW/cm<sup>2</sup>, increase in shot number (Fig.3.4) results in the total disappearance of the SP peak in extinction spectra indicating destruction of the silver clusters. The broad residual absorption could be associated with the colour centre formation as well as by residual silver species and micro-defects induced in matrix.

Thus, the experimental data testify that the destructive processes are involved in the mechanism of the laser assisted deformation of the Ag nanoparticles. Moreover, **the red-side and blue-side dichroism is defined rather by the laser pulse intensity** indicating different intensity dependent mechanisms leading to the

formation of oblong Ag nanoparticles aligned parallel and perpendicular to the laser polarisation, respectively. The number of shots in such case enhances mostly effect of single shot modifications. It's very important to notice that an intensity range between red-side and blue-side dichroisms results in isotropic changes of the extinction spectra, which could be related to modified nanoparticles with spherical shapes (Fig.3.2D). Thus, using the laser beams with Gaussian intensity distribution could lead to generation of nanoparticles with different types of modified shapes. However, even by top-hat intensity profiles enhancement and localisation of the light intensity in the glass sample could be additionally expected due to nonlinear interactions of laser pulses with intern microdefects and inclusions in the glass resulting in inhomogeneous intensity distribution in excited volume.

The formation of the small silver clusters in the surrounding of the distorted nanoparticle, which can be seen in TEM pictures (Fig.3.2), also testifies the destruction of the silver clusters. Moreover, the red shift of the SP peaks in extinction spectra for the pulse intensities higher as 0.5-0.6 TW/cm<sup>2</sup> could be caused by the dipole-dipole interactions between distorted silver nanoparticle and surrounding metal clusters. In the range of 0.2-0.6TW/cm<sup>2</sup> SP bands of modified samples represent shift in opposite directions relative to the original SP band of spherical nanoparticles peaked at 418 nm. The rise of the pulse number in this case increases first the spectral gap between s- and p-polarised SP bands and then the system reach a steady state without any following spectral alterations. Obviously, under these circumstances induced red shift of the SP resonance for p-polarization far away from the excitation wavelength restricts the excitation of SP and following elongation of the silver clusters.

### 3.1.2 Angular dependences of the laser induced dichroism.

As it has been shown above, the fs laser irradiation of Ag nano-spheres near to the SP resonance induces the elongation of the cluster shape. However, presented transmission electron microscopy does not answer a question, whether fs laser pulses result only in plain shape transformations (elongated disks) or silver nanoparticles have a form of spheroids (ellipsoids). In order to clarify this point, we performed a series of irradiations with incident angle about of 60 deg. Irradiation was carried out

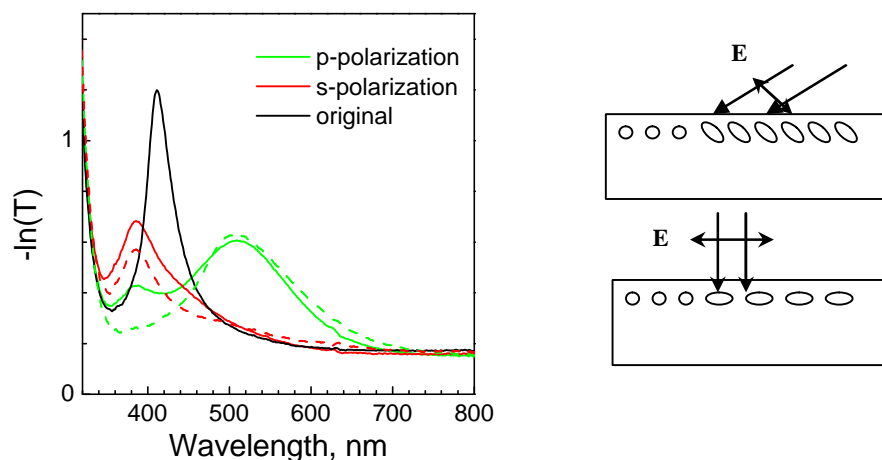


Fig.3.5. Extinction spectra of the glass samples with Ag nanoparticles: black solid line – original sample with spherical nanoparticles; dashed lines - irradiated at 400 nm with 150 fs laser pulses in multi-shot mode at normal incidence; solid lines - under incident angle of 60 deg. Laser polarization is parallel to the incidence plain. Scheme of the irradiation at an angle (top) and perpendicular (bottom) to the surface.

### *Chapter 3. Photomodification of single Ag nanoparticles embedded in soda-lime glass*

at 400 nm in multi-shot mode, peak pulse intensity of  $\sim 0.5 \text{ TW/cm}^2$ , and laser polarization parallel to the plane of incidence. As a result, irradiated samples demonstrated the laser induced dichroism, which was strongly dependent on the angle of observation. For instance, extinction spectra measured in direction perpendicular to the surface of the sample (solid line spectra in Fig.3.5) indicate in s-polarisation a SP band peaked at 380 nm, while two resonances can be seen in the p-polarisation centred at 380 nm and 510 nm. Change of the observation angle leads to the alteration of the extinction spectra. At angle near to the 60 deg (incident angle by irradiation) the extinction spectra are analogous to the case of the irradiation at normal to the surface: p-polarisation demonstrates single SP band at 510 nm (dashed spectra) and SP band in s-polarisation is centred at 380 nm. At the same time, the irradiated sample looks to be isotropic by observation at approximately -30 deg (approximately perpendicular to the direction of the irradiation). Such angular behaviour of the extinction spectra could be explained by formation of elongated silver nanoparticles uniformly oriented at an angle to the surface but parallel to the laser polarisation (Fig.3.5). In this case, the short wavelength maximum in the spectra for p-polarisation can be associated with the third axis of the cluster in direction of the laser beam propagation. Moreover, from the spectral positions of the short wavelength SP bands in s- and p-polarisations (peak at  $\sim 380 \text{ nm}$ ) we can conclude that two small axis are almost equal. In other words, the fs laser pulses cause transformation of the metallic nanospheres in spheroids.

On the other hand, if the laser polarization is perpendicular to the plain of incidence (actually parallel to the surface), extinction spectra don't demonstrate the short wavelength peak in p-polarisation and are similar to the spectra at normal angle irradiation indicating elongation of the nanoparticles along to the surface.

Therefore, we can conclude here that elongation of the Ag nanoparticles is strongly defined by the laser polarization and variation of the laser incident angle allows to produce spheroids with any given orientation in the glass.

#### *3.1.3 Subsequent modifications by multicolour irradiation.*

In this paragraph, we continue the study of the fs laser assisted modifications of Ag nanoparticles in soda lime glass. In particular, we will consider the excitation of silver clusters at different wavelengths affected on the induced dichroism. Foremost, we have to notice that all observed induced anisotropic modifications of Ag nano-spheres described above occurs by excitation of Ag nanoparticles at wavelengths near to the SP resonance. The spectral gap between the SP bands in polarized spectra, which is defined by the aspect ratio of the elongated clusters, can be tuned by variation of the peak pulse intensity and/or by the writing density (number pulses per spot). However, increased pulse intensity besides with the spectral shift leads to the destruction of the silver nanoparticles and bleaching of the SP bands, what actually undesirably decreases contrast of the induced dichroism. At the same time, shift of the SP band away of the laser wavelength upon multi-shot exposure to fs laser pulses with low peak intensity restricts the excitation of silver nanoparticles and the system comes to a steady state, where increasing number of pulses doesn't evoke any alterations in the extinction spectra. The far range spectral shift of the SP band could be apparently achieved by tuning of the laser wavelength towards SP resonance resulting in subsequent modifications of Ag nanoparticles.

In order to testify our assumption a glass sample with spherical Ag nanoparticles was irradiated first at  $\lambda = 400$  nm in multi-shot regime (peak pulse intensity about of  $0.5 \text{ TW/cm}^2$ , writing density about of 3600 pulses per spot). As can be seen from Fig. 3.6 the original plasmon band peaked at 413 nm (solid line) is split into two polarization dependent bands (dashed curves) at 390 nm and 480 nm for s- (perpendicular to the laser polarization) and p - polarization (parallel to laser), respectively. These two bands are attributed to SP resonances along short and long axis of the modified (oblong) silver clusters, which have a preferential orientation parallel to the laser polarization. The same area of the sample was then irradiated at 550 nm with appropriate laser polarization for excitation of SP in the absorption band centered at 480 nm (laser polarization parallel to the long axis of the oblong silver cluster). This leads to a further modification (Fig. 3.6) and additional red-shift of the SP band corresponding to the long axis of the modified nanoparticles (p-polarization) to 630 nm. At the same time, a blue-shift of the absorption peak in s- polarization to 360 nm indicates an increase of the aspect ratio of the ellipsoids. On the other hand, appearance of the second peak at about of 412 nm in p - polarization can be attributed to a quadrupole contribution in the SP resonance. It should be noticed here that irradiation of the modified (ellipsoidal) as well as of the original (spherical) Ag nanoparticles under the same circumstances (peak pulse intensity, writing density) but at wavelengths sufficiently far away from the SP resonance (transparent spectral range) did not evoke any measurable extinction changes.

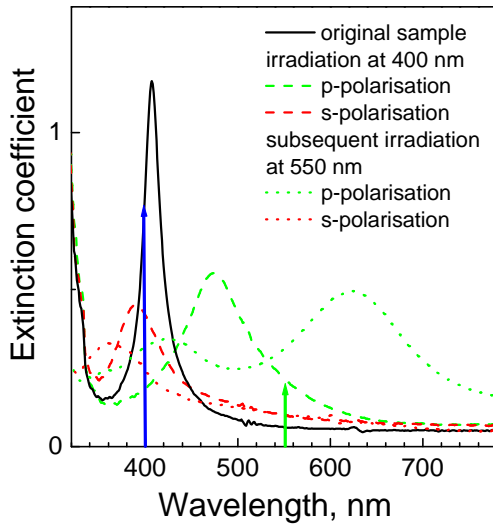


Fig.3.6 Extinction spectra of the glass sample containing single spherical Ag nanoparticles: solid curve - spectrum measured before irradiation; dashed curves - spectra obtained after irradiation by intense fs pulses at 400 nm; dotted curve - spectra after subsequent irradiation at 550 nm. Vertical arrows are indicating pump wavelengths.

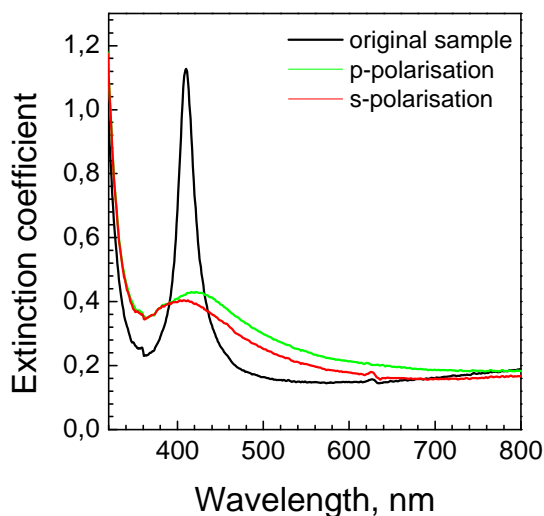


Fig.3.7. Extinction spectra of Ag nanoparticles irradiated by polarised fs laser pulses at 267 nm.

It should be noticed here that irradiation of the modified (ellipsoidal) as well as of the original (spherical) Ag nanoparticles under the same circumstances (peak pulse intensity, writing density) but at wavelengths sufficiently far away from the SP resonance (transparent spectral range) did not evoke any measurable extinction changes.

### 3.1.4 Modifications induced by fs laser pulses at 267 nm (interband effect).

Silver nanoparticles demonstrate an additional absorption band in the UV spectral range with maximum of  $\sim 310$  nm corresponding to the interband transitions of the electrons

### Chapter 3. Photomodification of single Ag nanoparticles embedded in soda-lime glass

(see Chapter 1). Thus, irradiation of composite glass with embedded Ag nanoparticles at 267 nm (the sum frequency of SH (400 nm) and fundamental radiation (800 nm)) with peak pulse intensity of  $\sim 0.33 \text{ TW/cm}^2$  (energy fluency of  $49 \text{ mJ/cm}^2$ ) and writing density of  $\sim 10^4$  shots/spot leads to transformation of the extinction spectra. In turn, as it can be seen in Fig.3.7, the intensity of the SP band decreases by the factor 3 and at the same time demonstrates induced dichroism: p-polarised absorption band shifts towards long wavelengths up to 421 nm, while absorption maximum for s-polarisation moves to 407 nm. Like in the case of excitation near to the SP resonance, such weak dichroism could be associated with Ag nanoparticles elongated in direction parallel to the laser polarisation. On the other hand, bleaching of the SP band in the spectra indicates destruction of the silver clusters upon exposure to UV laser pulses. However, it's still a question, if the observed modifications are caused by excitation of the Ag nanoparticles in interband or fundamental absorption in the soda-lime glass plays here a role.

#### 3.1.5 Femtosecond laser induced dichroism in composite glass with spherical Ag nanoparticles: first summary of the experimental data.

As it was discussed already in Chapter 1, fs laser pulse with moderate pulse energy can have extremely high peak intensity. In other words, electric field amplitude of the electromagnetic wave becomes very high in magnitude. Under these circumstances, exposure of a medium to the laser pulses could result in various nonlinear phenomena and even evoke structural modifications caused by multiphoton and tunnel ionisation. In Chapter 1 it was mentioned that the SP resonance of the metal nanoparticle is responsible for the local field enhancement in vicinity of the cluster, what in turn enhances the nonlinearity of the composite medium.

The experimental data presented above consider shape transformations of the spherical Ag nanoparticles in soda-lime glass upon exposure to fs laser pulses at wavelengths close to the SP resonance. As it was demonstrated, all observed laser induced modifications occur only in the given laser pulse intensity range ( $>0.2 \text{ TW/cm}^2$ ). Moreover, so called “red-side” and “blue-side” dichroism or in other words ***orientation of the modified silver clusters parallel or perpendicular to the laser polarisation is defined by the laser pulse intensity*** used for irradiation of the sample. The writing density (number pulses per spot) results in the accumulation of the induced modifications. However, it's quite obvious that ***by the multi-shot irradiation the laser induced spectral changes are playing a feedback role*** and restrict modification of the cluster shape. For instance, shift of the SP band towards long wavelengths for p-polarisation (red-side dichroism) is obviously limited by decreasing absorption from pulse to pulse at the excitation wavelength. Thus, for the laser pulse intensities less as  $0.6 \text{ TW/cm}^2$  modifications reach a steady state when following rise of the pulse number doesn't indicate some spectral alterations. However, tuning of the laser again towards the SP resonance stimulates subsequent modifications.

Observed anisotropic shape modifications are strongly combined, as it was demonstrated, with the laser polarisation indicating obviously nonlinear interaction of the SP with intense laser electromagnetic fields. In other words, the processes, which define a preferable orientation of the nanoparticles, should occur at time scales about of the laser pulse duration. At the same time, the thermal effects induced by the laser excitation of spherical Ag nanoparticles can only result in isotropic changes. Moreover, the experimentally observed fading of the SP band in extinction spectra

### *Chapter 3. Photomodification of single Ag nanoparticles embedded in soda-lime glass*

---

with increase in peak pulse intensity allows us to suppose that partial destruction or dissolution of Ag nanospheres is involved in the shape modification mechanism.

It's well known, that interaction of metal nanoparticles with intense laser pulses close to the SP resonance leads to the enhancement of the photoelectron emission from the cluster surface [3.19-3.29]. Even excitation of composite glass with Ag nanoparticles by ns laser pulses near to the SP causes a destruction of metal clusters accompanied by enhanced photocurrent [3.19] indicating a photovoltaic effect. Thus, it rather plausible to assume that interaction of intense fs laser pulses with silver inclusions in soda-lime glass results in SP assisted ionisation of metal clusters leading to the shape deformation and dissolution of the Ag nanoparticles. Moreover, by excitation of the SP with intense fs laser pulses the photoelectrons driven by the field on the surface of the metal nanoparticle, i.e. the superposition of the external field and induced polarisation, could assign the preferential direction for the modifications.

The laser pulse intensity of about  $0.2 \text{ TW/cm}^2$  (the threshold of the laser assisted modifications in the composite glass with Ag nanoparticles) could result in the photoionization of the silver clusters as well as glass matrix caused by multiphoton absorption. Moreover, such intensity corresponds to the electric field amplitude of electromagnetic wave to be in order of  $6.1 \times 10^6 \text{ V/cm}$ . Taking in to account the fact that excitation of Ag nanoparticles was performed near to the SP resonance, the enhancement of the local field in several orders of magnitude in comparison with incident wave makes the tunnel ionization probable.

On the other hand, it's quite obvious that the oblong shape of the Ag nanoparticle is fixed by surrounding solid matrix. Heating of the sample exposed by fs laser up to  $600 \text{ }^\circ\text{C}$  corresponding to the transition temperature in soda-lime glass causes a restoration of spherical shape of the modified Ag nanoparticles [3.14]. This allows us to assume that the fs laser assisted modification occurs under temperatures below of transition point. Otherwise, if the laser pulses result in the melting of the surrounding glass, keeping of the anisotropic shape by Ag nanoparticle is improbable.

Furthermore, the intense laser radiation can cause also the ionization of the glass matrix leading to structural transformations in it. Moreover, as it will be shown after, the soda-lime glass exposed to the fs laser pulses reveals an induced dichroism in visible spectral range caused by colour center formation. This can affect the electric permittivity of the glass and influence on the SP resonance of the incorporated metal clusters.

### **3.2 Modification of soda-lime glass by 150 fs laser pulses at 400 nm. Colour centres in the glass.**

It is known that the laser intensities of about  $10^{12}$  W/cm<sup>2</sup> lead to spectral changes in the transparent soda-lime glass caused by formation of color centers [3.30-3.32]. Moreover, generation of the color centers is characterised by the dielectric constant changes and can affect the position of the SP resonance in the extinction spectra of the composite glass. At the same time, ionization of the glass matrix and color centers formation can be involved in the processes of the shape modification of Ag nanoparticles.

Color center formation has been known since the XIX century and was extensively studied by exposure to  $\gamma$ -rays, UV radiation [3.33] as well as to intense laser pulses [3.30-3.32]. Whereas optical damage in glass is characterised by the formation of plasma and irreversible structural dislocations, the color centers formation takes a form of uniform slight discoloration of the medium through which the beam has been passed. The internal defects in the glass matrix or crystal (vacancies, interstitial ions and impurity ions of wrong valence) are characterised by an effective charge, which is able to attract and bind electrons and positive holes, which have been released in the matrix by exposure. Most of the electrons quickly recombine with the holes, that is, the electrons fall back into the stripped ions and reconstitute the normal ions. If before the recombination a free electron wanders near an interstitial cation or an anion vacancy, this positively charged defect can trap the electron in its Coulomb field. The positive holes that escape early annihilation also wander through the glass and are trapped at negatively charged defects, such as cation vacancies or interstitial anions. Moreover, trapped electrons or holes do not annihilate the charge of the defect but are only overlapping the surrounding of the vacancies or ions to an appreciable extent. Such trapped-electron or trapped-hole centers can be destroyed by warming the sample or by illuminating it with light of the appropriate wavelength. However, trapping of electrons by metal cations in the matrix leads to the reduction processes [3.35] and can bring even to a precipitation of metal colloids [3.32-3.34]. In such case, coloration in visible spectral range is determined by the SP band of metal clusters. In contrast with trapped electron and hole centers, which were discussed above, colloids mostly don't demonstrate a thermally induced bleaching in extinction spectra.

It should be mentioned that the concentration of the defects playing the role of trapping centers, strongly depends on composition of the glass. Thus, in the single component glass such as SiO<sub>2</sub> the substitution in the glass "random network" of Al<sup>3+</sup> for Si<sup>4+</sup> results in the creation of O<sup>-2</sup> vacancies or the simultaneous incorporation of aluminium cation interstitially playing a role of electron trapping centers. Formed charge imbalance in the matrix can be partially compensated by non-bridging oxygen contained in alkali silicate glasses in sufficient amounts. The non-bridging oxygen atoms together with cation vacancies are responsible for formation of hole-trapping centers in soda-lime glass [3.36].

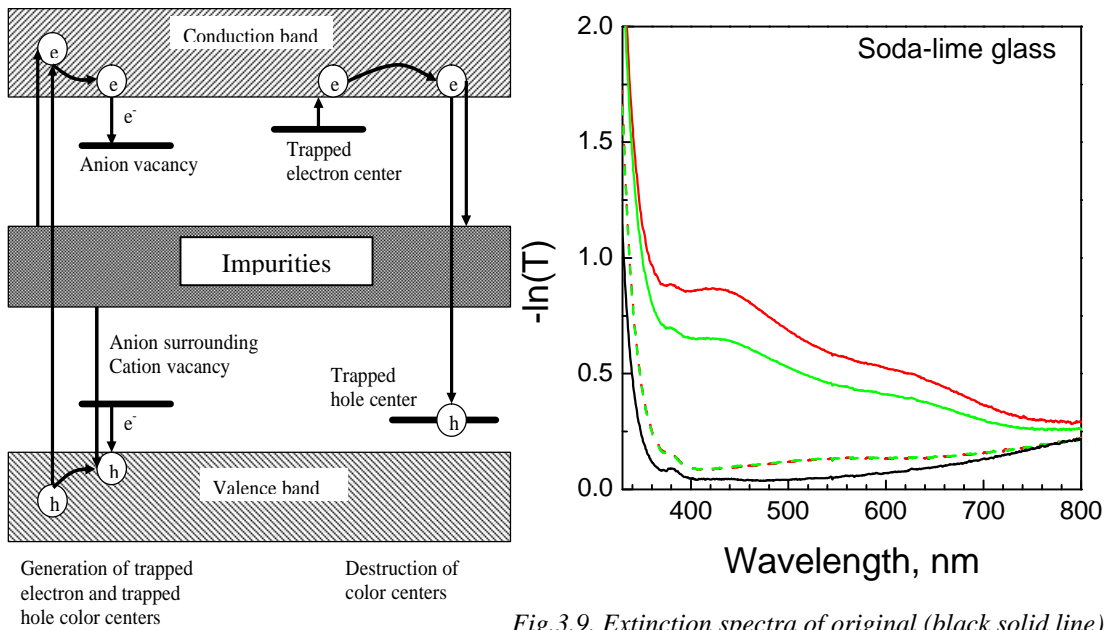


Fig.3.8. Schematic representation of the color center formation and destruction

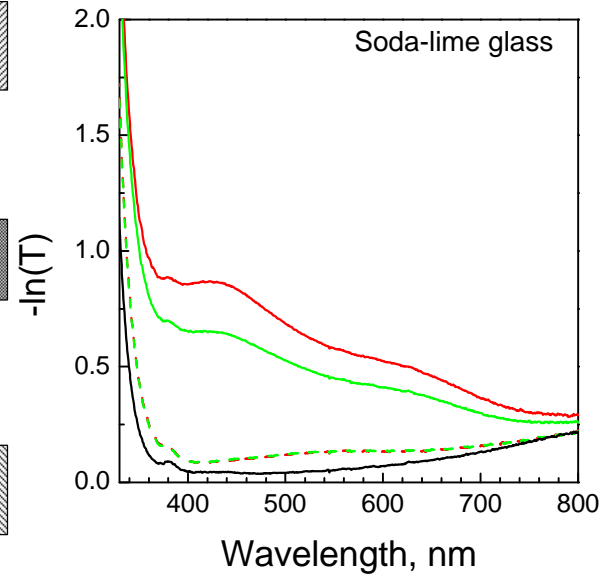


Fig.3.9. Extinction spectra of original (black solid line) soda-lime glass, irradiated at 400 nm: s-polarisation (red solid line) and p-polarisation (green solid line), heated at 150 °C for 3h glass (dash line).

Thus, formation of color centers requires a generation of mobile charge carriers in the glass via the photoinduced excitation of electrons from the valence band of silicate glass to the levels situated above the electron mobility threshold (Fig.3.8). For alkali-silicate glasses this threshold is placed in the region of the fundamental absorption edge ( $E_i \sim 5.4\text{eV}$ ) formed by transitions between levels in quasimolecular complexes  $\text{Si-O}\cdots\text{Na}^+$  (L-centers). Nonbridging oxygen defects  $\equiv\text{Si-O}^-$  in silica are responsible for 4.8 eV absorption [3.36]. Hence, exposure of glasses to radiation with photon energy less than intrinsic absorption edge cannot cause photoionization of glass matrix. However, irradiation with high power laser pulses with  $h\nu < E_i$  causes the multiphoton ionization of the glass matrix and formation of color centers [3.30-3.32]. On the other hand, sensitivity of the glasses can be significantly enhanced by impurities incorporated in the glass (like  $\text{Ce}^{3+}$ ,  $\text{Fe}^{2+}$ ,  $\text{Tb}^{3+}$ ,  $\text{Eu}^{3+}$  and so on), which form intermediate electron energy levels in the band gap of the glass matrix. Hence, ionization of impurities in the photosensitive glasses requires lower photon energies to induce electron transitions from intermediate energy levels in conduction band. In turn, the metal inclusions with Fermi energy level placed between valence and conduction bands can play a role of donor of electrons.

In our experiments, the original glass substrate (72.47  $\text{SiO}_2$ , 14.36  $\text{Na}_2\text{O}$ , 0.7  $\text{K}_2\text{O}$ , 6.1  $\text{CaO}$ , 4.05  $\text{MgO}$ , 1.49  $\text{Al}_2\text{O}_3$ , 0.133  $\text{Fe}_2\text{O}_3$ , 0.131  $\text{MnO}$ , 0.37  $\text{SO}_3$ , weight %) used for Na-Ag ion-exchange and Ag nanoparticles preparation was irradiated by 150 fs laser pulses at 400 nm with peak pulse intensity about of  $2.4\text{ TW/cm}^2$ . Irradiation was performed in multi-shot mode with writing pulse density of approximately  $4 \times 10^3$  pulses per spot. As it can be seen in the Fig 3.9, the original glass sample is absolutely transparent in visible spectral range and demonstrates a wing of absorption band centred in NIR about of 1100 nm and attributed to impurities of  $\text{Fe}^{2+}$  [3.34]. The irradiation with fs laser pulses leads to coloration of glass in whole exposed volume characterised by a strong rise of the absorption in UV and visible spectral range (Fig.3.9). The extinction spectra of exposed glass

Chapter 3. Photomodification of single Ag nanoparticles embedded in soda-lime glass

demonstrate two broad absorption bands centred at 430 nm and 640 nm corresponding to the trapped hole color centers ( $H_2$  and  $H_4$ ) [3.31-3.35]. The broad spectra in visible region as well as the absorption in UV can be associated with contribution of other types of trapped electron and hole centers presented in the Table 3.1.

**Table 3.1 Spectroscopic parameters of the absorption bands of intrinsic Color Centers in Soda Lime Glass (according to Ref. 3.34)**

Peak Position, eV	Peak Position, nm	Halfwidth, eV	Charge State	Designation
0.9	1380	0.4	+	$H_1$
1.6	770	0.7	-	$E_1$
2.0	620	0.5	+	$H_2$
2.1	580	0.8	-	$E_2$
2.4	517	0.45	+	$H_3$
2.85	435	1.1	+	$H_4$
3.2	388	0.45	-	$E_3$
3.7	335	0.8	-	$E_4$
4.1	302	0.9	+	$H_5$
4.75	261	0.9	+	$H_6$
5.2	238	1.05	-	$E_5$
5.8	214	0.8	+	$H_7$

Moreover, extinction spectra reveal an induced dichroism in the glass sample after irradiation by fs laser pulses indicating higher absorption in s-polarisation in contrast to the p-polarised spectra. This can be explained by anisotropic optical bleaching of  $H_4$  centers associated with laser polarisation dependent reorientation of those centers demonstrated by Glebov et al. [3.37]. However, Glebov and co-workers demonstrated effect of polarised laser irradiation at 435 nm on color centers induced by UV light. In our case, irradiation of glass samples at 400 nm by 150 fs laser pulses results in formation of color centers via multiphoton absorption. The following interaction of the fs laser pulses with  $H_4$  hole trapped centers owing to the absorption peak at  $\sim 420$  nm causes the bleaching and reorientation of them.

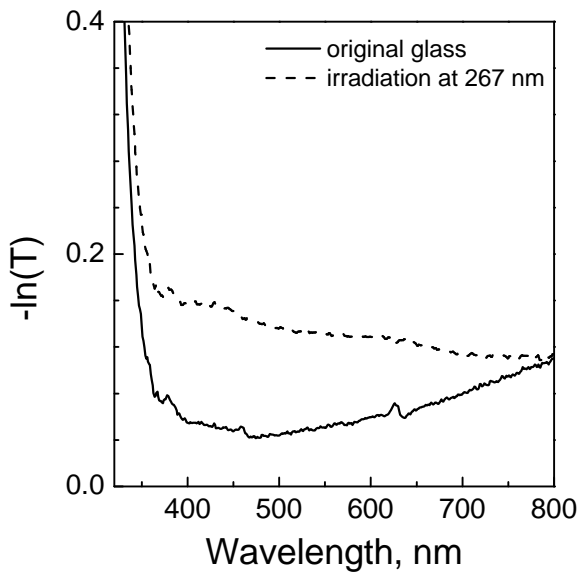


Fig.3.10 Extinction spectra of soda-lime glass before and after irradiation by 150 fs laser pulses at 267 nm

The spectral modifications in the glass induced by exposure at 400 nm are stable at room temperature retaining coloration unchangeable up to several years. However, thermal development of the irradiated glass at 150°C for 3 hours leads to the fading of the induced absorption (Fig.3.9) indicating recombination of color centers.

Similar spectral modifications were observed by irradiation of glass at 267 nm (Fig.3.10). However, in comparison with excitation at 400 nm penetration depth of the laser at 267 nm is much lower due to strong absorption in glass and

### *Chapter 3. Photomodification of single Ag nanoparticles embedded in soda-lime glass*

---

formation of color centers, which occurs only in the thin surface region. In the spectra two absorption peaks at 420 nm and 620 nm attributed to the hole trapped centers can be still resolved but their contribution in the spectra is much lower in comparison with the 400 nm excitation. This indicates apparently decrease of the proportion of the hole and electron trapped centers, which for example could be explained by contribution of  $\text{Fe}^{2+}$  (absorption peaks at 4.4eV and 5.1eV) to generation of free electrons by excitation at 267 nm (4.7eV) [3.32, 3.35, 3.38, 3.39]. It's well known that electron trapped centers are not stable at room temperature and the coloration in the glass induced at 267 nm disappeared in couple of days, while absorption bands formed by exposure to 400 nm were relative stable at 20 °C and bleaching was activated at 150 °C. Moreover, irradiation at 267 nm doesn't demonstrate the anisotropic modifications of the soda-lime glass, which support the assumption of the polarisation dependent bleaching of the hole trapped centers by exposure to 400 nm.

In summary, the irradiation of the soda-lime glass with 150 fs laser pulses at 400 nm, below the fundamental absorption edge, results in multiphoton ionization of glass matrix and in the formation of trapped electron and hole color centers indicating induced absorption in UV and visible spectral range. Moreover, observed laser polarisation dependent dichroism in modified glass was associated with anisotropic bleaching and reorientation of the hole trapped centers  $\text{H}_4$ . Trapped color centers are not stable to the heating and temperature treatment at 150 °C for 3h results in discoloration of the exposed region. Thus, obtained data indicate that the laser pulse intensities typical for Ag nanoparticle modifications at 400 nm also leads to the structural anisotropic transformations in the host matrix. In turn, effect of color centers formation on the extinction spectra of modified samples containing Ag nanoparticle can appear in two ways. First, induced absorption spectra of color centers in composite glass add to the absorption of silver clusters. Second, the color centers situated near to the surface of Ag nanoparticle increases the polarizability of the surrounding and will affect the surface plasma oscillations via dipole-dipole interactions as well as via influence of static effective charge redistribution shifting the SP peaks toward long wavelengths. Moreover, taking into account that the irradiation of Ag nanoparticles embedded in the glass was carried out near to the SP resonance, the enhancement of the local electromagnetic field can result in acceleration of the ionisation of the matrix near to the surface of metal cluster leading to formation of color centers, defects and even high ionised plasma (if the magnitude of the field is high enough) in the surrounding.

### 3.3 Effect of the temperature on the laser induced modifications of Ag nanoparticles.

As it was shown in section 3.1, excitation of spherical Ag nanoparticles in soda-lime glass at SP resonance by intense fs laser pulses results in polarisation dependent shape elongations. However, the mechanism of this laser induced deformation has not yet been elucidated in detail. A crucial question in this context is the possible ionization of the nanoparticles by intense femtosecond laser pulses. Moreover, as it was demonstrated in the Section 3.2, fs laser pulses at 400 nm with intensities exceeding the threshold of the laser induced modifications of the composite glass can stimulate the multiphoton ionization in the host glass matrix. This results in generation of trapped electron and hole color centers responsible for the induced absorption and dichroism in visible spectral range. Thus, the processes of color center formation could also be involved in the mechanisms of shape transformation of Ag nanoparticles. In turn, the color centers evoke modification of dielectric properties of the surrounding of the silver clusters and could affect on the surface plasma oscillations. Moreover, since the color centers are not stable by increase of the temperature, the temperature treatment of the exposed sample could reveal information according the laser assisted electron photoemission from Ag nanoparticles. On the other hand, the cluster ionization should lead to increase of silver ions content in the glass.

Since silver ions in glass as well as structural changes in the glass matrix can be identified by their characteristic photoluminescence, we have performed a series of luminescence measurements, combined with thermal treatment, of several samples: neat glass (i), ion-exchanged glass (ii), glass containing silver nanoparticles before (iii) and after (iv) laser induced deformation. The study is completed by extinction spectra demonstrating the effect of annealing on the latter type of samples. In the following it will be shown that the luminescence data provide interesting new information on the role of Ag nanoparticle ionization in the process of their laser induced shape modification.

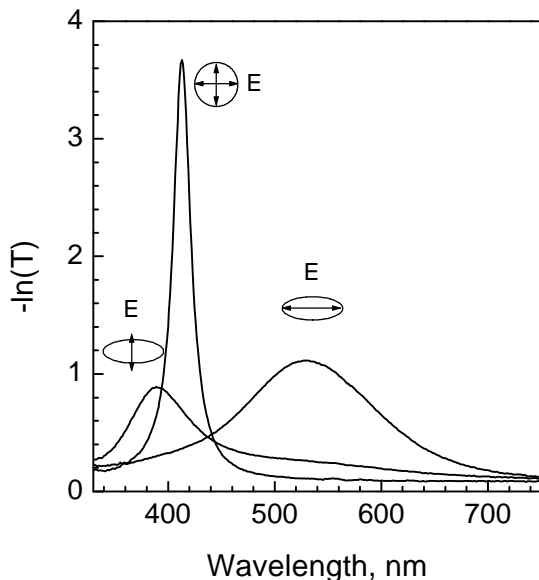


Fig.3.11. Extinction spectra of original (spherical) and oblong (after irradiation by intense fs pulses at 400 nm) Ag nanoparticles in soda-lime glass.

#### 3.3.1 SP bands modification by temperature treatment

The glass samples with spherical Ag nanoparticles used in the experiment were irradiated by 150 fs laser pulses at 400 nm in multi-shot mode. The peak pulse intensity was  $\sim 0.5\text{TW}/\text{cm}^2$ . Using X-Y translational stage a homogeneous field with size of  $3\times 3\text{ mm}^2$  was written with pulse density of  $\sim 4\times 10^4$  shots/ $\text{mm}^2$ .

Under these conditions the effect of the laser irradiation on the extinction spectra, as shown in the Fig.3.11, is a splitting of the original plasmon band at 413 nm in two polarization dependent bands centered at 390 nm and 540 nm for s- (perpendicular to the laser polarization) and p-polarization (parallel to the laser polarization), respectively. As it was discussed in the Section 3.1, these two bands can be attributed to the SP resonances of the modified (oblong) silver clusters.

After irradiation, samples were heated in oven at 100°C, 200°C and 400°C and it was observed that the extinction bands due to the surface plasmon resonances of the elongated Ag nanoparticles are modified during temperature treatment (Fig.3.12). Upper, center and lower panel refer to 100°C, 200°C and 400°C, and the different curves (as specified in the legend of Fig. 3.12) represent the spectra measured before and after 5, 15, 45, 60, and 120 min of annealing. Common to all temperatures is a continuous reduction of the band width with simultaneous blue shift of both p- and s-polarization bands, accompanied by an increase of the

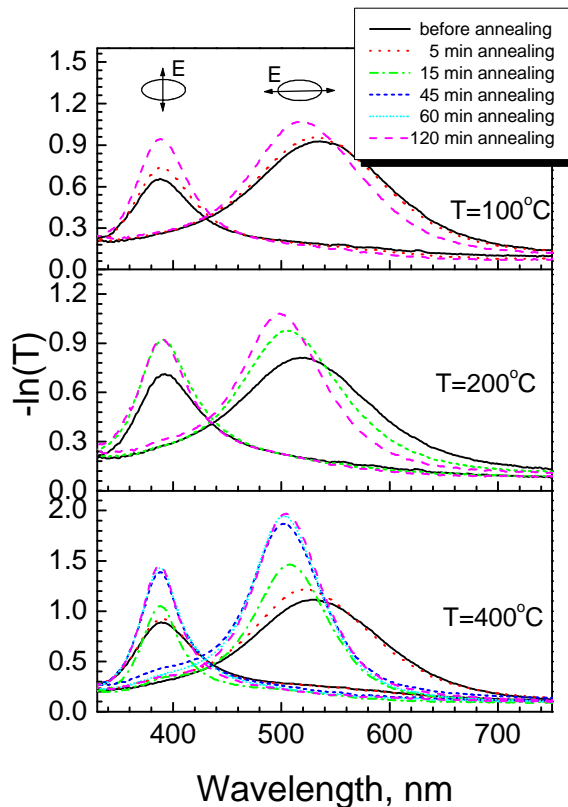


Fig.3.12. Extinction spectra of samples with Ag nanoparticles after irradiation by intense fs pulses at 400 nm, and thermal treatment (as specified in the figure).

maximum absorption strength. As it can be seen, the changes occur much faster at higher temperatures, so that, e.g., at 400°C no more modifications are observed after 45 min. In contrast to these findings, extinction spectra of non-irradiated samples with spherical Ag nanoparticles do not change at all during thermal handling.

Observed changes in the extinction spectra of the irradiated composite glass induced by temperatures much below the glass transition temperature to be about of 600 °C and silver melting point exclude the reshaping of the metal nanoparticles observed by M. Kaempfe [3.14] and can be interpreted in terms of modifications of the silver nanoparticle surrounding. Moreover, acceleration of the modification processes at temperature about of 100 °C allows us to assume a contribution of the trapped color centers, which are not resistant to the heating.

### 3.3.2. Luminescence study of the temperature induced modifications

The luminescence studies of the irradiated samples could help us in understanding of origins for the temperature induced modifications in the surrounding matrix and clarify the processes caused by interaction of Ag nanoparticles with ultrashort laser pulses.

### Chapter 3. Photomodification of single Ag nanoparticles embedded in soda-lime glass

The first examples for luminescence spectra, as given in Fig.3.13, refer to the original glass (dash-dotted curve), ion-exchanged samples before annealing (dashed and solid curves), and an annealed, but not irradiated sample containing spherical silver nanoparticles (dotted curve); the excitation wavelength in all cases was 266 nm.  $\text{Ag}^+$  ions in soda-lime glass are known to show upon UV-excitation a green-yellow luminescence due to the spin-forbidden electronic transition from the  $^3\text{D}$  manifold to the ground state  $^1\text{S}_0$  [3.40,3.41]. Corresponding to this expectation the ion-exchanged sample 1 shows under excitation at 266 nm a luminescence band peaked at 540 nm (solid curve).

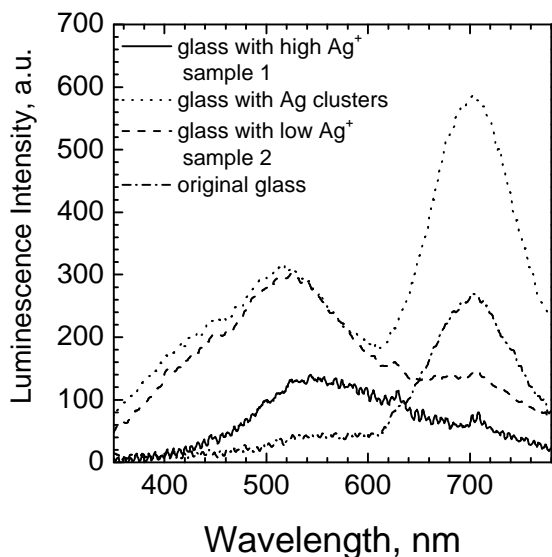


Fig.3.13. Luminescence spectra (excitation wavelength 266 nm) of  $\text{Ag}^+$ :glass samples 1 and 2 (see text for details), original glass and glass with Ag nanoparticles.

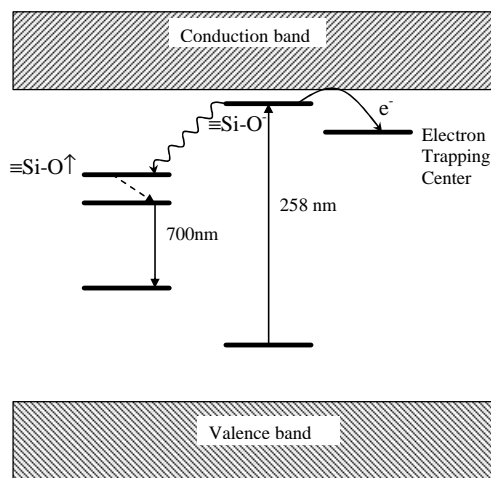


Fig.3.14 Energy band diagram of the non-bridging oxygen centers in the soda lime glass.

Therefore, the shoulder observed near to 430 nm in the emission spectra can be explained by silver ions with lower concentration in the depth of the glass substrate [3.41].

The second, stronger emission band obtained from the sample containing spherical silver nanoparticles (peaked at 700 nm), was detected also from original clear glass (dash-dotted line). This band could be associated with nonbridging oxygen defects in the glass, which were studied in details in Ref. [3.42]. As it was mentioned in the Section 3.2, nonbridging oxygen anions  $\equiv\text{Si-O}^-$  are assigned as the cause of the 4.8 eV absorption and playing a key role in formation of hole trapped centers. Thus, illumination of soda-lime glass at 267 nm results in excitation of nonbridging oxygen anion and following electron transition from excited state on the energy levels of neighbouring electron trapping centers (Fig.3.14). Formed trapped

hole centers are in excited state and following transition in ground state energy level is accompanied by luminescence at 700 nm. However, electron and hole trapped centers are not stable and the system rapidly comes in the initial state. It is important to notice that the concentration of nonbridging oxygen centers is strongly dependent on impurities in the glass matrix [3.33]. It is rather plausible to assume that during the ion exchange process (which is connected with heating) most of these defects are 'healed', while reduction of the silver ions and aggregation to Ag nanoparticles may create new defects, in particular in the vicinity of nanoparticles. This scenario would explain the behaviour of the emission band at 700 nm.

When the sample containing silver particles is irradiated by intense 400 nm

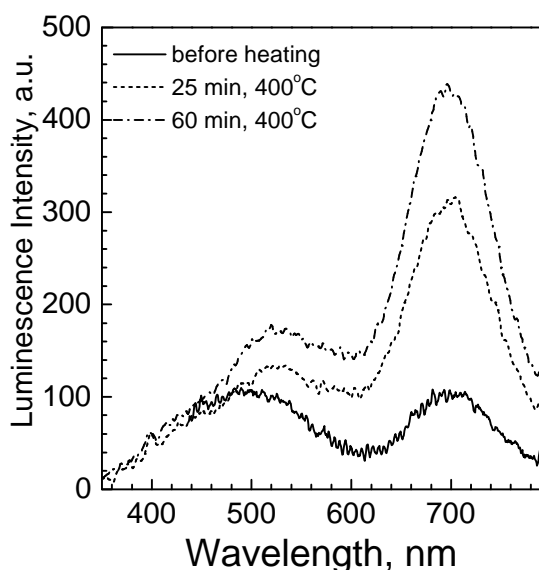


Fig.3.15. Luminescence spectra (excitation wavelength 266 nm) of samples with Ag nanoparticles irradiated by intense fs laser pulses, before and after heating.

laser pulses in the above described way to modify the clusters, the luminescence observed upon excitation at 266 nm changes to the shape shown in Fig.3.15 as solid curve; compared to the emission spectrum before 'destructive' irradiation (dotted curve in Fig.3.13), mainly the intensity of the band around 700 nm is decreased. Thermal treatment of the sample (1 hour at 400°C) again increases the intensity of this luminescence band at 700 nm, which can be explained by modifications of the glass matrix. At the same time, the band attributed to the silver ions does not show significant spectral changes. So the experiments at 266 nm excitation wavelength

alone can not prove the ionization of silver clusters during laser induced shape modifications.

We have performed additional luminescence experiments with an excitation wavelength of 400 nm, where the photon energy is too low to excite photoluminescence of  $\text{Ag}^+$  ions, but sufficient to observe luminescence around 600 nm due to very small charged clusters like  $\text{Ag}_2^+$ ,  $\text{Ag}_2^{2+}$ ,  $\text{Ag}_3^+$  and  $\text{Ag}_3^{2+}$  [3.40]. **No noticeable luminescence intensity was observed from clear glass and samples containing silver nanoparticles, even if they have been irradiated by the intense pulses for deformation. Also heating of samples with spherical nanoparticles does not evoke the luminescence upon 400 nm excitation.**

However, in case of previously irradiated samples the situation changes dramatically under thermal treatment: the Fig.3.16 shows the evolution of the luminescence spectra obtained from such a sample at 3 different temperatures (upper panel: 100°C; center panel: 200°C; lower panel: 400°C). The individual spectra are labeled with small letters (a) to (e) referring to 5, 15, 45, 60 and 120 minutes of annealing at the given temperature.

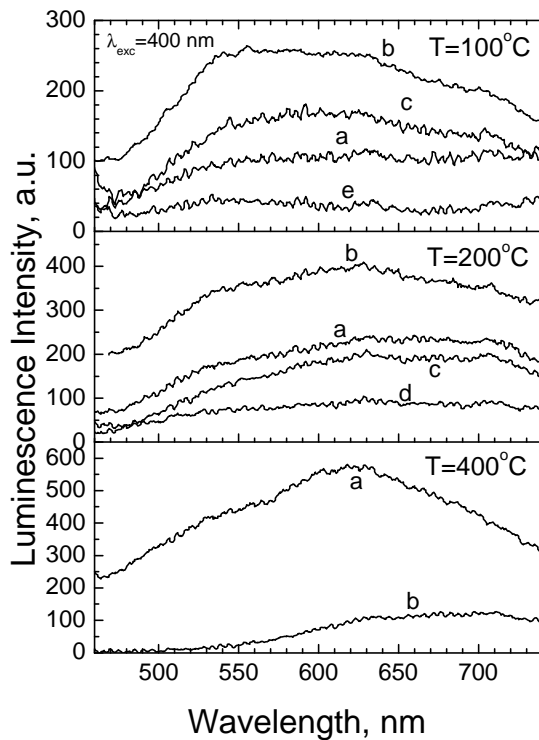


Fig.3.16. Luminescence spectra (excitation wavelength 400 nm) of irradiated samples with Ag nanoparticles, annealed at 100 °C (upper panel), 200 °C (center panel), 400 °C (lower panel) for 5 min (a), 15 min (b), 45 min (c), 60 min (d), 120 min (e).

of 400 nm. As plotted in Fig.3.17, this sample with high Ag doping concentration yields a very similar strong luminescence band at 600 nm indicating the presence of the  $\text{Ag}_2^+$ ,  $\text{Ag}_2^{2+}$ ,  $\text{Ag}_3^+$  and  $\text{Ag}_3^{2+}$  species [3.40]. It is an obvious conclusion that the orange luminescence from irradiated samples containing deformed nanoparticles originates from those small silver ion complexes, which are being formed during

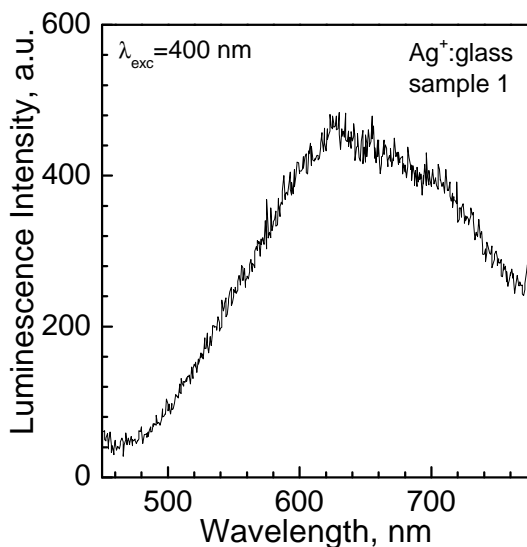


Fig.3.17. Luminescence spectra (excitation wavelength 400 nm) of  $\text{Ag}^+$ :glass (sample 1).

At all temperatures a broad emission band around 600 nm develops during heating, but on quite different time scales: at 100°C the intensity of luminescence rises for the first 15 min, then decreases again until it has vanished after 2 hours; with increasing time, the maximum of this luminescence band shifts from 540 nm to longer wavelengths. At 200°C the increase and following fading of the luminescence happens more rapidly and the equilibrium is achieved after 60 min; finally, at 400°C the emission reaches its maximum intensity within 5 min, and already after 15 min no measurable luminescence around 600 nm was detected any more. In addition, Fig.3.16 clearly shows that the maximum luminescence intensity is higher at higher temperatures. It is interesting to compare these spectra with one obtained from glass after Na-Ag ion exchange (sample 1), again with an excitation wavelength

of 400 nm. The position of the emission band of small silver clusters ( $\text{Ag}_2$ – $\text{Ag}_8$ ) depends strongly on their size and ionization state [3.43]. The emission band maximum is shifted to the red spectral range when the number of atoms in a cluster increases. Thus, the observed shape modifications of the emission band at 600 nm in the spectra of irradiated samples could be explained by inhomogeneous spectral broadening due to a wide distribution of silver species in size and charge ( $\text{Ag}_n^{k+}$ ,  $n = 2, 3, \dots$ ;  $k = 1, 2, \dots$ ).

3.3.3. Effect of the temperature on the laser assisted modifications.

In the previous section, we demonstrated that the temperature treatment of the irradiated samples by fs laser pulses stimulates the spectral changes caused by structural modifications in the composite glass with silver nanoparticles. Obtained results raise a question how the temperature will effect on the irradiation procedure and laser induced modification of spherical Ag clusters. To answer this question the laser exposure of the glass samples with embedded Ag nanoparticles was performed

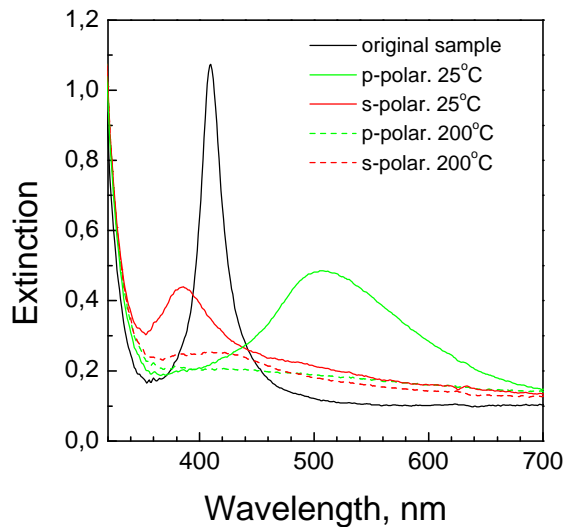


Fig.3.18. Extinction spectra of soda-lime glass with Ag nanoparticles irradiated at 400 nm at room temperature (25°C) and heated up to 200°C.

at different temperatures. Irradiation by 150 fs laser pulses at 400 nm was carried out in multi-shot mode using the same technique and parameters as for the samples studied in the section 3.3.1. However, the peak pulse intensity here was about of 0.4 TW/cm<sup>2</sup>.

As it can be seen in the fig.3.18, laser excitation at room temperature leads to the similar results reported above: SP band peaked at 413 nm splits in two polarisation dependent bands with maxima at 380 nm and at 510 nm for s- and p-polarisation, respectively. On the other hand, preheating of the sample up to 200 °C and following irradiation under the same circumstances did not

demonstrate the induced dichroism in extinction spectra and led to an absolute bleaching of the original SP band, which in turn could be explained by total destruction of the silver clusters in the heated glass upon fs laser irradiation.

3.3.4. Interpretation and discussion of the temperature assisted effects.

The results presented above give evidence that Ag<sup>+</sup> ions are produced in the glass matrix in the course of laser induced deformation of silver nanoparticles: the occurrence of a strong luminescence band around  $\lambda = 600$  nm under excitation at 400 nm, which was only observed for irradiated samples (containing oblong Ag nanoparticles), clearly indicates the formation of the mentioned small silver ion species Ag<sub>2</sub><sup>+</sup>, Ag<sub>3</sub><sup>+</sup> etc.; as those can not be created from Ag clusters purely thermally, they are obviously due to clustering and partial reduction of previously produced Ag<sup>+</sup> ions. It is quite reasonable that these ions are produced during the laser induced ‘destruction’ of nanoparticles, since enhanced photoelectron emission has been observed upon excitation of Ag nanoparticles by fs laser pulses near the SP resonance [3.19-3.29]. In the course of this ionization the positively charged core of ionized clusters will no longer be stable, and due to the Coulomb forces Ag ions will leave the clusters and form a local positive charge near to the surface of a particle. However, in our experiments using an excitation wavelength of 266 nm for

luminescence there was no unambiguous proof for an increase of concentration of free silver ions after high-intensity irradiation (compare Fig.3.14). The most plausible explanation for this problem is the fact that the emitted silver ions remain in the immediate vicinity of the silver clusters, producing a rather high local concentration of  $\text{Ag}^+$ -ions; for such a situation strong luminescence quenching was observed [3.41]. In addition, the non-irradiated samples containing Ag nanoparticles still show a relatively intense emission at 520 nm due to the residual free silver ions in the sample, which is present after annealing in reduction atmosphere (where the formation of silver species is limited and emission at 600 nm was not detected [3.44]) and formation of silver clusters, but also after laser irradiation and repeated annealing (Fig.3.14). So it is reasonable that silver ions produced during irradiation close to the silver particles do not cause remarkable changes of the  $\text{Ag}^+$ -ion luminescence band centered at 520 nm (under excitation at 266 nm).

Putting the above arguments together, it is obvious that the broadband luminescence observed after heat treatment around 600 nm (excitation at 400 nm) must be attributed to small silver ion species (like  $\text{Ag}_2^+$ ,  $\text{Ag}_3^+$ ,  $\text{Ag}_3^{2+}$ ), which are produced from silver ions created near to the Ag nanoparticles during laser induced ionization and Coulomb explosion. This conclusion is supported by the fact that luminescence at 600 nm was not detected in original samples with spherical nanoparticles subjected to heating. At this point it should be mentioned that color centers, which appear in the original transparent soda-lime glass by intense laser irradiation at 400 nm, as it was discussed above, disappear completely after annealing at 150 °C for 120 min. Apparently, heating initiates the dissociation of the electron trapping centers in glass and reduction of silver ions, and the consecutive formation of the small charged Ag clusters. This fact and the relatively low activation temperature of 100°C for modification processes allows us to suppose an influence of the trapped electron color centers on formation of silver ion species. When the annealing temperature is increased up to 200°C and 400°C, the dissociation of color centers is accelerated, and the evolution of the observed luminescence spectra reflects the formation and ripening of charged silver ion aggregates. Fading of luminescence with time is a result, apparently, of growth of the small ionized silver clusters playing the role of nucleation centers for silver colloids [3.40] and finally of their coalescence with the original silver particles (Ostwald ripening).

This interpretation is confirmed by the effects of the heating on the extinction spectra of irradiated samples with Ag nanoparticles, i.e., narrowing and blue-shift of the SP bands (Fig. 3.12), which are obviously caused by modifications in the surroundings of silver particles: after irradiation by intense laser pulses causing particle deformation, there will be silver ions near to the remaining particles, and photoelectrons caught by trapping centers in the glass matrix. While the silver ions in the vicinity of Ag particles may affect their plasma oscillation via a DC electric field, the photoelectrons caught in trapping centers in the glass could change the polarizability of the cluster surroundings and thus the effective dielectric constant of the matrix. Both effects will contribute to broadening and red-shift of the surface plasmon bands, where the broadening may also be due to the inhomogeneous distribution of local environments. Apparently, the effect of heating then is the dissociation of the electron trapping centers and reduction of silver ions, followed by aggregation of small ionic silver clusters. Finally, these silver ion species will diffuse back to the remainder of the original (disrupted) nanoparticle and reaggregate with it, probably forming larger species before their final coalescence. The latter can be concluded comparing the temporal evolution of both extinction spectra (Fig. 3.12)

### Chapter 3. Photomodification of single Ag nanoparticles embedded in soda-lime glass

and luminescence at 600 nm (Fig. 3.16) under temperature treatment: as long as the luminescence is rising, the extinction bands show only very weak changes; the more significant changes, in particular the increase of extinction strength, are observed when the luminescence is already decreasing or even practically vanished. This is most evident at the higher temperatures (200°C and 400°C); in the latter case no more spectral changes are observed after 45 minutes indicating that the surroundings of the Ag nanoparticles is in an equilibrated state already. For the lower temperatures the extinction spectra after 2 hours of heating differ from that one obtained at 400°C, and – in full agreement with the expectation for thermally activated processes – appear not to have reached their equilibrium situation yet.

Furthermore, fs laser induced ionization of the Ag nanoparticles is obviously responsible for the bleaching of the SP band observed by irradiation of the glass samples heated up to 200 °C. The fact is that an increase of the glass temperature stimulates high diffusion mobility of the silver cations. Thus, the silver cations ejected by the positive charged core are diffusing in the glass out from the Ag nanoparticle preventing the formation of the positive charged shell of the silver cations around the silver clusters and resulting in dissolution of them. This indicates that the local increase of the silver cation concentration in vicinity to the cluster surface are protecting the nanoparticles from total dissolution and are involved obviously in the processes of the shape modifications. Indeed, following reduction of the silver cations by emitted electrons in direction parallel to the laser polarisation and precipitation of the species in vicinity to the cluster core could result in the elongation of the Ag nanospheres.

As a prove of proposed mechanism of temperature induced alteration of extinction spectra a series of TEM images of irradiated samples before and after annealing at 300 °C for approximately 3 hours were recorded and presented in the Fig.3.19. As it was demonstrated above in the Section 3.1 and shown in the Fig.3.19A,D, irradiation of the samples by fs laser pulses near to the SP resonance leads to the formation of oblong as well as nearly spherical silver nanoparticles with surrounding small clusters. Here we have to point out that the aggregation of the small metal species could be caused by inescapable temperature increase due to

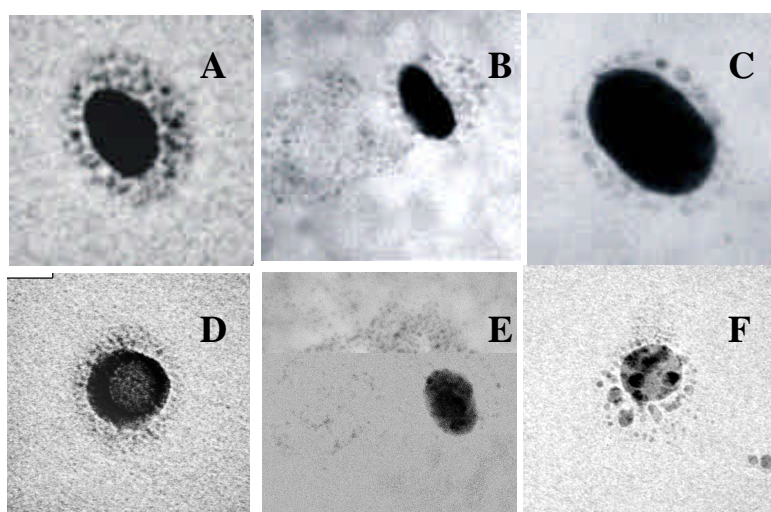


Fig.3.19. Transmission Electron Microscopy of Ag nanoparticles in soda-lime glass: A,D – irradiated at 400 nm by 150 fs laser pulses; B, C,E and F – irradiated samples subjected to the temperature treatment at 250 °C for 3h.

### *Chapter 3. Photomodification of single Ag nanoparticles embedded in soda-lime glass*

---

action of mechanical polishing and exposure to ion-beam during preparation of the samples over a long time for the TEM studies. As it was shown above, irradiated samples are very sensitive to the increase of the temperature and demonstrate changes in extinction spectra even at 100°C. Nevertheless, after temperature treatment irradiated samples are evidently (Fig.3.19 B,C,E,D) indicating modifications of the surrounding of distorted Ag nanoparticle: concentration of small silver clusters drastically decreases accompanied by their ripening; a little bit far away from modified nanoparticle aggregation of small silver cluster were detected, which can form an anisotropic shape. The formation of the aggregates in the long ranges over the nanoparticle is indicating obviously generation and diffusion of silver cations during exposure to fs laser in glass matrix away from the hot metal cluster, which, in turn, reduced and agglomerated in silver species by following temperature treatment. According to the observed anisotropy of the species distribution around of modified elongated nanoparticle it's rather plausible to assume that photoemission of electrons in the direction of laser polarization leads to a partial reduction of the silver cations and re-aggregation of silver atoms with disrupted silver cluster resulting in anisotropic distribution of the silver ions around of nanosphere. Thus, these high mobility active silver cations are diffusing without any obstacle in other direction. However, we have to notice, that the last assumption has to be proven carefully by the additional experiments. Nevertheless, these observations in general confirm the interpretation of spectral studies given above.

As a summary, by studying luminescence spectra, novel information has been obtained about the role of silver ions in the process of the fs laser pulse induced permanent deformation of spherical Ag nanoparticles in soda-lime glass to oblong ones. Samples with Ag nanoparticles show, after irradiation and only moderate temperature treatment at 100°C, a strong broad band luminescence (excitation wavelength 400 nm) centered at 600 nm, which can be attributed to small silver complexes  $\text{Ag}_2^+$ ,  $\text{Ag}_3^+$ ,  $\text{Ag}_3^{2+}$ . Additionally, temperature induced modifications of extinction spectra in the region of the SP bands indicate changes of the nanocluster environment by aggregation of the mentioned silver ion species. The fact that temperature treatment of original samples (containing spherical Ag nanoparticles, without irradiation) has no influence on the extinction spectra and also doesn't evoke the luminescence upon 400 nm excitation, allows us to conclude that small silver ion complexes are formed from  $\text{Ag}^+$  ions being created during fs laser irradiation by way of ionization and Coulomb explosion of silver nanoparticles. Actually, the increase of the local  $\text{Ag}^+$  ion concentration near to the cluster, followed by reduction and cluster precipitation could play a key role in the processes of the fs laser induced modification of the shapes of Ag nanoparticles in soda-lime glass. Increase of the temperature of the sample during the laser irradiation leads to the total dissolution of the Ag nanoparticles in soda-lime glass, what in turn supports the proposed model.

### 3.4 Dynamic of the laser induced modifications of Ag nanoparticles in soda-lime glass.

The ultrafast dynamics of SP resonance excitation by ultrashort laser pulses has been studied extensively in the last years, in particular in the low intensity regime, where any spectral changes are completely reversible [3.45-3.50]. On the other hand, as it was shown above, fs laser pulse with intensities higher as  $10^{11} \text{W/cm}^2$  reveal irreversible processes like cluster ionization and glass matrix structural modifications. Furthermore, these processes could play a significant role in transformations of the shape of silver nanospheres, which are responsible for induced dichroism of the SP bands in the extinction spectra. A first series of time-resolved single-color pump-probe experiments demonstrated a comparably slow relaxation process on a time scale of several 100 ps accompanying the deformation of Ag nanoparticle embedded in soda-lime glass by laser intensities about of  $16.7 \text{ TW/cm}^2$  (energy fluency of  $2.5 \text{ J/cm}^2$ ) in single shot mode [3.51]. However, laser pulses with peak intensity about of  $2.4 \text{ TW/cm}^2$  reveal the ionization of the original soda lime glass and formation of the color centers resulting in darkening of the glass. It raises the question, whether ionization and formation of trapped centers can create a directional preference for material transport, which is necessary for the deformational process, but can only happen on clearly slower time scales.

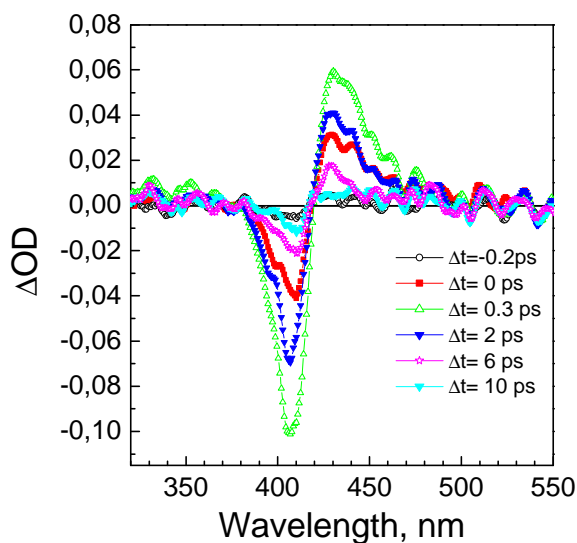


Fig. 3.20 Transient differential absorption spectra obtained on the glass sample containing spherical Ag nanoparticles at different delay times; Excitation peak pulse intensity about of  $2.6 \times 10^9 \text{ W/cm}^2$  (energy fluence  $0.4 \text{ mJ/cm}^2$ )

The first series of time-resolved single-color pump-probe experiments demonstrated a comparably slow relaxation process on a time scale of several 100 ps accompanying the deformation of Ag nanoparticle embedded in soda-lime glass by laser intensities about of  $16.7 \text{ TW/cm}^2$  (energy fluency of  $2.5 \text{ J/cm}^2$ ) in single shot mode [3.51]. However, laser pulses with peak intensity about of  $2.4 \text{ TW/cm}^2$  reveal the ionization of the original soda lime glass and formation of the color centers resulting in darkening of the glass. It raises the question, whether ionization and formation of trapped centers can create a directional preference for material transport, which is necessary for the deformational process, but can only happen on clearly slower time scales.

For the detailed discussion of the time evolution it is more instructive to look at time-resolved data at some characteristic wavelengths.

Here we present results of time-resolved pump-probe experiment with 150 fs pump pulses at 400 nm and supercontinuum probe pulses giving important information about the possible source of the directional memory of the samples.

The first experiments were performed with low pulse intensities much below to the permanent modification threshold to be about of  $0.2 \text{ TW/cm}^2$  (see Section 3.1). The fig. 3.20 shows some characteristic differential transient spectra measured on a sample with 50  $\mu\text{m}$  thickness containing Ag nanoparticles, which indicate two regions of induced absorption (300-380 nm and 420-550 nm), and a region of bleaching between these two. In general, the three regions seem to evolve quite similarly as a function of time showing a fast rise and a slower decay on a time scale of several picoseconds.

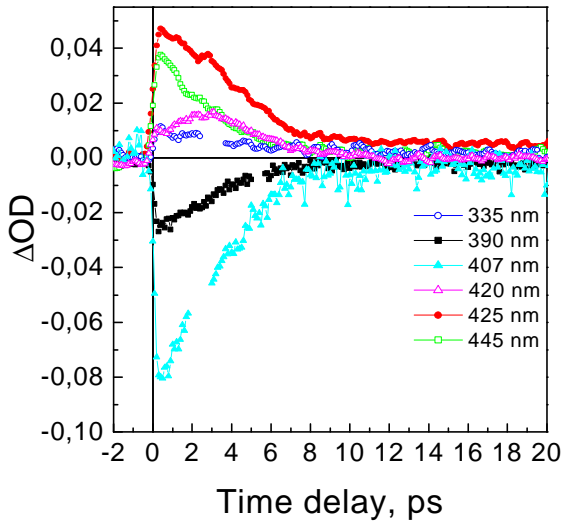


Fig. 3.21 Time dependence of the optical density changes in absorption spectra of glass containing Ag nanoparticles at different wavelengths. Excitation peak pulse intensity about of  $2.6 \times 10^9 \text{ W/cm}^2$  (energy fluence  $0.4 \text{ mJ/cm}^2$ ).

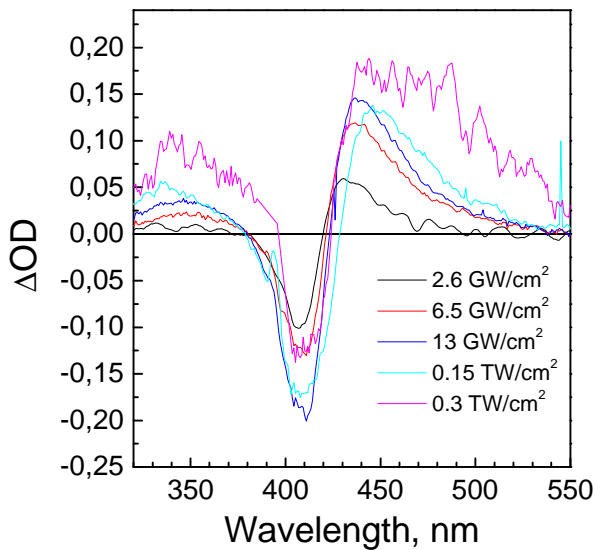


Fig.3.22 Transient differential absorption spectra obtained on the glass sample containing spherical Ag nanoparticles for different excitation pulse intensities. Delay time was 0.3ps

transitions due to the hot electron system, as has been observed previously [3.53].

Increase of the intensity of the pump pulse slightly modifies the differential absorption spectra (Fig. 3.22) indicating the rise of the optical density in the UV spectral region and simultaneous broadening and red shift of the growing absorption band in the other side of the SP resonance. At the first sight, such behaviour of the differential absorption spectra could be associated with strong heating of the electron

As can be seen in the Fig. 3.20 and 3.21, at all wavelengths the signal rises for the first 0.3 ps. This is in general compatible with previous findings [3.52-3.54] in the weak perturbation regime, where the main changes around the SP resonance can be assigned to the non-instantaneous establishment of an electron temperature after excitation, i.e., the signal rise is determined by the thermalization time of the electron gas due to electron-electron, electron-surface and electron-phonon scattering. As the thermalization of this initially athermal electron distribution happens within a few hundreds femtoseconds for the amount of energy injected in our experiments, it's easily understood that the signal rise more or less follows the integral over the pump-probe correlation. Following relaxation of the induced spectral changes with characteristic decay time about of 3.2 ps is associated obviously with transfer of electron energy to the lattice and later to the glass matrix. The transient spectra in the low perturbation regime can be described simply as a broadening and slight red-shift of the SP band caused by perturbation of metal complex dielectric constant. Our data are very similar to this behaviour at wavelength  $>380 \text{ nm}$ , but exhibit an additional induced absorption at shorter wavelengths, which could be explained by an overall increase of the interband

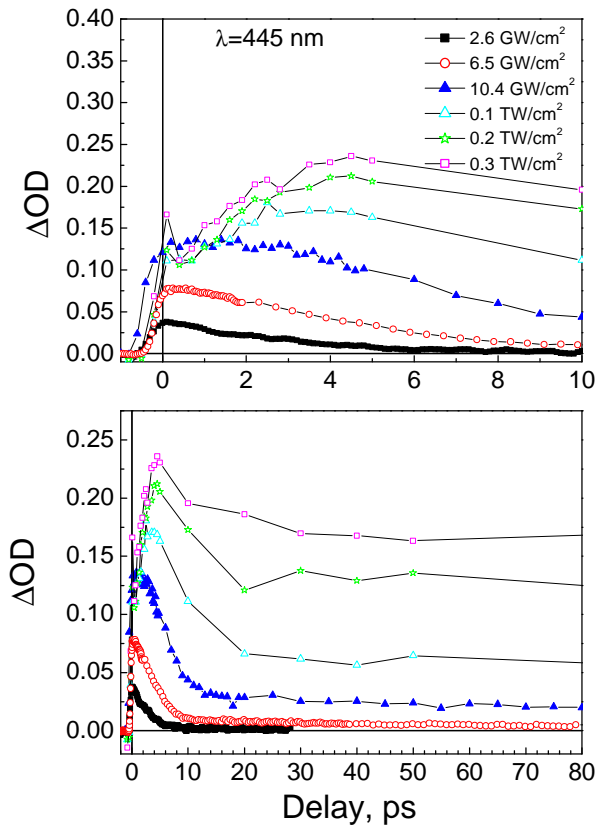


Fig.3.23 Time dependence of the optical density changes in absorption spectra of glass containing Ag nanoparticles at 445 nm for different pump pulse intensities.

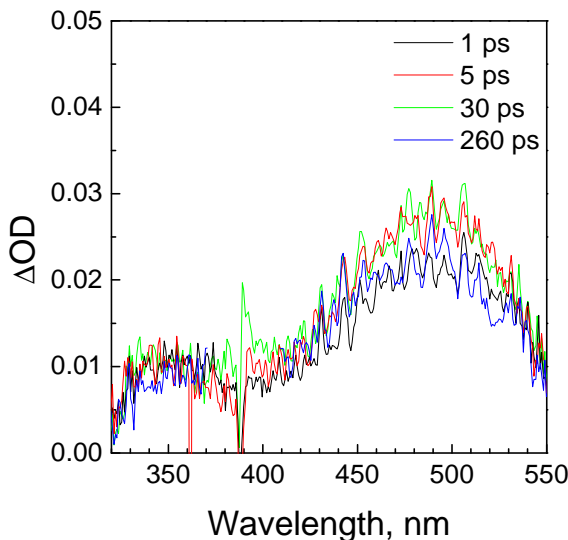


Fig.3.24 Differentiation absorption spectra of the soda-lime glass for different time delays between pump and probe pulses.

gas induced by pulses with high energies. However, relaxation dynamic of the silver nanoparticles by excitation with the intense pump pulses (Fig.3.23) reveals an appearance of the additional long time relaxation component with decay time up to  $\sim 1 \mu\text{s}$ . Moreover, increase of the pump pulse intensity up to  $0.3 \text{ TW}/\text{cm}^2$  leads to the significant contribution of the long life absorption in the transient spectra. Here, we have to point out, that the modification threshold of the Ag nanoparticles in soda-lime glass was estimated in the Section 3.1 to be about of  $0.2 \text{ TW}/\text{cm}^2$ . So it may be concluded that observer long life absorption component at the intensities applied here are reflecting an additional physical process associated with the modification of Ag nanoparticles. An idea about the nature of this process can be acquired from a comparable experiment performed on the neat soda-lime glass substrate (Fig.3.24), where the only difference is the significantly increased pump pulse intensity of approximately  $1.2 \text{ TW}/\text{cm}^2$ . Under such circumstances the initially transparent glass develops a weak, broad absorption with just the same time behaviour as extracted from the above data for the composite glass: at any position within that absorption band signal rises within 500 fs and then remains nearly constant or at latest decays only on a very slow time scale up to  $1 \mu\text{s}$  (Fig.3.25). The most obvious explanation for this transient spectra is the multiphoton ionization of soda-lime glass and

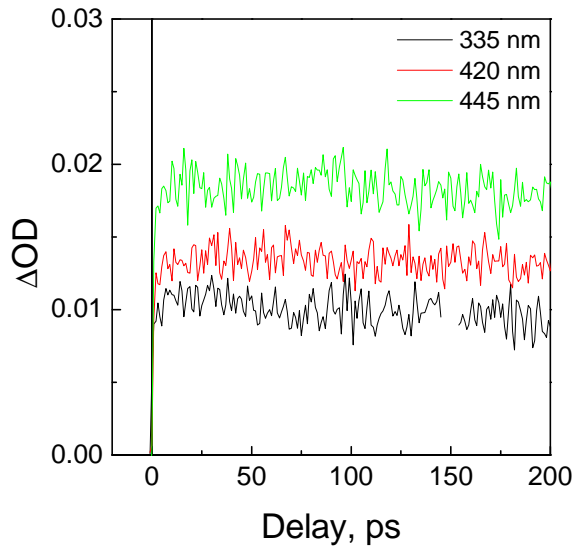


Fig.3.25 Relaxation dynamics of the soda lime glass excited by 150 fs laser pulses at 400 nm.

the generation of trapped electron and hole color centers in the glass, which can produce, as it was shown in the Section 3.2, absorption bands in the visible spectral range, and are known to have rather long lifetimes up to being thermodynamically stable at room temperature. It's plausible to assume that the long-lived absorption observed in the samples containing silver nanoparticles has the same origin (electron trapped in the glass matrix). The nanoparticles incorporated in the glass matrix can play in such case a role of short cuts for electron transitions

in the composite glass reducing band gap between Fermi level of the free electrons in metal inclusion and conduction band of the glass matrix. Moreover, SP assisted local field enhancement in vicinity of the metal cluster can lead to the ionization of the surrounding matrix.

Obtained results find an excellent agreement with the experimental data presented in previous sections of this chapter. The measured dynamics of the SP excitations of Ag nanoparticles for different pump laser pulse intensities explicitly indicate appearance of the long time absorption component in transient spectra referred to the ejection of electrons and probably induced plasma in surrounding glass matrix leading to the following formation of the trapped color centers. It's important to notice that this rise of absorption was observed at laser pulse intensities of about  $10^{11}$  W/cm<sup>2</sup>, what is in good agreement with the threshold of the laser induced permanent changes of extinction spectra of composite glass with spherical Ag nanoparticles determined in the Section 3.1. Furthermore, photoemission of electrons results obviously in positive charging of silver clusters and following Coulomb explosion with formation of free silver cations in surrounding, what, in turn, was manifested by the luminescence studies of irradiated glass samples with Ag nanoparticles presented in the Section 3.3.

### **3.5. Mechanism of the anisotropic shape modifications of spherical Ag nanoparticles in soda-lime glass upon fs laser irradiation.**

The aim of this last section of the current chapter is to summarize experimental data and to propose mechanism of the SP assisted shape modifications of spherical Ag nanoparticles embedded in soda-lime glass by excitation with intense ultra-shot laser pulses. Performed investigations of the effects accompanying the anisotropic modifications in the composite glass allow us to manifest the following experimental facts:

- 1) the laser assisted modifications occur only by appropriate laser pulse intensity (higher than  $0.2 \text{ TW/cm}^2$  by excitation at 400 nm) and exposure wavelength near to the SP resonance;
- 2) orientation of the modified silver clusters (parallel or perpendicular to the laser polarization) is defined by the laser pulse intensity used for irradiation; the number of laser pulses in this case plays mostly accumulative role;
- 3) fading and following total disappearance of the SP band in extinction spectra at higher peak pulse intensities indicate that the partial destruction or dissolution of silver cluster is involved in modification mechanism;
- 4) pump-probe experiments and luminescence studies testify the SP assisted electron photoemission and drastic increase of the content of silver cations in vicinity of disrupted nanoparticle; thus, the destruction of the silver nanoparticles occurs obviously due to Coulomb explosion during ionisation of the silver cluster;
- 5) resulting positive charged shell of the silver cation is playing apparently a key role in the shape modifications; thus, preheating of the sample up to  $200^\circ\text{C}$  increases the mobility of the silver cations and prevents formation of the cation shell in the vicinity of the cluster leading to total dissolution of the Ag nanoparticles upon laser irradiation.

Therefore, the experimental data testify rather complex mechanism of the fs laser assisted modifications of Ag nanoparticles incorporated in glass. Nevertheless, the whole process could in general be formulated as a consequence of the SP assisted electron photoemission (ionization), which leads to the following recharge in the matrix, Coulomb explosion of the metal nanoparticle and precipitation of Ag nanoparticle with asymmetric shape. Thus, the photoelectron emission from the metal cluster is the central point in the observed effects and deserves an attention of more detailed consideration.

#### *3.5.1. Surface Plasmon assisted photoemission from metal nanoparticles.*

Coming to the basics of the photoeffect, it's well known that in order to induce a free electron carrier, the photon energy of the radiation have to overcome the electron work function, needed to exceed the binding energy of electrons with the surface (extrinsic photoeffect), or to excite transition of electrons from ground state into conduction band of dielectric (intrinsic photoeffect). However, as it has been already discussed in Chapter 1 and in Section 3.2, intense laser pulses even with  $h\nu$  less than the work function can evoke emission of electrons due to multiphoton, tunnel and even avalanche ionization.

In the last years the SP assisted photoelectron emission from supported Ag nanoparticles has been extensively studied upon excitation with intense ultrashort

laser pulses [3.20-3.29]. Therefore, the electron work function from the silver clusters defined as an energy gap between the Fermi level and the energy of the free electron in the vacuum is of about 4.3 eV [3.1,3.22,3.26]. Moreover, it was testified [3.29] that excitation near to the SP resonance extremely enhances the two-photon photoemission yield from the Ag nanoparticles.

In the composite glass, containing metal nanoparticles probability of the SP assisted photoemission can be strongly affected by a structure of electron energy manifold in the host matrix. In turn, an energy level scheme of the soda-lime glass with embedded Ag nanoparticles can be presented as a junction of the dielectric with a metal (Fig.3.26). The work function of the valence electrons in pure silica is about of 10.6 eV. Moreover, the edge of the fundamental absorption about of 9 eV in pure silica is caused by electron transitions from valence band in to conduction band. As it

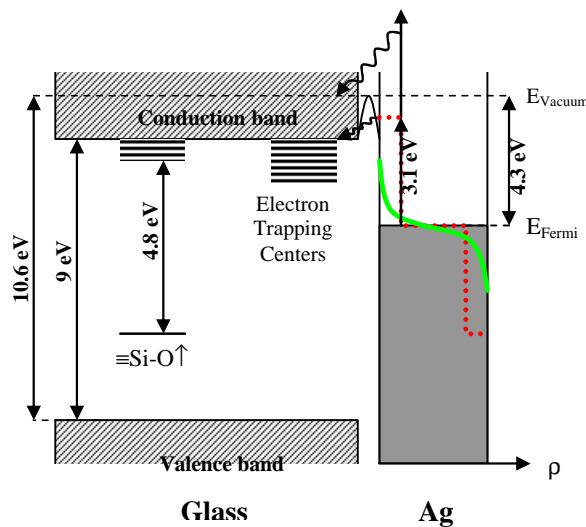


Fig.3.26 Energy level scheme of the electrons in the composite glass containing silver inclusions. The red dotted line indicates a non-thermal distribution of the electrons in Ag nanoparticle caused by excitation of SP resonance. The green one –distribution of the electrons after thermalization.

in to conduction band of the surrounding glass matrix, even by single photon absorption.

Excitation of the Ag nanoparticles near to the SP resonance ( $\sim 3$  eV) by the fs laser at 400 nm (3.1eV) leads to a non-thermal distribution of the electrons in the conduction band of the metal (the Fig.3.26, red dotted line). Since the maximal electron energy in these case exceeds the bottom of the conduction band of the matrix in 0.4 eV, the electron injection in the conduction zone of the glass could be possible. Here we have to point out that the photoemission opens up an additional channel for energy relaxation of the metal clusters. Following thermalization of the electrons with characteristic time of a few hundreds of femtoseconds (the Fig.3.26, green line) obviously restricts the photoemission processes. On the other hand, upon the two-photon plasma excitation the electrons overcome the ionization energy level and without any obstacles penetrate in the glass matrix. Even during thermalization the energy of the electrons could be high enough to jump in the conduction band of the glass. In turn, the injection of the electrons from metal inclusions in conduction band of the surrounding matrix is obviously the origin of a rise of conductivity in the

### Chapter 3. Photomodification of single Ag nanoparticles embedded in soda-lime glass

composite glass with Ag nanoparticles upon fs laser irradiation near to the SP resonance [3.19].

On the other hand, induced free carrier in the glass causes the broad absorption in the visible spectral range, which was observed in the composite glass as well as in the original soda-lime glass upon excitation with 150 fs laser pulses at 400 nm (see the Section 3.4). The fact that the threshold of the laser induced modifications is in quite good agreement with the laser pulse intensity indicating the

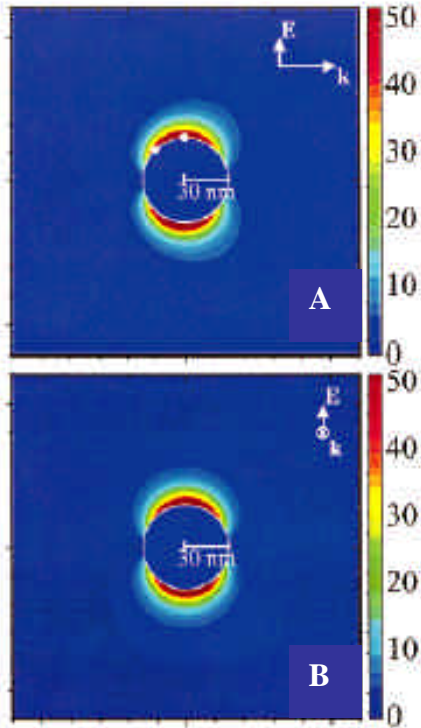


Fig.3.27. Electric field contour for a spherical Ag nanoparticle with radius of 30 nm excited by polarised light near to the SP resonance (the figure adopted from Ref.[3.55]).

free carrier absorption in the nanocomposite glass, allow us to associate the modification threshold with injection of photoelectrons in the glass matrix. During the plasma relaxation, the free electrons in the glass could be trapped by positive charged defects in the matrix leading to formation of color centers indicating long time relaxation component in the induced absorption spectra (see Section 3.4).

However, the proposed mechanism provides only isotropic photoemission of the electrons by the metal nanosphere. However, in the case of SP excitation we can not exclude an effect of the local field enhancement in vicinity of the Ag nanoparticle. Moreover, by excitation with polarized light the E-field enhancement (Fig.3.27) occurs in special points on the surface [3.1, 3.2, 3.55]. The local field enhancement depends on the wavelength (on-resonance or off-resonance) and can reach several orders of magnitude higher than the incident field. In our experiment, the threshold of laser assisted modifications was determined to be about  $0.2 \text{ TW/cm}^2$ . This corresponds to the electric field amplitude of the electro-magnetic wave of about  $6.1 \times 10^6 \text{ V/cm}$ . The highest peak pulse intensity about of  $2.4 \text{ TW/cm}^2$  gives the magnitude of the electric field amplitude of  $9.45 \times 10^7 \text{ V/cm}$ . Increase of the electric field in the vicinity of the silver cluster due to SP resonance could strongly suppress energy levels (see Chapter 1) on the metal-dielectric junction and induce effective electron carrier flow from the surface of nanoparticle parallel to the laser polarisation. The anisotropy in this case is determined by anomalous distribution of the local electric field over nanosphere (Fig.3.27). On the other hand, the electric field in the vicinity of the metal cluster could overcome a breakdown threshold of the glass resulting in the high density electron plasma formation and even ablation of the glass matrix on the poles of the nanosphere.

Therefore, the nonlinear photoionization of the silver nanoparticles are in good agreement with experimental data explaining the intensity threshold of the laser induced modifications and appearance of the broad band induced absorption with long relaxation time, which could be associated with the conduction electrons in the glass and following formation of the colour centers. In turn, as it was indicated by study of the temperature induced effects (the Section 3.3), the colour centers influence on the SP resonance of the Ag nanoparticle in extinction spectra apparently

### Chapter 3. Photomodification of single Ag nanoparticles embedded in soda-lime glass

via dipole-dipole interactions. Moreover, the SP assisted local field enhancement can evoke an anisotropic photoemission of electrons from Ag nanoparticle resulting in anisotropic distribution of the induced defects (electron trapped colour centers) in surrounding glass matrix, which could play an important role in the anisotropic shape modifications.

#### 3.5.2. Dipole-dipole interactions of the SP with induced free electron carrier in the surrounding glass matrix.

The laser induced ionization of the Ag nanoparticles results in generation of high density free electrons in the matrix, which in turn, after relaxation, lead to formation of the electron trapped colour centers in the vicinity of the Ag nanoparticle. The free electrons as well as the colour centers are indicating strong absorption at SP resonance and can result in resonant coupling of SP oscillations with matrix [3.56]. In this case, the dipole-dipole interactions between silver nanoparticle and surrounding media are responsible for an additional channel of SP damping and anisotropic energy transfer into matrix.

The dipole moment of the SP oscillation of metal nanoparticles with frequency of  $\omega_{SP}$  given as  $\vec{D}(t) = \vec{D}_0 e^{i\omega_{SP}t}$  creates at distance  $\vec{r}$  from the center of cluster an oscillating field  $\vec{E}(t, \vec{r}) = \vec{E}_0(\vec{r}) e^{i\omega_{SP}(t-r/c)}$ . The electric field amplitude  $\vec{E}_0$  could be expressed according to the Ref.[57] as:

$$\vec{E}_0(\vec{r}) = \frac{3\vec{n}(\vec{D}_0 \cdot \vec{n}) - \vec{D}_0}{4\pi\epsilon_0 \mathbf{e}' r^3}, \quad 3.1$$

where  $\vec{n}$  is a unit vector in the direction of the radius vector,  $\mathbf{e}'$  is the real part of the complex relative permittivity of the surrounding medium  $\mathbf{e} = \mathbf{e}' + i\mathbf{e}'' = 1 + \mathbf{c}' + i\mathbf{c}''$  (see Chapter 1, Eq.1.17). This electric field induces a polarization given as:

$$\vec{P}(t, \vec{r}) = \text{Re}(\mathbf{e}_0 \mathbf{c} \vec{E}(t, \vec{r})), \quad 3.2$$

where  $\mathbf{c}$  is the complex linear electric susceptibility of the medium. The average power absorbed per unit volume according to Ref.[58] can be expressed as:

$$W = \overline{E(t, \vec{r}) \dot{P}(r, t)} = -\frac{\omega_{SP} \mathbf{e}_0}{2} \mathbf{c}'' |E_0(\vec{r})|^2 \quad 3.3$$

Substituting the Eq.3.1 in Eq.3.3 and after a couple elementary derivations we receive the angular dependent average power absorbed by the matrix:

$$W(r, \Theta) = -\frac{\omega_{SP}}{32\pi^2 \mathbf{e}_0 \mathbf{e}'^2 r^6} \mathbf{c}'' D_0^2 (1 + 3\cos^2(\Theta)), \quad 3.4$$

where  $\Theta$  is the angle between dipole of the SP oscillations and the radius vector. Thus, according to the Eq.3.4, if the absorption coefficient of the surrounding matrix

Chapter 3. Photomodification of single Ag nanoparticles embedded in soda-lime glass

is not equal to 0 at frequency of the SP resonance, the power flow is expected from the nanoparticle via dipole-dipole coupling of metal cluster and host matrix. Moreover, the energy absorption is more intense in direction of the laser polarisation (direction of the dipole orientation). Thus, strong interaction of the SP with the generated in the surrounding glass matrix free electrons and colour centers can result in highly anisotropic excitation of free electron carrier in the vicinity of the surface of nanosphere, which in turn could induce an anisotropic plasma formation, anisotropic temperature distribution and stress in the matrix.

3.5.3 Ionization assisted anisotropic shape transformation of spherical Ag nanoparticles in soda lime glass.

As it has been discussed above, excitation of the Ag nanoparticles with intense fs laser pulses near to the SP resonance induces the electron photoemission

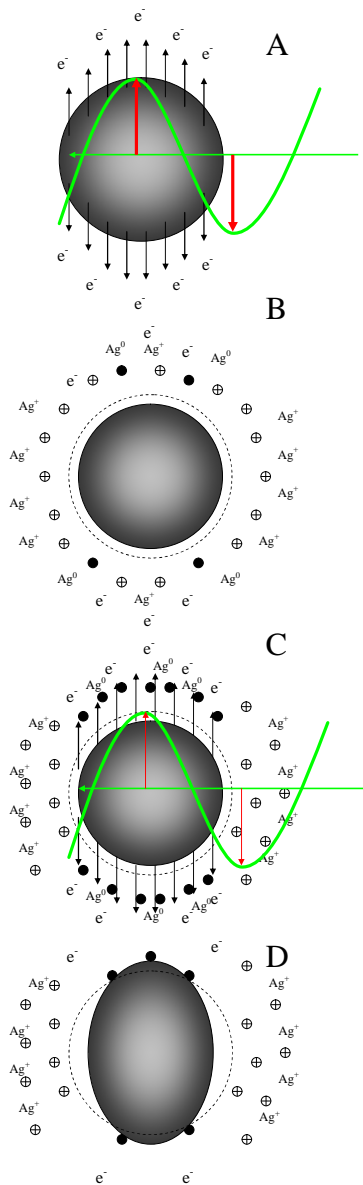


Fig.3.28. Laser assisted shape modification of the metal nanosphere via ionization and precipitation .

from the surface of the metal clusters. Moreover, electron flow in the direction of the laser polarisation (Fig.3.28A) and polarisation dependent resonant SP coupling with the glass matrix can result in formation of the high density electron plasma localised in glass near to the surface of the metal nanospheres in direction of the laser polarisation. Following relaxation of electrons leads to the formation of trapped electron centers concentrated mostly on the poles of the sphere. At the same time, resulting positively charged nanoparticles is not stable any more and eject silver cations driven by the Coulomb forces forming, as it was mentioned in section 3.3, a positively charged shell near to the disrupted cluster (Fig.3.28B). Moreover, the diffusion length of the silver cations in the glass matrix is restricted obviously by the mobility of  $Ag^+$  and rapid thermal relaxation of the Ag nanoparticle. Here we have to point out that the energy transfer from the nanoparticle into the matrix results in considerable increase of the temperature in the cluster surrounding. However, the temperature should be below the transition temperature in the glass. Otherwise, the oblong shape of the cluster can not be fixed (it is proved by heating experiments at  $600^{\circ}C$  [3.14]). Nevertheless, under these circumstances the silver cations could be reduced by the electrons located in the matrix defects and evoke precipitation of silver aggregates in vicinity of the nanoparticle with following coalescence with the cluster. Moreover, the silver cations could play a role of electron trapping centers by the next laser pulse (Fig.3.28C) leading in intense precipitation and growing of the silver cluster in the direction of the laser polarisation. Apparently, this mechanism leads to the anisotropic distribution of the  $Ag^+$  ions in direction

perpendicular to the laser polarisation (Fig.3.28D), which was demonstrated by the experimental data (Fig.3.19B). Furthermore, the precipitation mechanism of the shape elongation is additionally approved by the laser assisted dissolution of the Ag nanoparticles in preheated sample up to 200°C. Increase of the temperature enhances the diffusion mobility of the silver cations in glass and apparently prevents formation of the cationic shell in vicinity of the metal cluster.

According to the proposed mechanism, formation of the high fraction of silver cations near to the cluster and photoemission of electrons in direction of the laser polarisation are responsible for precipitation of oblong silver nanoparticles embedded in soda-lime glass parallel to the laser polarisation.

On the other hand, this mechanism evidently works at laser pulse intensities slightly above the threshold of the laser induced modifications. Increase of the laser pulse intensity causes a rise of the temperature in the surrounding glass and diffusion mobility of the silver cations. This leads to expansion of the radius of the cationic shell and decrease of the concentration of  $Ag^+$ -ions near to the nanosphere. Thus, the precipitation and the anisotropic ripening of the Ag nanoparticles become less probable and extinction spectra as well as TEM demonstrate the isotropic changes (see Section 3.1). Moreover, if the laser pulse intensity is high enough, the plasma formation is probable on the interface of the glass and the silver inclusion in special points, where local electric field is maximal (on the poles of the sphere along to the laser polarisation). Moreover, the electron density of the electrons in the induced plasma is defined by the local electric field strength as well as by direct absorption of

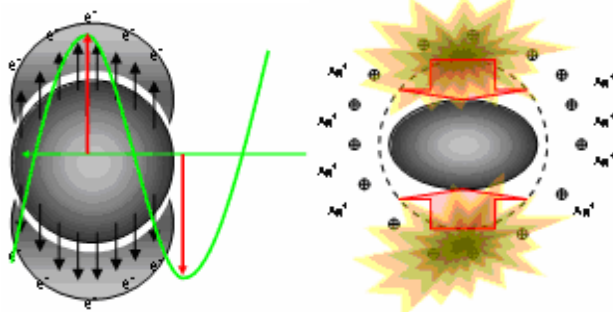


Fig.3.29. Laser assisted shape modification of the metal nanosphere via high density plasma formation in surrounding matrix.

the laser radiation by free electrons and energy transfer from the nanoparticle to matrix via resonant SP coupling with the free electrons. The last two processes can induce very rapid increase of the electron density due to avalanche ionization of the glass. The following plasma relaxation leads to the transfer of the energy from electrons to the lattice (glass) on the time scale much faster than the thermal

diffusion time. This can result in ablation of the material on the interface between glass and metal inclusion leading to partial destruction of the nanoparticle on the poles (Fig.3.29). Moreover, the shock due to expansion of the matrix evokes compression of the metal cluster in direction parallel to the laser polarisation.

In conclusion, in this section we discussed possible mechanism of the laser induced shape modifications of spherical Ag nanoparticles embedded in soda-lime glass. The main point of the proposed scenario is the SP assisted photoelectron emission of the electrons from the metal surface upon excitation with 150 fs laser pulses. The following development of the processes strongly depends on the applied laser pulse intensity: slightly above the modification threshold the Coulomb explosion and anisotropic ripening of the Ag nanoparticles results in elongation of the cluster parallel to the laser polarisation; intense laser pulses evoke the dense electron plasma on the glass-metal interface, which leads to ablation and compression of silver nanosphere resulting in orientation of the cluster perpendicular to the laser polarisation.

## Chapter 4.

# **Laser assisted structural modifications of strongly aggregated Ag nanoparticles in soda-lime glass**

In the previous chapter, we discussed anisotropic shape transformation of single spherical Ag nanoparticles upon exposure to intense fs laser pulses near to the SP resonance. Here, excitation of aggregated systems with metal nanoparticles where the gap between nanoparticles is much smaller than the particle size is studied. Under these circumstances, by consideration of the structural transformations we can not neglect a mechanical contact between metal nanoparticles. Moreover, the aggregated nanoparticles with high polarizability (noble metals) strongly interact via dipolar forces, or more generally, multipolar coupling, which manifest unique linear and nonlinear optical properties [4.1, 4.2] and can affect the modification processes in the composite medium. At the same time, high fraction of metal inclusions leads to the increase in deposited pulse energy density in the system (due to extremely high absorption). Thus, the thermal effects like melting and coalescence of the metal clusters could reveal a considerable contribution in structural alterations.

In turn, in this chapter we will discuss modification of structural and optical properties of aggregated Ag nanoparticles (filling factor about of 0.7) in thin glass layers upon exposure to intense fs and ns laser pulses.

#### 4.1 Anisotropic nanostructures created by fs laser irradiation in glass containing aggregated Ag nanoparticles

As it has already been mentioned, increase in the filling factor of metal nanoparticles leads to the strong multipolar interactions, which have significant influence on the optical properties of the composite materials and apparently could affect the structural modifications upon exposure to fs laser pulses. Here we will demonstrate new phenomena occurring in the composite glass containing Ag nanoparticles with filling factor up to 0.7 (the Fig.4.1) by irradiation with intense 150 fs laser pulses at various wavelengths.

The extinction spectra of the sample shown in the Fig.4.2 demonstrate strong broad absorption band in the visible spectral range, which can be referred to inhomogeneously broadened SP band of the silver nanoparticles embedded in the glass. The broadening is obviously caused by collective interactions between Ag nanoparticles distributed in the glass with filling factor up to 0.7 decreasing in the depth. Here we are mostly interested in studies of modifications induced only in the upper layer with maximal filling factor, which defines the high reflectivity of the sample. The reflection spectrum of the sample with strongly aggregated Ag nanoparticles is shown in the Fig.4.2 and demonstrates a broad reflection band centred at about of 580 nm, which could be referred to the SP resonance of the silver aggregates. The large red shift of the SP is caused by strong interparticle interactions. The reflection coefficient in the maximum reaches a value of 47%. Since the reflection of the sample is defined by the upper layer with maximal filling factor of the Ag nanoparticles, the structural changes can be monitored by alteration of original reflection spectra. The laser processing of the composite glass was performed with 150 fs laser pulses at 400 nm, 528 nm and 800 nm. Using an ordinary technique of multi-shot irradiation, square fields with size of 3x3mm were irradiated on the sample. The peak pulse intensity was chosen to be  $\sim 0.6-0.7$  TW/cm<sup>2</sup> for each case. The polarised reflection spectra were then measured.

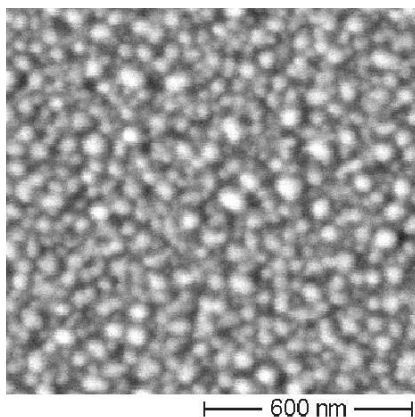


Fig.4.1 SEM picture of the composite glass with Ag nanoparticles

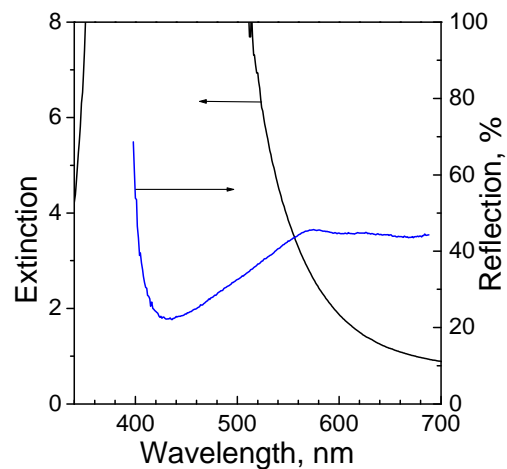


Fig.4.2 Extinction and reflection spectra of the glass with aggregated Ag nanoparticles.

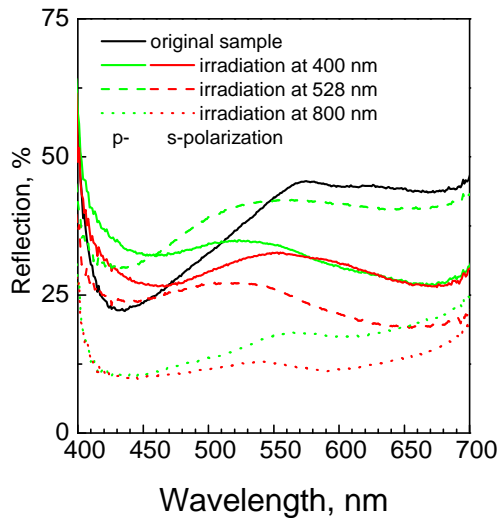


Fig.4.3 Reflection spectra of the aggregated Ag nanoparticles in the glass: effect of the fs laser irradiation at 400 nm, 528 nm, 800 nm.

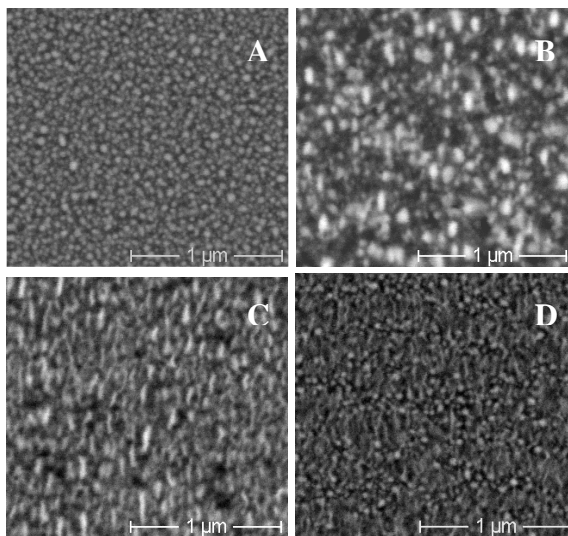


Fig.4.4. SEM image (BSE mode) of the glass with Ag nanoparticles: A: original sample with spherical Ag clusters; B: sample irradiated at 400 nm; C: sample irradiated at 528 nm; D: sample irradiated at 800 nm. The laser polarization was in vertical direction.

First observation of the exposed areas indicates visible anisotropic changes in the sample. Reflection spectra presented in the Fig.4.3 also reveal drastic dichroic modifications. Moreover, as it was testified by the experiment, the dichroism is strongly dependent on excitation wavelength. For instance, irradiation of the composite glass at 400 nm leads to rise of reflection coefficient in the region 400-500 nm. Moreover, in p-polarisation (green line) reflection coefficient is considerably higher than in s-polarisation (red line). At the same time, reflectivity of the sample decreases in spectral range above 500 nm and does not demonstrate any dichroism in this spectral range. Exposure of the sample at 528 nm also evokes dichroic alterations of the reflection spectra. Moreover, in p-polarisation strong changes occur only in the spectral range 400-550 nm indicating growth of the reflection coefficient. At the same time, s-polarized spectrum reveals significant drop of the reflectivity above of 450 nm. In contrast, irradiation of the sample at 800 nm leads to significant decrease of the reflection coefficient approximately by factor 4 in visible spectral range demonstrating only a little dichroism above 540 nm. However, as it can be seen, in all three cases reflectivity in p-

polarisation is considerably higher than in s-polarization .

Scanning electron microscopy of the irradiated samples reveals anisotropic structural changes (Fig.4.4), which are responsible for alterations of the reflection spectra and induced dichroism. In particular, as can be seen in the Fig.4.4B, irradiation at 400 nm considerably decreases fraction of the silver clusters in the glass layer in comparison with the original one (Fig.4.4A). At the same time, initially spherical particles drastically grow in size and simultaneously demonstrate elongation of the shape in direction parallel to the laser polarization. These structural transformations could be explained by a junction of several nanoparticles of the aggregated system in the single cluster upon laser pulse excitation. Increase in the

distance between nanoparticles abates the contribution of the dipolar interaction of metal clusters and should be responsible for the decrease of reflectivity in the spectra above 500 nm (Fig.4.3). Moreover, the oblong shape of the clusters is obviously responsible for the observed dichroism in the spectra.

Similar polarization dependent structural changes can be also seen in the sample subjected to irradiation at 528 nm (Fig.4.4C). However, the aspect ratio of the resulted metal clusters here is much higher than in the sample irradiated at 400 nm and can even reach values of up to 10 for longest structure. Moreover, elongated clusters are still compact packed and in the direction of the long axis they are almost contacting each other, while in other direction the distance between nanoparticles is considerably higher than diameter of the initial spherical nanoparticles. Thus, in this case the dichroic alteration of the reflection spectra can be caused by anisotropic shape of the single clusters as well as by their distribution in the glass layer. In particular, the reflection spectrum in p-polarisation is scarcely affected by the laser radiation, while in s-polarisation reflection strongly decreases above 450 nm indicating weak dipole-dipole interactions.

By irradiation at 800 nm, where absorption is mostly defined by collective SP excitations, SEM image of the modified sample indicates significant reduction of amount of aggregated spherical Ag nanoparticle and localized formation of extremely long tiny island structures (Fig.4.4D). Apparently, the structural changes from one side cause the common fading of the reflection and from other side are responsible for the observed dichroism in the red side of the reflection spectra.

Therefore, in general all three cases demonstrate similar formation of the oblong metal clusters upon exposure to intense fs laser pulses. Moreover, the aspect

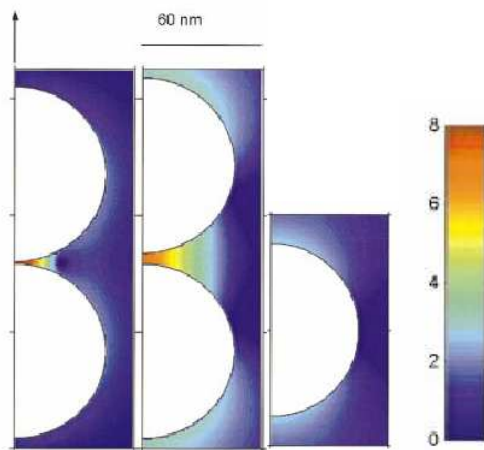


Fig.4.5 EM-enhancement factor at a cross section through three different silver particle configurations. The wavelength of the incident field is 514.5 nm with vertical polarization. The left-hand column illustrates the EM enhancement for dimer configurations of two spheres with a separation of 1 nm. The middle column shows the same situation, but with a separation distance of 5.5 nm. The right-hand column shows the case of an isolated single particle. Note that the color scale from dark blue to dark red is logarithmic, covering the interval  $10^0 < M_{EM} < 10^8$ . Regions with enhancement outside this interval are shown in dark blue and dark red, respectively. According to Ref.[3].

ratio of the clusters seems to be increasing with attenuation of the laser towards long wavelengths leading to a red shift of the maximal dichroism. It is rather plausible to suppose that observed structural modifications of the aggregated silver nanoparticles could be caused by anisotropic junction of the nanospheres in direction of the laser polarisation. In turn, this mechanism is completely different from the shape elongation of the single nanoparticles discussed in Chapter 3. Apparently, in the case of the aggregated system interparticle dipole coupling occurring during SP polariton excitation is responsible for the anisotropic structural changes.

Indeed, numerous theoretical estimations and experimental works testify arise of the “hot sites” located at junctions between closely spaced nanospheres, at certain positions in aggregates [4.3-4.9]. In turn, the local electromagnetic field enhancement of the incident wave in the system of two

## *Chapter 4. Laser assisted structural modifications of strongly aggregated Ag nanoparticles in soda-lime glass*

contacting spheres is strongly dependent on the particle size, the distance between nanoparticles as well as on excitation wavelength. Extended Mie theory indicates, that local field enhancement can reach  $10^{11}$  [4.3-4.4] in hot nanojunctions (Fig.4.5) leading to enormous enhancement of the nonlinear response from the random composite medium [4.2, 4.3, 4.5]. In particular, as it was shown in Ref.[4.3] and in the Fig.4.5, excitation of the couple of silver nanospheres near to the SP resonance with light polarization parallel to the axis of the dimer indicates a drastic local field enhancement in the space between the two clusters, caused by strong dipole-dipole interaction. In turn, increase of the distance between nanospheres decreases the enhancement factor. At the same time, under the same excitation parameters the magnitude of the local field in vicinity of the single nanoparticles is several orders lower than in nanojunctions. Such strong interparticle interaction evokes an optical forces acting on the nanospheres pulling them together [4.4]. Would the aggregated metal nanoparticles be placed in liquid or gas matrix, we could expect a narrowing and following coalescence of the interacting spheres driven by the optical forces. However, a fluid matrix is not able to fix anisotropic shape of the metal nanoclusters (without additional molecular stabilizers) and formation of the anisotropic aggregates in solutions was not published. On the other hand, the shape and location of the metal nanoparticles in the glass is stabilized by the matrix and the distance between nanoparticles is fixed preventing, in turn, the optical forces to pull the nanospheres together. Nevertheless, extremely high intensity of the local field could induce a multiphoton and tunnel ionization leading to ablation of the glass matrix in vicinity of the junction leading to a coupling of nanospheres.

In our case, the laser peak pulse intensity about of  $0.6 \text{ TW/cm}^2$  corresponds to the electric field amplitude of the incident wave (Chapter 1, Eq.1.34) to be about  $10^7 \text{ V/cm}$ . Under these circumstances, increase of the electric field in several order of magnitude in the space between nanospheres will obviously result in ionization of the glass, high density plasma formation and following ablation of the thin glass layer between nanoparticles. This leads to coalescence of nanoparticles and formation of anisotropic clusters aligned parallel to the laser polarisation.

Apparently, proposed scenario is responsible for the formation of the oblong metal nanostructures by excitation of the aggregated Ag nanoparticles in glass matrix with 150 fs laser pulses. Moreover, the wavelength dependence of the structural modifications could be explained by excitation of different anisotropic modes in the aggregated system. For instance, attenuation of the laser towards long wavelength obviously leads to excitation of the longest chains of spherical nanoparticles oriented parallel to the laser polarization and demonstrating a maximal red spectral shift of the SP band [4.7-4.9].

## 4.2 Modification of optical and structural properties of aggregated Ag nanoparticles in glass by exposure to ns laser pulses near to the SP resonance.

All experimental data presented above in the thesis were dedicated to the SP assisted anisotropic structural modifications of spherical Ag nanoparticles induced by intense fs laser pulses. In spite of the effect of the filling factor on occurring shape transformations, the polarization dependence of the induced anisotropy testifies the fact that intense electromagnetic laser fields in combination with SP assisted local field enhancement in vicinity of the cluster are playing the key role in processes of the shape elongation. At the same time, ns laser pulses at 527 nm affected the glass samples only with oblong nanoparticles (laser modified and mechanically stretched) leading to restoration of spherical shape of the clusters caused by heating of the glass matrix up to transition temperature. In samples with embedded spherical Ag nanoparticles increase of the pulse fluence even up to  $2.5 \text{ J/cm}^2$  (the peak pulse intensity  $\sim 12 \text{ MW/cm}^2$ ) resulting in the melting of the glass layer did not induce any dichroism. On the other hand, if the fraction of the silver clusters in glass is very high, excitation with ns laser pulses leads to new phenomena, which will be discussed in this part of my work.

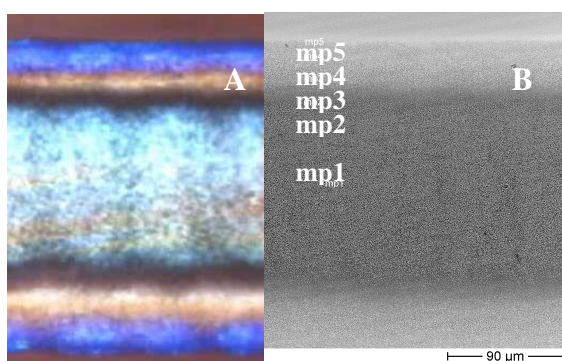


Fig.4.6 Modified composite glass with Ag nanoparticles by 200 nm laser pulses at 527 nm: A - optical microscope image in reflection; B - corresponding SEM image in BSE mode.

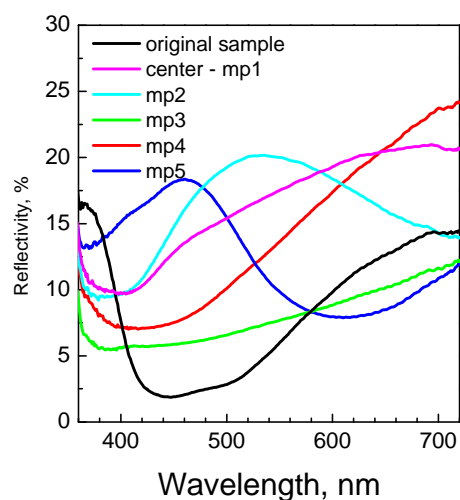


Fig.4.7 Local reflection spectra measured across of lines burned on the sample with Ag nanoparticles (Fig.4.6A) by the 200 ns laser pulses at 527 nm.

In experiments we studied the samples with high filling factor of Ag nanoparticles provided by the CODIXX AG. Irradiation was carried out in multi-shot mode at 527 nm using SH from Q-switched Nd:YLF laser with pulse duration of 200 ns, pulse energy up to 10 mJ and repetition rate of 1 kHz. The beam was focused on the sample to a spot with diameter of  $150 \mu\text{m}$  and the pulse energy didn't exceed the value of  $200 \mu\text{J}$  (the fluence of  $2.2 \text{ J/cm}^2$ , the peak pulse intensity of  $11 \text{ MW/cm}^2$ ). Using X-Y translational stage series of lines were written on the sample.

As it can be seen in the Fig.4.6A, effect of the laser expose reveals unusual coloration of the sample and drastic increase of the reflectivity of the modified area in visible spectral range. For instance, on the border of the burned line the glass changes initial dark brown colour on bright blue (mp5 – see the

## Chapter 4. Laser assisted structural modifications of strongly aggregated Ag nanoparticles in soda-lime glass

Fig.4.6). Towards to the center of the line the colour smoothly changes to light red (mp4) and then to light blue-green (mp1-mp2). The local reflection spectra measured across to the modified line (Fig.4.7) represent details of the spectral alterations. In original glass with Ag nanoparticles a broad reflection band above 550 nm in the spectra defines the dark brown reflection and is caused apparently by aggregated silver nanospheres in the upper glass layer. The reflection spectrum recorded in the center (a violet curve labelled as mp1 in the Fig.4.7) of the modified line demonstrates appearance of a broad reflection band formed by two overlapping peaks centred at about of 460 nm and 650 nm. A little bit away from the center near to the dark region (mp2) the spectra indicates a single intense reflection band peaked at 520 nm. Following shift in the thin dark area (mp3) demonstrates rise of the reflectivity in the spectral interval 400-600 nm, while initial reflection band in the NIR slightly goes down. The next region in direction to the edge of the line (mp4) is characterised by homogeneous increase of the reflectivity with maximum shifted towards long wavelength responsible for the red coloration of the sample. The border of the irradiated line with blue coloration (mp5) demonstrates in the reflection spectra a band at 450 nm. At the same time, a maximum of the initial red reflection band seems to be shifted far in NIR spectral range.

Observed drastic changes in optical properties of the composite glass with aggregated Ag nanoparticles are obviously caused by some inhomogeneous structural modifications in the sample upon exposure to 200 ns laser pulses near to the SP resonance. First, a SEM overview of the modified area in BSE mode (Fig.4.6B) demonstrates a fading of the image brightness of the exposed line indicating considerable decrease of metal content in the center of the irradiated area. Further investigation of the electron microscopy images of the exposed region (Fig.4.8) at appropriate distances from the center of the line corresponding to the recorded reflection spectra (Fig.4.7) uncovers evident differences in structural alterations in the composite glass. In particular, the middle area with blue-green coloration (Fig.4.8B) is characterized by formation of large aggregated metal nanoparticles and even island films with diameter up to 500-600 nm. The metal

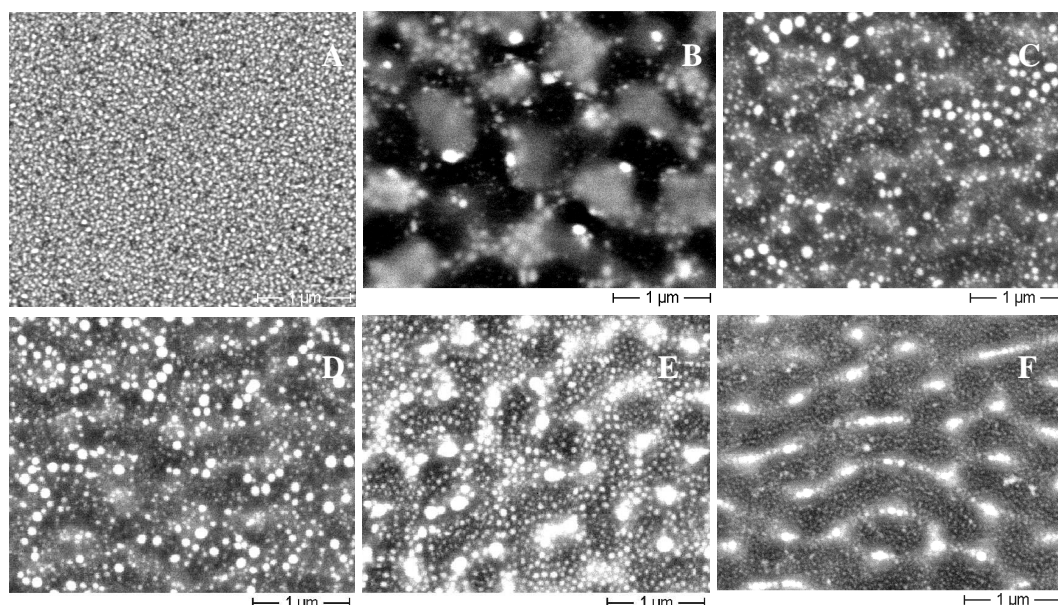


Fig.4.8 Scanning electron microscopy (BSE) of the glass with aggregated Ag nanoparticles: A – original sample; B – center of the modified line (mp1); C – structures in the area mp3 (see the Fig.4.6); D – mp4; E – mp5, F – edge of the modified area. Corresponding reflection spectra are shown on the Fig.4.7.

## Chapter 4. Laser assisted structural modifications of strongly aggregated Ag nanoparticles in soda-lime glass

islands structures are quite homogeneously distributed in the glass and separated by gaps about of 500 nm. Moving off from the center we can see appearance of disordered, large, spherical silver nanoparticle with diameter up to 150 nm (Fig.4.8C). At longer distances from the center a fraction of the large Ag nanoparticles considerably grows (Fig.4.8D). In the border region (Fig.4.8E) the SEM image demonstrates a nonuniform ripening of the silver nanoparticles and formation of almost quasiperiodical distribution of large single clusters (globes) with diameter of  $\sim 150$  nm. The distance between silver globes was estimated to be about of 500-550 nm. Moreover, in the gaps between globular clusters, as it was observed, the initial aggregated Ag nanoparticles are also growing in size by factor of 2. On the edge of the modified region SEM indicates the growth of thin wire structures of Ag nanoparticles quite uniformly aligned parallel to the border of the modified line (Fig.4.8F) and spaced in about 500 nm. Here we have to point out that additional experiments performed with various laser polarisation did not reveal any polarisation dependence in orientation of the metal nanowires.

As it can be seen in the Fig.4.9, the laser radiation mostly affects a very thin region leading to coalescence and formation of large Ag clusters beneath the surface. At the same time, SEM image in cross section demonstrates strong distortion of the surface and agglomeration of the metal on the top. All these effects are caused by an anomalous increase in the temperature on the surface of the composite glass upon exposure to 200 ns laser pulses at 527 nm. This evokes the coalescence of the aggregated Ag nanoparticles, diffusion and evaporation of the silver on the top of the sample, melting and re-crystallisation of the surface.

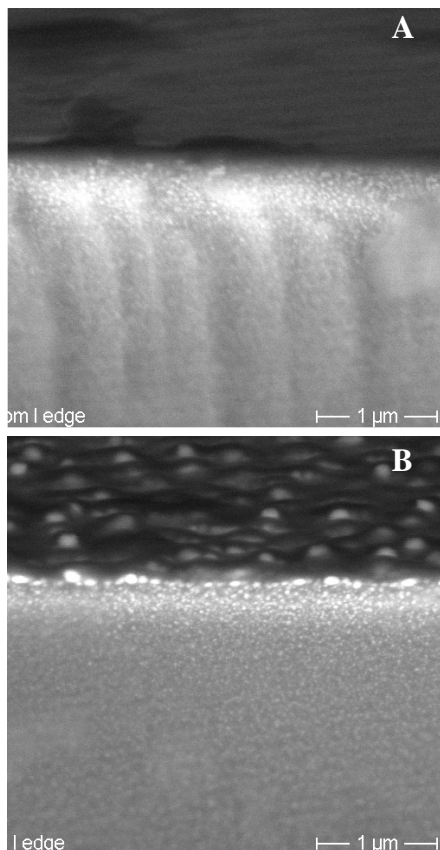


Fig.4.9 SEM image (BSE mode) of the cross section of the glass with Ag nanoparticles before (A) and after (B). The pulse energy fluence was about of  $0.55 \text{ J/cm}^2$ .

As it was shown in Chapter 1, the size, shape and distribution of the metal nanoparticles in the dielectric matrix determines the effective dielectric constant of the composite medium and as consequence strongly affect the dispersion, absorption and reflectivity of the metalodielectric glass. Thus, alterations of the reflection spectra (Fig.4.7) induced by the laser irradiation could be explained by modifications of the optical properties of thin upper layer itself. However, contribution of the interference due to strong modulation of the refractive index near to the surface of the exposed glass, which rather plausible to assume by such inhomogeneous structural changes in the depth, can not be excluded. At the same time, quasiperiodical silver arrays (in the border region) and even metal island (in the central part) on the top of the sample form opal like structures producing wavelength selective diffraction driven in turn by the size of the structures and the magnitude of the gap between them (grating order). As it was shown above, achieved structures are spacing in about of 500 nm from each other and

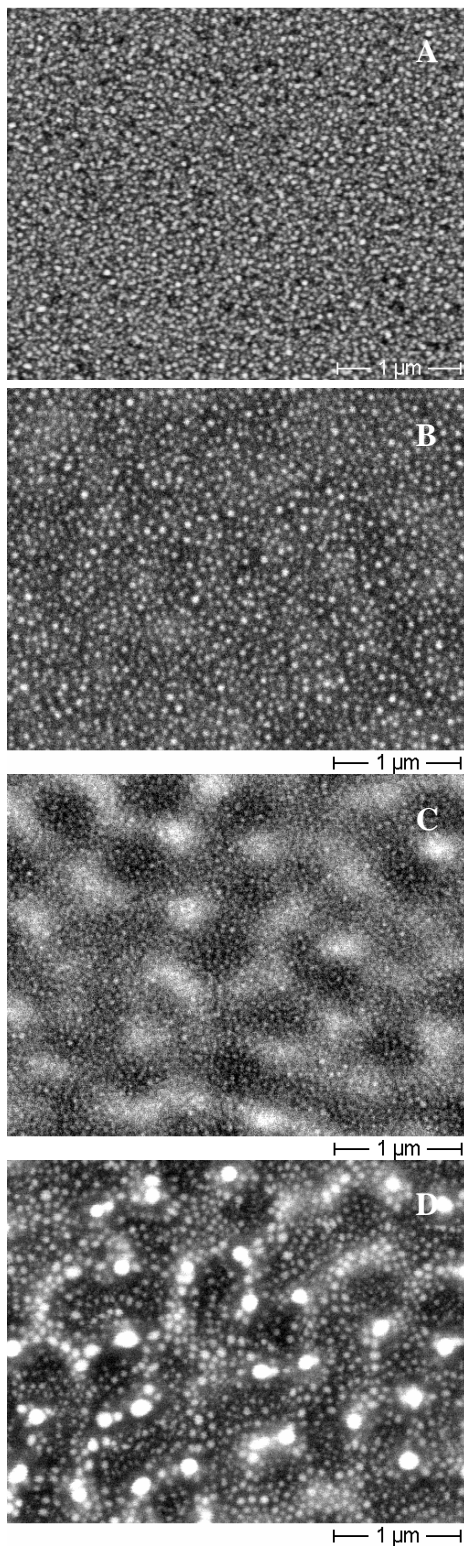


Fig.4.10. SEM image of the glass containing Ag nanoparticles: A - original sample; B,C,D – image of the area at the same distance from the center; B – writing density of 200 pulses per spot (150 $\mu$ m); C – writing density of 1000 pulses per spot; D – writing density of 2000 pulses per spot. The pulse energy fluence was 2.2J/cm<sup>2</sup> and the spot diameter about of 150  $\mu$ m.

should reveal strong effect on spectral properties in the visible spectral range.

Therefore, the metallic structures created in the composite glass with Ag nanoparticles upon exposure to 200 ns laser pulses near to SP resonance could be considered as photonic crystals [4.10-4.12] with optical properties defined by the periodical band gaps in the medium. Recently, the metalodielectric photonic crystals have been proposed and extensively studied as possible candidate for creation of photonic band gaps in the optical wavelength range [4.13-4.16]. The localised SP resonance of the single nanosphere in such materials forms the photonic band gaps in analogy with electron energy levels of an isolated atom in a crystal [4.16-4.18]. In turn, this allows to apply the tight-binding formalism developed for the case of the atomic orbitals in description of the metalodielectric photonic crystals [4.16]. On the other hand, dependence of the SP resonance on the size, shape and distribution (filling factor) of the metal clusters as well as on the dielectric properties of the host matrix opens a new route for control of the band gap characteristics and development of novel PC media with unique optical properties. For instance, the wavelength selective mirrors for the visible spectral range can be created using photonic glass with colloidal Ag particles [4.19]. The maximum of reflectivity in these materials was settled by appropriate radius of the silver sphere, which defined the band gap size. Recently, we demonstrated a creation of 1D metaloglass photonic crystal analogue [4.20] using a novel technique of DC electric field assisted dissolution of silver nanoparticles in soda-lime glass [4.21, 4.22]. Variation of the applied voltage and annealing time at moderate temperatures allows to control the band gap size and to retune position of the reflection band in visible spectral range. Furthermore, the spectral properties (in particular – the reflection spectra) of structured composite glass exposed to 200 ns laser pulses have to be discussed in terms of 3D band gaps in

## *Chapter 4. Laser assisted structural modifications of strongly aggregated Ag nanoparticles in soda-lime glass*

metalodielectric photonic crystals and still need additional investigation. The detailed analysis of optical properties of created plasmonic periodical structures in soda-lime glass is an aim of my future investigations, which deserves consideration in a separate article and certainly will be published at appropriate time. Here, it's rather reasonable to focus our attention on the processes responsible for the formation of the regular structures in the composite glass.

According to the experimental conditions, the periodical metal structures in the glass containing aggregated Ag nanoparticles occur upon multi shot irradiation by 200 ns laser pulses near to the SP resonance. This fact allows us to suppose a contribution of some type of selforganisation processes in formation of the regular structures. In other words, we believe that the periodical chains are not a product of the single laser pulse, but are growing and stabilising with following laser pulses. As it can be seen on the Fig.4.10, exposure of the sample with various pulse writing densities (the number of laser pulses per spot) clearly indicates progressive ripening of the regular structures with increase of the number of pulses. For instance, irradiation with writing density of 200 pulses per spot leads to the considerable increase of the size of Ag nanoparticles and simultaneous sinking of the silver fraction in the upper layer (Fig.4.10B) in comparison with original sample (Fig.4.10A). Increase of the writing density up to 1000 pulses per spot results in growth of large clusters (Fig.4.10C), which could play apparently a role of nucleation centers for periodical structures created in the glass by writing density of 2000 pulses (Fig.4.10D). Thus, the metal ripples are developing with rising number of pulses indicating a selforganisation mechanism. Moreover, the distance between globular aggregates is about 500 nm, which is in a good correlation with the excitation wavelength. This apparently indicates that we are dealing in such case with so-called Wood's anomalies induced by the laser radiation in solids.

The first observation of laser-assisted ripples [4.23] is related to the time of first laser creation (Ruby laser 1960 by Maiman). In fact, it was testified that almost any material could generate on the surface highly periodic permanent structures. Since then formation of laser induced Wood's structures has been extensively studied for last four decades upon exposure of different media with CW, pulsed  $\mu$ s, ns and fs lasers [4.24-4.36] indicating the universality of the observed phenomena. The ripples were observed in metals [4.27, 4.29, 4.31], semiconductors [4.23-4.25, 4.28, 4.31, 4.36] and also in dielectrics [4.34, 4.35]. In spite of the different laser induced processes in the matter, the periodical structuring appears as the result of the nonlinear growth process initiated by the scattering of the incident laser radiation by random irregularities initially present in the surface as roughness or been induced by the laser radiation on the interface. Thus, the interference of the incident beam with the scattered light propagating at grazing angle to the surface produces a special modulation of the light intensity on the top of the sample with periodicity corresponding to the laser wavelength. This intensity variation could result in increase of the amplitude of the irregularities in the interference maxima. Thus, formed special frequency component of the surface irregularities has an appropriate periodicity to diffract the incidence radiation in the first order at the same angle along to the surface increasing the strength and contrast of the interference, which can cause further growth of the corresponding surface irregularities. Therefore, the creation of the interference pattern on the top of the sample is the common feature of the observed phenomena. The periodicity of the produced interference between incident and scattered light on the surface can be given as:

$$\Lambda = \frac{\lambda}{n(1 \pm \sin(\Theta))}, \quad 4.1$$

where  $\lambda$  is the laser wavelength,  $n$  is the refractive index of the medium, which the scattered wave is propagating in,  $\Theta$  is the angle of incidence of the laser beam. According to the Eq.4.1, the periodicity of the generated regular structures inversely depends on the refractive index, which can be affected by the nonlinear interactions of the intense laser pulses with the medium (high nonlinear cubic susceptibility, generation of the free current, colour centers formation). At normal incidence ( $\Theta = 0$  deg) the pattern period is  $\Lambda = \lambda/n$ .

Therefore, it's quite obvious that all the observed structural modification are induced in the silver containing glass due to strong inhomogeneous heating in the sample caused by absorption of specially modulated laser radiation on the surface. Due to high optical density, the penetration depth of the laser radiation in the sample is about 1  $\mu\text{m}$ . However, the pulse duration of 200 ns is obviously much longer than thermal relaxation time of the metal clusters and pulse energy released in the thin upper layer with high fraction of the Ag nanoparticles is dissipated due to the heat diffusion in the depth of the sample. The characteristic heat diffusion length can be given as [4.37]:

$$l_T = 2\sqrt{\frac{\gamma\tau}{c\rho}}, \quad 4.2$$

where  $\gamma$  is the thermal conductivity,  $c$  is the sample heat capacity,  $\rho$  is the sample density,  $\tau$  is the laser dwell time (i.e. the laser pulse duration of 200 ns). Since the filling factor of the Ag nanoparticles is very high, we can take for rough estimations parameters of the bulk silver ( $\rho=10.5$  g/cm<sup>3</sup>,  $c=0.237$  J/gK,  $\gamma =4.27$  W/cm K). Thus, according to the Eq.4.2 the heat diffusion length is about of 11.7  $\mu\text{m}$ . This length could be associated with the heat penetration in the depth of the sample during the laser pulse. In other words, the volume of the matter, which the pulse energy is released in, can be extended up to  $V = 2\pi\omega^2 l_T$ , where  $\omega$  is the laser beam waist (in our case  $2\omega=150$   $\mu\text{m}$ ). Having this in mind, the increase in the temperature of the exposed area caused by single laser pulse can be expressed as:

$$\Delta T = \frac{E}{cl_T\rho}, \quad 4.3$$

where  $E$  is the laser pulse energy fluency. Thus, according to the Eq.4.3, the single laser pulses with energy fluence about of 2.2 J/cm<sup>2</sup> could enhance the temperature of irradiated spot on the sample up to 780°C, which in turn is more than the transition temperature in the glass. It has to be pointed out that for the temperature estimation due to high silver fraction we used parameters of the bulk silver. However, for the composite glass with distribution gradient of metal clusters in the depth the thermophysical properties of the medium strongly vary as a function of the distance from the surface and should be described in terms of an effective medium (metal+glass). In turn, using the thermal parameters for the bulk glass ( $\rho=2.51$  g/cm<sup>3</sup>,  $c=0.86$  J/gK,  $\gamma =0.011$  W/cm K) the heat diffusion length and the maximal temperature induced by the single laser pulse according to the Eqs.4.2 and 4.3 were

#### *Chapter 4. Laser assisted structural modifications of strongly aggregated Ag nanoparticles in soda-lime glass*

estimated to be about 0.63  $\mu\text{m}$  and 16200°C, respectively. Such unrealistic temperature increase leads to destruction of the material. However, it corresponds to an idealistic case, when the whole pulse energy (energy fluence of 2.2 J/cm<sup>2</sup>) is absorbed in the thin upper layer of glass to be less than the heat diffusion length. However, this could be true in a system with a thin layer (a few hundreds nm) containing aggregated metal nanoparticles deposited on the glass substrate. Then, excitation in SP band can evoke anomalous temperature increase and ablation of the material.

It's obvious that our situation is somewhere in between and single laser pulses produce strong inhomogeneities in the top of the sample caused by melting, evaporation, aggregation and coalescence of the Ag nanoparticles.

According to the discussion above, the most plausible scenario for the formation of the quasiregular metal structures in the composite glass with high fraction of Ag nanoparticles by exposure to 200 ns laser pulses near to the SP resonance seems to be as follows. At the start, the role of the initial random scatter centers in the metalocomposite glass could be assumed by the silver nanoparticles, which have extremely high scattering cross section near to the SP resonance. At the same time, the anomalous heating of the exposed area by the single laser pulse could evoke the surface acoustic wave (SAW), which can contribute in the scattering processes. If the temperature overcomes the melting threshold, which is the case here, two additional instabilities could be involved: the capillary wave instability (CW) and the interference evaporation instability (IEI) [4.36]. Thus, the static and induced surface irregularities induce the scattered light, which interferes with initial incident laser radiation producing a special modulated light array on the surface. Since the optical density of the sample near to the surface is very high, the absorption of the interference patterns on the top results in an appropriate periodically modulated heating of the surface and following nonuniform coalescence of silver nanoparticles, melting and evaporation of silver from the top. In this way after relaxation a frozen grating of metal ripples embedded in glass with the periodicity  $\Lambda$  could be formed. As the next laser pulse comes, the preformed grating on the surface reinforces the intensity of the interference fringes playing a role of the positive feedback in growth of the regular structures presented in the Fig.4.10. In turn, the orientation as well as periodicity of the regular structures could be strongly affected by many factors: the type of the surface irregularities mostly contributing in the scattering processes (surface roughness, growing Ag nanoparticles, SAW, CW, IEI); temperature gradient induced by the Gaussian intensity profile of the laser beam; the angle of the incidence and laser wavelength. In conclusion, we have acknowledged the interference to be the cause of the formation of the periodical structures and briefly discussed probable physical mechanisms. However, observed effect still needs additional investigations, which certainly will be done in the in the near future.

## Chapter 5

# **First steps towards application of the fs laser induced dichroism in composite glass with spherical Ag nanoparticles**

In Chapter 3, we considered SP assisted modifications of the single spherical Ag nanoparticles embedded in soda-lime glass upon exposure to intense 150 fs laser pulses. The experimental data are indicating that the polarization dependent elongation of the shape of metal clusters is responsible for the laser induced dichroism in the composite glass. However, the linear and nonlinear optical properties of the composite medium caused by the SP resonance are strongly dependent on the host matrix, size, and shape as well as on distribution of the metal clusters. These factors could apparently affect the shape transformation processes induced by fs laser pulses. In this chapter, we will study the fs laser modifications in soda-lime glass with inhomogeneous distribution of the Ag nanoparticles. For instance, the opportunity of three-dimensional (3D) anisotropic structuring in samples with a fill factor gradient of silver clusters in the depth by multicolour irradiation with fs laser pulses. The idea is based on a selective wavelength excitation of Ag nanoparticles with proper fill factor, which in turn defines the spectral width and position of SP band. On the other hand, multicolour irradiation of such type of samples and subsequent laser modifications allow production of high contrast dichroic filters. This aspect will also be described in this chapter too. One should be noticed that in contrast with the samples containing aggregated Ag nanoparticles (filling factor about of 0.7) studied in previous chapter, experiments presented here were performed on the samples with maximal filling factor about of 0.3 near to the surface and decreasing in the depth. In spite of the considerable inhomogeneous broadening of the SP band caused by multipolar interactions between nanospheres, the distance between them is still longer than the size of the single particle. Thus, the induced dichroism presented in this chapter should be referred to as modification of the separated silver nanoparticles. Proposed techniques could be used in manufacturing of different 3D, polarization and wavelength selective micro-devices such as polarizers, filters, gratings, displays and rewriting optical data storage devices.

### 5.1. 3D anisotropic structuring in the glass with filling factor gradient of Ag nanoparticles in the depth.

As it has been shown in the Section 2.5, composite glass with Ag nanoparticles distributed near to the surface of the sample with fill factor gradient in the depth reveals the dependence of the absorption spectra on the depth. This opens a way for the wavelength selective excitation and modification of the nanoparticles with proper filling factor by fs laser pulses.

Irradiation of the samples was performed in multi-shot mode at three different wavelengths: by linearly polarized pulses at 400 nm derived from second harmonic generator (SHG), also 500 nm and 550 nm generated by optical parametric amplifier (OPA) with following sum frequency of signal and fundamental wavelength at 800nm. In each case, pulses with energy up to 20  $\mu\text{J}$  and temporal width of 150 fs were focused on the sample using a lens with focal length of 300mm yielding to a spot diameter of approximately 150 $\mu\text{m}$ . The sample was mounted on a motorized X-Y translation stage with its glass surface towards the incident beam. In each case square areas of approximately 3x3 mm<sup>2</sup> were written on the sample using multi shot

regime of the laser with a pulse density of approximately  $2 \times 10^4$  shots/mm<sup>2</sup>.

Under these conditions, irradiation of the samples by fs laser pulses resulted in similar changes of the extinction spectra as in the case of single nanoparticles (Chapter 3), i.e. splitting of the SP band and red-shift of the p-polarized band. However, in contrast to samples with low fill factor now also the longer laser wavelengths 500 nm and 550 nm caused strong spectral changes responsible for dichroitic coloration (Fig.5.1). In other words, a wavelength dependent dichroism is produced. Here we have to notice that irradiations of the samples were carried out from the glass substrate side as it is

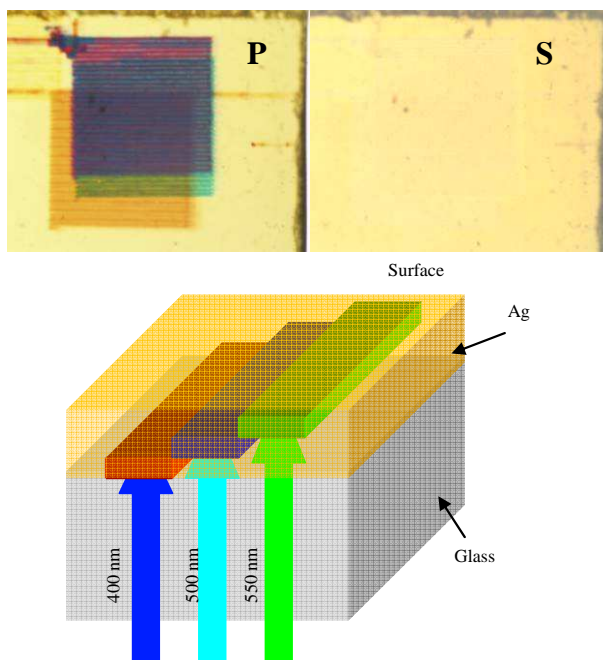


Fig.5.1 The glass sample with Ag nanoparticles irradiated at 400 nm (red), 500 nm (blue) and 550 nm (green) by 150 fs laser pulses. Images for p- and s-polarizations. Bottom: scheme of the sample irradiation.

shown in bottom of the Fig.5.1.

As is seen in Fig.5.2 (giving the p-polarized spectra), irradiation at  $\lambda = 400$  nm leads to the appearance of a SP band (seen as shoulder) at 470 nm, irradiation at 500 nm results in a band peaked at 570 nm, and irradiation at 550 nm produces a SP band at 660 nm. Here apparently the observed different red-shift of the SP peaks after irradiation at different wavelengths has to be explained by a combination of different aspect ratio of the particles and different dipol-dipol interactions between ellipsoids in different depths (i.e., at different fill factor). In all three cases there remains a strong absorption band close to 400 nm, indicating that a considerable part

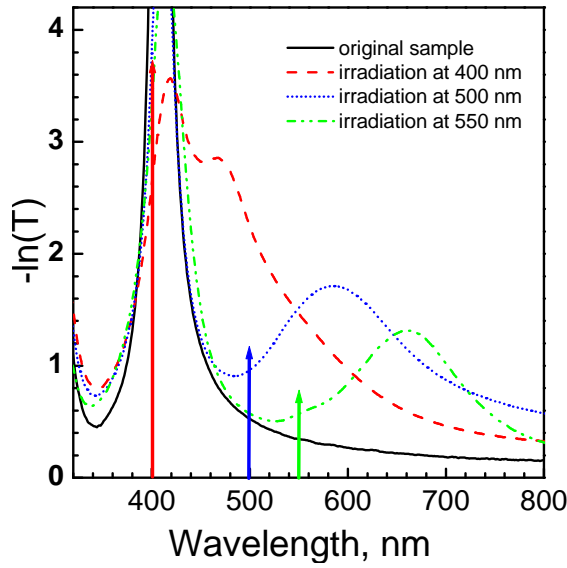


Fig.5.2 Extinction spectra (measured with light polarized parallel to the laser polarization) of original glass sample containing Ag nanoparticles with fill factor gradient; original spectrum (solid curve) and spectra after irradiation by fs laser pulses at  $\lambda = 400$  nm (dashed), 500 nm (dotted) and 550 nm (dash-dotted).

we define for the SP bands created by the different irradiation wavelengths a polarization contrast  $P$  given as the value of the peak absorption constant  $A_{\max}(\lambda)$  of the difference extinction spectra ( $A(\lambda) = \alpha_p(\lambda) - \alpha_s(\lambda)$ ), where  $\alpha$  denotes the usual absorption constant. This value  $P$  is closely

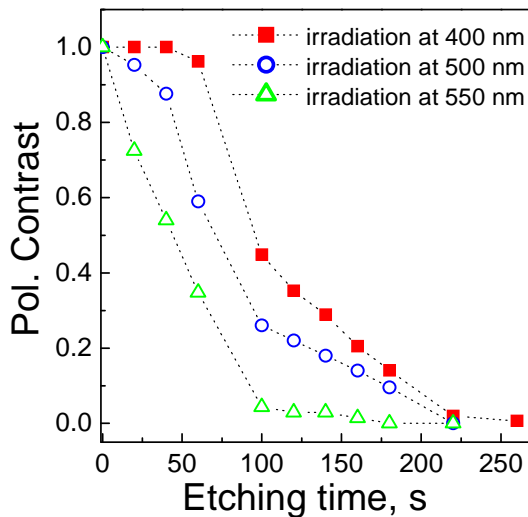


Fig.5.3 Evolution of Polarization contrast  $P$  (see text for definition) as a function of etching time in 12% HF acid, determined for three different sample regions, which were irradiated by fs laser pulses at  $\lambda = 400$  nm (squares), 500 nm (circles) and 550 nm (triangles).

of the silver nanoparticles has not been deformed to non-spherical shape. This can be taken as evidence for an inhomogeneous broadening of the SP band caused by the fill factor gradient of Ag nanoparticles (see Chapter 2), and for the possibility to deform particles in different depths selectively by irradiation of laser wavelengths adjusted to the SP band position (and thus fill factor) in that depth.

A second, direct proof for the modifications being located in different depths was obtained by etching of the sample in 12% HF acid and monitoring in a time interval of 20 seconds separately the extinction spectra of that etched areas, which had before been modified by irradiation at 400, 500, or 550 nm wavelength.

For convenience of presentation, we define for the SP bands created by the different irradiation wavelengths a polarization contrast  $P$  given as the value of the peak absorption constant  $A_{\max}(\lambda)$  of the difference extinction spectra ( $A(\lambda) = \alpha_p(\lambda) - \alpha_s(\lambda)$ ), where  $\alpha$  denotes the usual absorption constant. This value  $P$  is closely correlated with the anisotropic SP extinction bands of modified Ag nanoparticles with oblong shape (and uniform orientation), and can thus be used as an indicator for the content of such modified particles in the sample. Fig.5.3 gives the values we obtained during etching for the 3 different areas, normalized to the same starting value, as a function of etching time. Clearly the fading of the polarization contrast depends strongly on the excitation laser wavelength. While, e.g., the content of the Ag nanoparticles modified by irradiation at 550 nm has decreased by 50% already within the first 50 seconds, the polarization contrast  $P$  of the areas irradiated at 400 nm and 500 nm is almost unchanged after that time. The content of Ag nanoparticles modified at 500 nm (400 nm) reaches the level of 50%

## Chapter 5. First steps towards application of the fs laser induced dichroism in composite glass with spherical Ag nanoparticles

only after 75 s (100 s). In other words, irradiation at 550 nm affects mostly Ag nanoparticles with the highest fill factor, which are located near to the surface of the sample (see a picture in bottom of the Fig. 5.1), irradiation at a wavelength of 500 nm results in modifications in an intermediate region in larger distance from the sample surface, and the changes in extinction spectra induced by excitation at 400 nm are caused by modifications in the deepest layer (with respect to the sample surface) where collective interactions between Ag nanoparticles are negligible. It should be noted that this interpretation corresponds well with the visual impression which can be observed using a conventional stereo microscope.

It was tried also to irradiate the sample from the side containing Ag nanoparticles, as opposed to the irradiation from the glass substrate side used for all experiments described above. This approach did not lead to the same results, mostly because of the significant losses for each excitation wavelength caused by the broad absorption band of the upper layers with a high fill factor of Ag nanoparticles (compare Section 2.5, the Fig.2.12). Thus, in the case of irradiation onto the particle containing side one has to increase considerably the intensity of the laser pulses in order to increase the penetration depth of the laser light into the sample. This, however, results in spectral changes mostly in the upper layer preventing the selective modifications in the depth obtained by irradiation through the neat glass side. On the other hand, in the Section 5.3 of this chapter it will be shown how multicolor exposure from the layer side can be used for producing of high contrast wavelength selective dichroic filters.

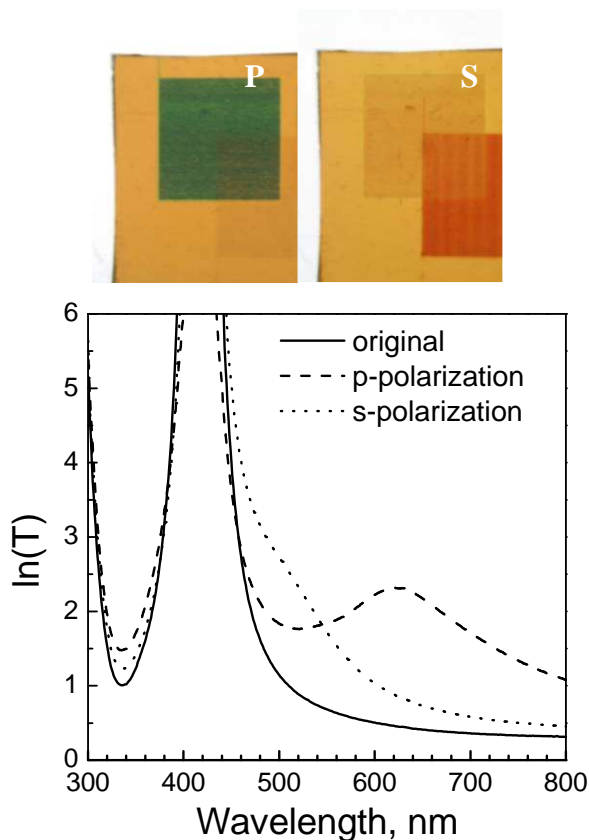


Fig. 5.4 Irradiation of the samples with Ag nanoparticles at 400 nm and 550 nm in crossed polarizations: in top – image of the sample in polarized light; bottom – polarized extinction spectra of overlapping area between irradiated fields on the sample.

It is obvious that presented technique has a large potential for a number of applications including 3D micro-structured, dichroic optical devices or optical 3D data storage, which in turn will be discussed in the next section. In this context it is important to notice that the sequence of irradiation wavelengths of the fs laser pulses should be done in the direction of wavelength decrease (550 nm, 500 nm, 400 nm), since otherwise, due to the red-shifted SP band (p-polarization) of the deformed oblong nanoparticles, the modifications in the deeper layer will be partially ‘destroyed’ by the laser pulses at longer wavelengths necessary to manipulate regions closer to the sample surface. Applying instead subsequently wavelengths in a decreasing order, one can first modify the close-to-surface layers with maximal fill factor, showing maximal red shift of the SP band in the spectra (Section 2.5, the

## *Chapter 5. First steps towards application of the fs laser induced dichroism in composite glass with spherical Ag nanoparticles*

Fig.2.12). Then by tuning of the laser radiation towards shorter wavelengths, the deeper regions having a lower fill factor of silver inclusions can be addressed, moving the region where modifications happen away from the sample surface, while the already modified areas remain unchanged.

As the proposed technique of multicolor irradiation gives an opportunity to create the discrete dichroic layers in the composite glass containing silver clusters, there are not obstacles to use multicolor laser pulses with different polarization for production of layered structures with special optical properties. For instance, two fields shown in the top of Fig.5.4 were irradiated at 550 nm and 400 nm with crossed polarizations to each other. Indication of p-polarization corresponds in this case to the direction of the laser polarization at 550 nm, while s-polarization is assigned parallel to the laser polarization at 400 nm. This procedure is changing the original yellow color of the exposed at 400 nm and 550 nm fields on the sample into red (s-polarization) and green (p-polarization), respectively. Furthermore, rotation of the light polarization demonstrates an alternating bleaching of the both irradiated regions (Fig.5.4). At the same time, overlapping area between the irradiated fields represents combination of optical properties of both. Thus, change of the polarization switches the color of the mixed region from green into red. Furthermore, extinction spectra of the irradiated areas (Fig.5.4) demonstrate appearance of the additional absorption bands in right side from original SP resonance with maximum about of 413 nm: at 500 nm after irradiation at 400 nm and at 620 nm after exposure at 550 nm. In both cases, these bands we observed only in polarization parallel to the polarization of laser pulses used for modification. However, overlapping area demonstrates both resonances in mutually perpendicular polarizations (see Fig.5.4). This result is an additional convincing prove of the formation of the independent dichroic layers in the depth upon multicolor irradiation with fs laser pulses.

In addition, as well as in the work of Dr. M. Kaempfe [5.6], we have observed that heating of the sample to approximately 600 °C or re-radiation of modified regions by a cw- or Q-switched laser at 532 nm near to the SP band restores the original extinction spectra, being identical within experimental accuracy with those of the samples before irradiation. This indicates a relaxation of the silver nanoparticles back to their initial, spherical shape. For 532 nm laser irradiation, the laser polarization had to be appropriately aligned for effective excitation of SP band. This results in local heating of the sample over the glass transition temperature and relaxation of modified Ag nanoparticles. Thus, the whole transformation process described here is in principle reversible, and thus the nanostructured materials consisting of metal nanoparticles in glass, in combination with tunable fs or ps laser sources, could potentially be used for very long-lived, but nevertheless rewritable data storage devices. In turn, the next section we will consider an opportunity to use the composite glass with embedded Ag nanoparticles in 3D optical data storage.

## 5.2 Composite glass with Ag nanoparticles as a promising media for 3D optical data storage by spectral coding.

In the last two decades composite materials containing metal nanoparticles found various applications in different fields of science and technology. The fact that the SP strongly depends on the host matrix, shape and distribution of metal nanoparticles [5.1, 5.2, 5.7], allows to use the composite materials in development of novel optical devices with unique linear and nonlinear optical properties. For instance, the dependence of the SP resonance on the shape of Ag nanoparticles was used for optical data storage by spectral coding [5.8-5.9]. In combination with the fs laser assisted shape modification of spherical Ag nanoparticles in glass this method opens up a route for using composite material containing Ag nanoparticles as medium for optical data storage. Moreover, the capacity of the optical data storage devices can be extremely enhanced using multiple wavelengths and multiple coding layers [5.10-5.11]. In turn, in the last section we demonstrated an opportunity to control the depth of the anisotropic modifications in the composite glass with varying fill factor of Ag nanoparticles by attenuation of the excitation wavelength. Moreover, the fs laser induced dichroism in composite glass opens a way to enhance the data capacity using the laser polarization for spectral data coding. Reversibility of the fs laser induced modifications by heating of the sample up to glass transition temperature let us to discuss a creation of the new rewritable 3D optical data storage devices on the basis of the Ag nanoparticles incorporated in glass matrix.

The storage capacity of an optical disk (Fig.5.5) can be expressed as follows

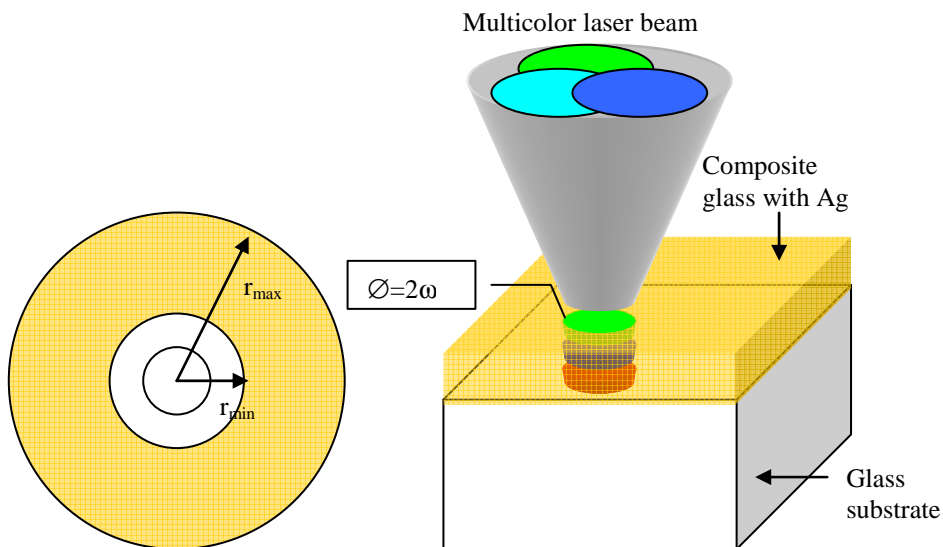


Fig.5.5 Schematic illustration of multiwavelength multilayer optical disc.

$$C = \frac{NM(r_{\max}^2 - r_{\min}^2)}{\omega^2}, \quad 5.1$$

where  $\omega$  is the spot size of the modified area (storage unit),  $r_{\max}=58$  mm and  $r_{\min}=25$  mm are typical values for the standard CD,  $N$  is a number of the layer used in the storage unit,  $M$  is a number of bits stored in the single layer of the storage unit. According to the Eq.5.1 there are three ways for enhancement of the data capacity of an optical disc: 1) minimization of the size of the modified region (storage unit); 2) usage of the multilayer structures; 3) increase of a number of logical states in the single layer of the storage unit.

Hence, in this part of my thesis we will show a principle, which could be used for creation of high density 3D optical data disc on the basis of composite glass with embedded Ag nanoparticles.

### 5.2.1. Effect of the peak pulse intensity on the spot size of the modified area in composite glass with Ag nanoparticles.

Since invention of the first optical CD in 1981 and development of the first CD-ROM in 1985 by Philips and Hitachi the optical storage technology stirred much interest of many researcher groups and manufacturers working on enhancement of the data storage capacity of novel optical storage media. A drastic increase of the data capacity of the recent developed optical discs in the last decade was mainly achieved by minimization of the size of burned defect in the active layer as well as by reduction of the gap between burned bits. Moreover, since writing technique is based on thermal effects induced in the active layer by CW lasers, the size of the stored bits is defined by the diffraction limit of the focused laser beam. In turn, as it has already been discussed in Chapter 2, the spot size (spot radius) of a laser beam can be given as

$$\omega = \frac{\lambda M^2}{\pi \cdot N.A.}, \quad 5.2$$

where  $\lambda$  is the laser wavelength, N.A. is the numerical aperture of a focusing objective,  $M^2$  is the beam quality factor. Thus, shorter laser wavelengths and larger N.A. lead to the decrease of the laser spot size and consequently minimization of the burned bit on the disc. In turn, change of the writing wavelength from 780 nm (CD) to 640 nm (DVD) (Fig.5.6)

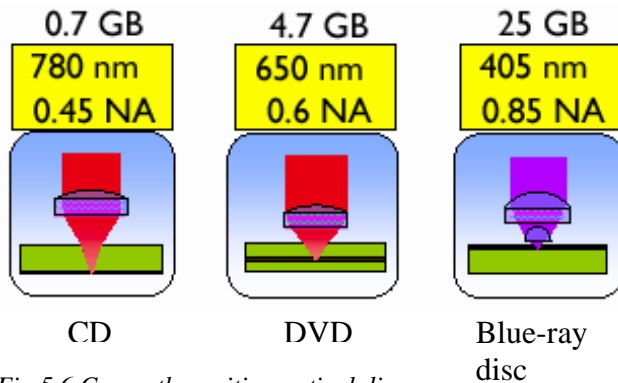


Fig.5.6 Currently exciting optical discs.  
Origin: Ref.[5.12]

allowed to increase the storage capacity from 700 MB on CD up to 4.7GB on DVD. Appearance of the blue laser diodes emitting at 405 nm has facilitated to raise the recording data volume up to 25 GB in so-called Blue-ray discs. Moreover, in October 2004 JVC, also known as Victor Company of Japan, announced that it has

## Chapter 5. First steps towards application of the fs laser induced dichroism in composite glass with spherical Ag nanoparticles

developed the world's first single lens with a numeric aperture of 0.95. In principle, the new lens can boost the capacity of a 12cm-diameter single-layer disc to more than 40GB of data. However, the diffraction limit is still a main restricting factor for the size of the logical unit.

One of the ways to overcome the diffraction limit is via usage of the intense

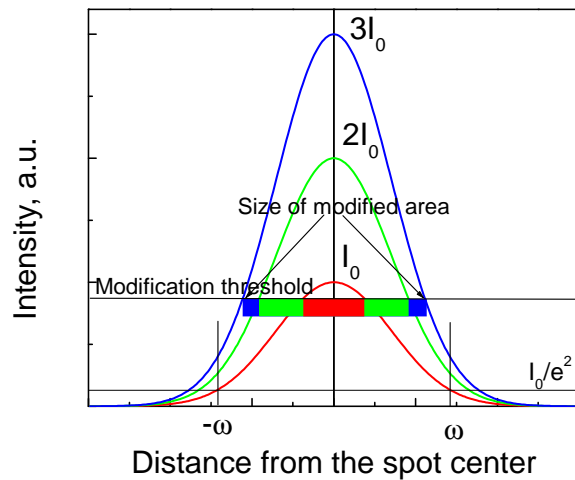


Fig.5.7 Schematic explanation of the size control of modified area by variation of the peak pulse intensity.

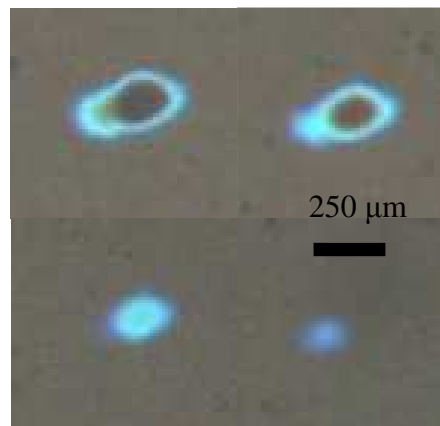


Fig.5.8 Dichroic spots on the sample formed by laser pulses with different peak pulse intensities.

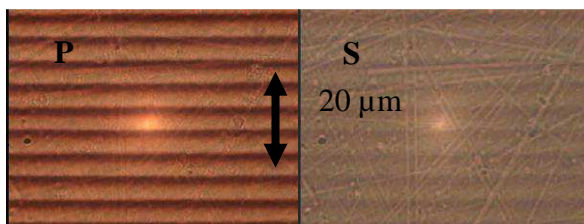


Fig.5.9. Dichroitic grating written in composite glass containing Ag nanoparticles with fs laser pulses at 400 nm.

fs laser pulses and nonlinear processes in the media for recording of information. As a fact, production of 100 nm structures is possible by ablation of chromium film exposed to induced fs laser pulses at 780 nm [5.13]. The idea was to use the peak laser fluence slightly above the ablation threshold. In such case modifications occurs only in the central part of the beam producing sub-diffraction structures.

In Chapter 3 it has been shown that fs laser assisted anisotropic modifications in the composite glass with Ag nanoparticles appear only by overcoming of a certain threshold. Obviously, using pulses with peak intensities slightly above the modification threshold (see Fig.5.7) allows to minimize the modified region in composite glass.

Presented in Fig.5.8 sample was irradiated at 400 nm with 150 fs laser pulses and was actually used to study intensity dependences presented in Chapter 3. The laser beam was focused in the spot with diameter about of 270  $\mu\text{m}$  by the lens with 300 mm focus length (the sample wasn't placed in the focus). Four spots on the sample shown in the Fig.5.8 are corresponding to the pulses with energies 100  $\mu\text{J}$  (2.4  $\text{TW}/\text{cm}^2$ ), 60  $\mu\text{J}$  (1.44  $\text{TW}/\text{cm}^2$ ), 40  $\mu\text{J}$  (0.96  $\text{TW}/\text{cm}^2$ ), 20  $\mu\text{J}$  (0.45  $\text{TW}/\text{cm}^2$ ). As it was predicted by the scheme in the Fig.5.7, decrease of the peak pulse intensity leads to significant reduction of the diameter of the modified region being much smaller as the laser spot width. Moreover, usage of the 15x mirror objective with N.A. = 0.28 allows to

## Chapter 5. First steps towards application of the fs laser induced dichroism in composite glass with spherical Ag nanoparticles

achieve in our conditions the laser spot size not less as 2  $\mu\text{m}$ . However, appropriate selection of the peak pulse intensity allows to generate modifications in submicron scales. Fig.5.9 presents a dichroic grating with lines width lower as 1  $\mu\text{m}$  and distance of 5  $\mu\text{m}$  obtained in the glass with Ag clusters.

Obviously, optimization of the focusing system and laser beam quality ( $M^2$ ) of the burning system allows to overcome the diffraction limit and to minimize the size of modified region down to wavelength scales.

### 5.2.2. Spectral data coding in composite glass with Ag nanoparticles exposed to fs laser pulses

In previous section we discussed an opportunity to increase the data recording density in the glass containing Ag nanoparticles by minimization of the modified area. On the other hand, the high storage density in optical discs can be achieved by coding of information in several active layers [5.10, 5.11]. In section 5.1 the formation of the discrete anisotropic layers in the glass samples with inhomogeneous distribution of Ag nanoparticles in the depth was demonstrated by exposure to multicolor fs laser pulses. Moreover, the depth of the modified layers is defined by the excitation wavelength. Simplicity of the proposed procedure allows us to suggest this technique for coding of information in anisotropic layers created by fs laser excitation. In this case, the number of wavelengths used for the disc burning defines number of active layers and increases linearly the data capacity. In Section 5.1 we demonstrated irradiation of the samples at tree different wavelength (400 nm, 500 nm and 550 nm). However, there are not visible obstacles to increase a number of incident wavelengths using for example wavelength division of the supercontinuum generated in the photonic crystal fiber [5.14, 5.15]. At the same time, samples used for 3D optical data storage require an optimization of the distribution function of the metal clusters in the depth. Obviously, the ideal medium for such type of the data storage would be a disk with stacked glass layers containing Ag nanoparticles, which differ from each other by filling factor of silver clusters. In this case, each layer excited independently by appropriate wavelength.

In addition, multiplexing of the data in each dichroic layer can be obtained by spectral data coding using the polarization dependence of the SP resonance of ellipsoidal metal nanoparticles [5.8]. In our case, the orientation of the modified Ag

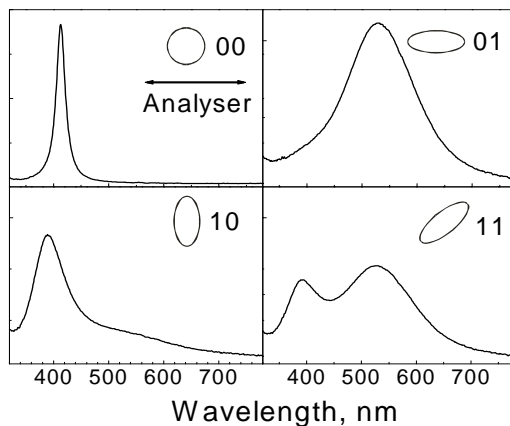


Fig.5.10 Spectral coding of two bits of information by variation of writing laser polarization and shape modification of spherical Ag nanoparticles in glass

nanoparticles embedded in the glass is assigned by direction of the laser polarization during irradiation and can be simply switched during burning process. Thus, by irradiation of a single layer using three different orientations of the laser polarization (angle between the laser polarization and polarization of analyzer is  $0^\circ$ ,  $45^\circ$  and  $90^\circ$ ), it is possible to achieve four independent logic states given by a set of four extinction spectra of modified Ag clusters (see Fig. 5.10). In turn, the spectra were measured by constant polarization direction of the

## *Chapter 5. First steps towards application of the fs laser induced dichroism in composite glass with spherical Ag nanoparticles*

---

analyzer. Obtained set of the four different spectra corresponds with two data bits of the storage unit in the single layer. Using even three wavelengths and three laser polarization directions to exposure the glass sample with filling factor gradient of Ag nanoparticles the storage density of the disc can be enhanced by factor 6. It means that the data capacity of the simple DVDs could be enhanced up to 30 GB, which is higher than modern HD-DVD and Blue-Ray Discs. Appropriate choice of the peak pulse intensity and reduction of the spot size, in addition to increase of the number of wavelengths used for multicolor burning and optimization of the fill factor gradient and usage of discs with several silver containing layers could significantly enhance the capacity of this optical disc.

In addition, as it has already been pointed out, observed fs laser induced modifications in composite glass with Ag nanoparticles are reversible by heating at approximately 600 °C or re-radiation of the modified region by a cw or Q-switched laser at 532 nm near to the SP band. This fact demonstrates a significant advantage of the proposed technique, which allows development of high-density rewritable optical glass discs with embedded metal nanoparticles.

### 5.3. Preparation of high contrast structural polarizer in composite glass with Ag nanoparticle by multicolor fs laser irradiation

In Chapter 3 we considered modification of the single spherical Ag nanoparticles in the soda-lime glass upon exposure to intense fs laser pulses near to the SP resonance. This procedure leads to the laser induced dichroism of the SP bands in extinction spectra caused by the elongation of initially spherical shape of the Ag clusters. Obviously, observed effects could find a broad application in the different fields of science and technology. For instance, in previous section we proposed technique for 3D high density optical data storage using fs laser induced dichroism in the composite glass containing silver clusters. Here it will be shown that fs laser processing of such glass can be used for manufacture of wavelength selective high contrast structured polarizers.

The laser induced dichroism studies in Chapter 3 were carried out on the samples, where the thickness of the glass layer with Ag nanoparticles was less or equal to the laser beam penetration depth. Such optically thin samples allow us to achieve maximal homogeneity of the irradiated region. On the other hand, the low optical density restricted the contrast of the induced dichroism. In order to produce high contrast dichroitic filters we need obviously samples with thick photosensitive layer containing high concentration of Ag nanoparticles. In particular, increase of the fill factor of Ag clusters in the glass allows CORNING and CODIXX AG to produce broad band polarizers with optical density much higher as 3 and the contrast up to  $10^5$  just by mechanical stretching of glass heated up to transition temperature.

On the other hand, the depth of modifications in composite glass with high fraction of silver nanoclusters is restricted by small laser beam penetration in the sample due to high absorption coefficient. Increase of the peak pulse intensity will evoke inhomogeneous modifications of silver clusters in the depth: near to the surface high pulse intensity leads to the destruction of the nanoparticles giving the

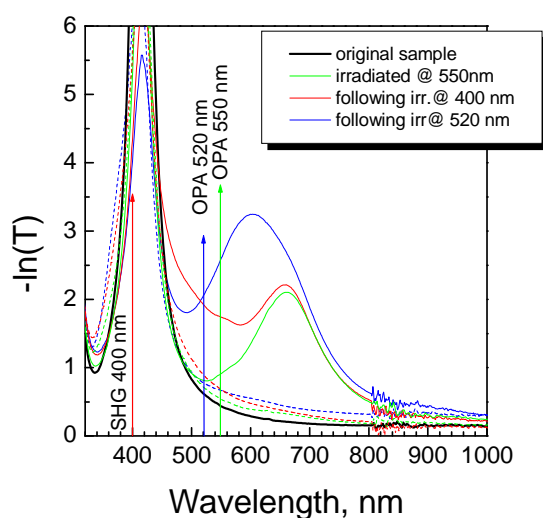


Fig.5.11 Extinction spectra of the composite glass with silver nanoparticles subjected to the multiple irradiation at 400 nm, 520 nm and 550 nm. Solid lines - p-polarisation, dotted lines - s-polarisation.

isotropic contribution in extinction spectra (see Chapter 3) and minor elongation of Ag clusters in the depth responsible for the observed dichroism. However, this problem can be solved using subsequent modification by multicolor fs laser irradiation. The idea is to use attenuation of the excitation wavelength to modify samples layer by layer in the depth.

For experiments, we used samples with spherical Ag nanoparticles provided by CODIXX AG. Irradiation conditions were similar to the case of 3D anisotropic structuring (see Section 5.1): three wavelengths 400 nm, 520 nm and 550 nm were used for

## Chapter 5. First steps towards application of the fs laser induced dichroism in composite glass with spherical Ag nanoparticles

excitation. However, exposure of the samples was carried out from the side with layer containing Ag nanoparticles. The peak pulse intensity was chosen slightly above the modification threshold. This allows to achieve modifications only in thin layer (less than penetration depth).

First, we have exposed the sample to fs laser pulses at 550 nm leading to appearance of an additional absorption band near to 660 nm in p-polarized extinction spectra (Fig.5.11). As it has been shown in the Section 5.1, observed spectral changes can be associated with modification of the Ag nanoparticles with maximal filling factor and distributed near to the surface (Fig.5.12). After that, we irradiated the same area on the sample at 400 nm with the same laser polarization. Since the SP resonance of the nanoparticles in the upper layer is shifted towards longer wavelengths, the penetration depth of the laser pulses at 400 nm increases. Thus, the laser pulses affect on silver clusters

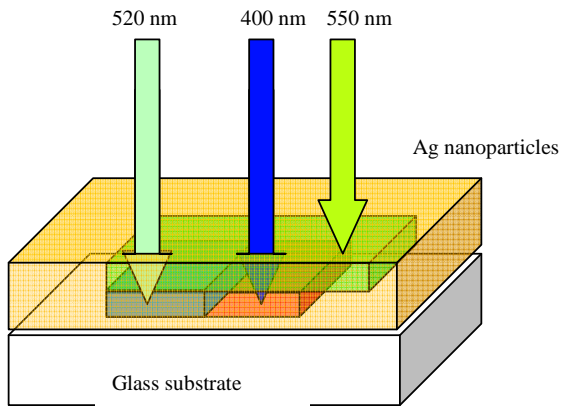


Fig.5.12 Scheme of the preparation of the high contrast dichroic filters by multicolour irradiation of the composite glass with Ag nanoparticles

placed in the deeper regions. This results in the following alteration in the extinction spectra indicating additive increase of the absorption between 500 and 600 nm. Scanning of the laser beam through the sample was performed many times until the spectral changes reach a steady state. It means that all the available nanoparticles for laser radiation are modified, and SP band was shifted in red spectral range but the residual absorption obviously prevents excitation of clusters in the depth of the sample. However, as it was found in Chapter 3, deformed by fs laser pulses Ag nanoparticles are able to subsequent modifications induced by excitation at second wavelength coinciding with SP resonance. Hence, irradiated sample was subjected to the following exposure at 520 nm resulting in subsequent particles transformations in recently modified layer responsible for the following shift of the SP resonance to 600 nm and spectral hole burning at 500 nm. In this way the absorption losses at 400 nm can be significantly decreased in modified layers (penetration depth is increased) and deeper regions in the sample become available for the following modification by fs laser pulses at 400 nm. This procedure can be performed many times until modification of whole amount of the nanoparticles in the sample. Using the chosen excitation wavelengths we obtained an dichroic area with absorption maximum in extinction spectra peaked near 600 nm. Moreover, the spectral contrast in the modified area (a ratio between transmittance of the sample in the s- and p-polarizations with extraction of the reflection losses from the glass surface) was calculated to be about 20 at 600 nm. Obviously, using another combination of the excitation wavelengths it's possible to produce filters with appropriate spectral characteristics. It's important to point out, that the thickness of the active layer in these samples was about 6  $\mu\text{m}$ . Since the contrast is exponentially rising with the thickness, increase of the silver containing glass layers will considerably improve the contrast of the dichroic filter produced by exposure to the fs laser pulses.

In conclusion to this chapter, the fs laser induced modifications have been studied in the composite glass with Ag nanoparticles distributed in the depth with

## *Chapter 5. First steps towards application of the fs laser induced dichroism in composite glass with spherical Ag nanoparticles*

---

strong filling factor gradient. It was shown that exposure of such samples to fs laser pulses at various wavelengths can lead to formation of discrete anisotropic layers in the depth. In turn, the distances of the modified layers from the surface as well as spectral properties are defined by the excitation wavelength and local fraction of Ag nanoparticles in the sample. Demonstrated technique opens us an opportunity for 3D microstructuring in the composite glass by means of fs multicolor laser radiation and can be used for various applications. For instance, 3D structuring as well as anisotropic character of the laser induced modification can be used for optical spectral data coding and offer the composite glass with Ag nanoparticles as a promising medium for development of novel optical high density storage devices. Moreover, the strong intensity dependence of the fs laser dichroism and appropriately chosen peak pulse intensity allow to overcome the diffraction limit of the size of burning unit, which will drastically increase the data storage capacity. The main advantage of the composite glass with Ag nanoclusters is that that the heating in oven as well as local heating by exposure to Q-switched or CW lasers near to the SP band result in the reversibility of the fs laser induced modifications. This allows to use this technique for creation of rewriting sources for optical data storage. On other hand, multicolour irradiation of the composite glass with Ag nanoparticles can be effectively used for manufacturing of high contrast structured polarizers and microfilters. Nevertheless, we believe that this approach could find many additional applications in development of different 3D polarization and wavelength selective microdevices such as polarizers, filters, gratings, RGB and DWDM devices, optical and plasmonic embedded circuits.

## Chapter 6

# Summary and outlook

Owing to the outstanding optical properties and growing demand on miniaturization of integrated optics, metal nanostructures become beyond all comparison to break a sub-diffraction limit in creation of integrated circuits and optical elements. Thus, studies of the plasmonic materials remain a hot, active and expanding field of science and technology. Moreover, manufacturing of novel nanocomposites, micro- and nanodevices with specific features require development of powerful and flexible techniques to control and optimize their structural and optical properties. In this context, studies of the laser assisted modifications in the composite glass with Ag nanoparticles presented in this work demonstrate a simple way to manipulate the shape and distribution of the metal clusters, which in turn define the alterations of optical properties.

For instance, excitation of the spherical single Ag nanoparticles embedded in soda lime-glass by polarized fs laser pulses close to the SP resonance results in formation of uniformly oriented oblong silver clusters. Moreover, the orientation perpendicular or parallel to the laser polarisation is defined by the laser peak pulse intensity used for irradiation. Thus, pulse intensities slightly above the modification threshold lead to the elongation of the silver nanoparticle parallel to the laser polarisation. On the other hand, increase in the peak pulse intensity in one order of magnitude results in spheroids aligned perpendicular to the laser polarization. The temperature effects, luminescence studies of the modified samples as well as relaxation dynamics measurements indicate the SP assisted photoemission of electrons and ionization of the silver nanoparticles resulting in growth of silver cation content in vicinity to the cluster. Moreover, experimental data indicate ionization and formation of colour centers in the glass matrix (apparently close to the surface of metal nanoparticle) accompanying the cluster modifications upon exposure to fs laser pulses. According to the acquired experimental results a mechanism of the shape modifications was proposed.

However, there are many questions, which still need additional investigations. One of them is that up to now we have very poor information concerning a time scale of dichroism formation in the composite glass. In order to clarify this fact, the polarisation dependent pump-probe experiments are required. On the other hand, the contribution of glass matrix in the modification processes should be thoroughly studied. In turn, according to the proposed model, the threshold of the induced modifications is defined by injection of photoelectrons in the glass matrix. Hence, the energy manifold of the host matrix should strongly affect the tunnelling

of electrons and apparently the modification threshold. Thus, the fs laser induced modification of Ag nanoparticles should be studied in glasses with various cationic compositions.

Other effects were demonstrated in the system with aggregated Ag nanospheres upon irradiation with fs and ns laser pulses near to the SP resonance. For instance, exposure of the compact packed metal clusters to intense fs laser pulses reveal a formation of oblong metal clusters aligned parallel to the laser polarization, which are responsible for the induced dichroism in reflection spectra. Detailed analysis of the experimental data clearly testifies that observed modification occurs due to junction of the contacting clusters in direction to the laser polarisation caused by strong dipole-dipole interactions. In turn, the wavelength dependence of the induced modifications was demonstrated and could be associated with excitation of different collective modes. However, this assumption needs additional investigations.

On the other hand, excitation of the aggregated Ag nanoparticles with the ns laser pulses at 527 nm near to the SP resonance produces high thermal inhomogeneities in the surface region and results in the ripening of the periodical chain-like silver structures distributed in the glass. The periodicity about 500 nm and development of the observed structures in multi-shot regime allowed us to suppose formation of the so called Wood's structures caused by interference between the light scattered by the induced inhomogeneities and the incident laser beam. The exposed region demonstrated strong alterations in the reflectivity caused by the induced structural modifications in thin upper glass layer with aggregated nanoparticles. However, these are only the first results and observed effects should be extensively studied in the future.

In conclusion, proposed techniques could find many applications in development of different 3D polarization and wavelength selective microdevices such as polarizers, filters, gratings, RGB and DWDM devices, optical and plasmonic embedded circuits, and optical data storage devices.

## References

- 1.1.A.Yariv, "Quantum Electronics", 3<sup>rd</sup> ed. Wiley&Sons, N.Y.1989.
- 1.2.A. Miller, D.M. Finlayson, "Laser sources and applications", Proceedings of the 47<sup>th</sup> SUSSP St.Andrews, 1995.
- 1.3.H.Rabin, C.L.Tang, "Quantum electronics: a treatise", 537 p. Acad. Press, N.Y. 1975.
- 1.4.R.A. Alfano, "The Supercontinuum Laser Source", 458 p., Springer Verlag, N.Y.1989.
- 1.5.O.M. Efimov, K.Gabel, S.V.Garnov, L.B. Glebov, S.Grantham, M.Richardson, M.J.Soileau, "Color-center generation in silicate glass exposed to infrared femtosecond pulses", JOSAB15, p.193 (1998).
- 1.6.C.B. Schaffer, PhD thesis, Harvard University (2001).
- 1.7.L.V.Keldish, Sov.Phys.JEPT 20, 1307 (1965).
- 1.8.G.Mie, Ann.Phys.(Leipzig) 25, 377 (1908).
- 1.9.U. Kreibig, M. Vollmer: *Optical Properties of Metal Clusters*, Springer Series in Materials Science, Vol. 25 (Springer Berlin 1995).
- 1.10. V. M. Shalaev: *Optical Properties of Nanostructured Random Media* (Springer Berlin 2001).
- 1.11. J. Tominaga, D.P. Tsai: *The Manipulation of Surface and Local Plasmons*, Topics in Applied Physics (Springer, Berlin, 2003).
- 1.12. J.D.Jackson, "Klassische Elektrodynamik", Walter de Gruyter, Berlin; N.Y., 1982.
- 1.13. V.V. Kresin, "Collective resonances in silver clusters: role of d-electrons and the polarization free surface layer", Phys. Rev. B 51, p.1844 (1995).
- 1.14. K.-J.Berg, A.Berger, , H.Hofmeister, Z. Physik D20, 309(1991).
- 1.15. A. Hilger, M. Tenfelde, U. Kreibig, " Silver nanoparticles deposited on dielectric surfaces ", Appl. Phys. B 73, 361–372 (2001).
- 1.16. J.Postendorfer, "Numerische Berechnung von Extinktions- und Streuspektren sphäroidaler Metallpartikel beliebiger Größe in dielektrischer Matrix", Dissertation, Martin-Luther University Halle-Wittenberg, 1997.
- 1.17. J.P. Marton, J.R. Lemon, Phys. Rev. B 4, 271 (1971).
- 1.18. G. Xu, M. Tazawa, P. Jin, S. Nakao, Appl. Phys. A (online first, 28 January 2004).
- 1.19. V.A. Markel, L.S. Muratov, M.I. Stockman, T.F. George: Phys. Rev. B 43, 8183 (1991).
- 1.20. V.A. Markel, V. Shalaev, E.B. Stechel, W. Kim, R.L. Armstrong: Phys. Rev. B 53, 2425 (1996).
- 1.21. S. V. Karpov, A. L. Bas'ko, A. K. Popov, V. V. Slabko, T. F. George, in: *Recent Research Developments in Optics, vol. 2*, pp.427-463 (Research Signpost, Trivandrum, India, 2002).
- 1.22. J.I. Gittleman, B. Abeles, „Composition of the effective medium and the Maxwell-Garnett predictions for the dielectric constants of granular metals“, Phys.Rev. B 15, p.3273(1977).

## References

---

- 1.23. W.Rechberger, A.Hohenau, A.Leitner, J.R.Krenn, B.Lamprecht, F.R.Aussenegg, „Optical properties of two interacting gold nanoparticles“, *Opt.Comm.* 220, p.137-141 (2003).
- 2.1. P.F. Moulton: *Opt. News* 8, 9 (1982)
- 2.2. P.F. Moulton: *J. Opt. Soc. Am. B* 3, 125 (1986)
- 2.3. P.F. Moulton: In *Tunable Solid-State Lasers*, ed. by P. Hammerling, A.B. Budgor, A.A. Pinto (Springer Ser. Opt. Sci. 47) (Springer, Berlin, Heidelberg 1985) pp. 4–10.
- 2.4. R. Rao, G. Vaillancourt, H.S. Kwok, C.P. Khattak: In *Tunable Solid-State Lasers* (OSA Proceedings Series), Vol. 5, ed. by M.L. Shand, H.P. Jenssen (Optical Society of America, Washington, DC 1989) pp. 39–41.
- 2.5. M.S. Pshenichnikov, A. Baltuska, R. Szipöcz, D.A. Wiersma: *Ultrafast Phenomena XI* (Springer, Berlin 1998) pp. 3–7
- 2.6. Z. Cheng, G. Tempea, T. Brabec, K. Ferenc, C. Spielmann, F. Krausz: *Ultrafast Phenomena XI* (Springer, Berlin 1998) p. 8
- 2.7. A. Baltuska, Z. Wei, M.S. Pshenichnikov, D.A. Wiersma: *Opt. Lett.* 22, 102 (1997).
- 2.8. M. Nisoli, S. De Silvestri, O. Svelto, R. Szipöcs, K. Ferenc, C. Spielmann, S. Sartania, F. Krausz: *Opt. Lett.* 22, 522 (1997)
- 2.9. A.E. Siegman, „Analysis of laser beam quality degradation caused by quadratic phase aberrations“, *Appl.Opt.*32, p.5893(1993).
- 2.10. A.E.Siegman, “Lasers”, Mill Valley, CA:Univ.Sci.Books,1986.
- 2.11. W.A.Clarkson, D.C.Hanna, *Opt.Lett.* 21, p.375(1996).
- 2.12. R.A. Alfano, “The Supercontinuum Laser Source”, 458 p., Springer Verlag, N.Y.1989.
- 2.13. S.A. Kovalenko, A.L. Dobryakov, J. Ruthmann, N.P. Ernsing, *Phys.Rev.A* 59, 1999, p.2369.
- 2.14. K.-J. Berg, A. Berger, H. Hofmeister, *Z. Phys. D* 20 (1991) 309
- 2.15. H.Hofmeister, W.-G. Drost, A. Berger, *Nanostruct. Mater.* 12, 207 (1999).
- 3.1.U. Kreibig, M. Vollmer: *Optical Properties of Metal Clusters*, Springer Series in Materials Science, Vol. 25 (Springer Berlin 1995).
- 3.2.V. M. Shalaev: *Optical Properties of Nanostructured Random Media* (Springer Berlin 2001).
- 3.3.J. Tominaga, D.P. Tsai: *The Manipulation of Surface and Local Plasmons*, Topics in Applied Physics (Springer, Berlin, 2003).
- 3.4.T. Wenzel, J. Bosbach, A. Goldmann, F. Stietz, F. Träger: *Appl. Phys. B* 69, 513 (1999).
- 3.5.F. Stietz: *Appl. Phys. A* 72, 381 (2001).
- 3.6.R. Jin, Y.W. Cao, C.A. Mirkin, K.L. Kelly, G.C. Schatz, J.G. Zheng: *Science* 249, 1901 (2001).
- 3.7.M. Kaempfe, H. Graener, A. Kiesow, A. Heilmann: *Appl. Phys. Lett.* 79, 1876 (2001).
- 3.8.A.L. Stepanov, D.E. Hole, A.A. Bukharaev, P.D. Townsend, N.I. Nurgazizov: *Appl. Surf. Sci.* 136, 298 (1998).

## References

---

- 3.9.A.L. Stepanov, "Modification of implanted metal nanoparticles in the dielectrics by high-power laser pulses", *Rev.Adv.mater.Sci.*4, p.123(2003).
- 3.10. I. Zergioti, S. Mailis, N.A. Vainos, P. Papakonstantinou, C. Kalpouzos, C.P. Grigoropoulos, C. Fotakis: *Appl. Phys. A* **66**, 579 (1998).
- 3.11. E.J. Bjerneld, F. Svedberg, M. Kaell: *Nano Lett.* **3**, 593 (2003).
- 3.12. M. Kaempfe, G. Seifert, K.-J. Berg, H. Hofmeister, H. Graener: *Eur. Phys. J. D* **16**, 237 (2001).
- 3.13. M. Kaempfe, T. Rainer, K.-J. Berg, G. Seifert, H. Graener: *Appl. Phys. Lett.* **74**, 1200 (1999).
- 3.14. M.Kaempfe, "Laserinduzierte deformation metalischer Nanopartikel in Glaeser", Dissertation, Martin-Luther University Halle-Wittenberg, 2000.
- 3.15. G. Seifert, M. Kaempfe, K.-J. Berg, H. Graener: *Appl. Phys. B* **71**, 795 (2000).
- 3.16. G. Seifert, M. Kaempfe, K.-J. Berg, H. Graener: *Appl. Phys. B.* **73**, 355 (2001).
- 3.17. D.Du, X.Liu, G.Korn, J Squier, G.Mourou, "Laser induced breakdown by impact ionization in SiO<sub>2</sub> with pulse widths from 7 ns to 150 fs", *Appl.Phys.Lett.* 64, 3071-3073 (1994).
- 3.18. D.Du, X.Liu, G.Mourou, "Reduction of multi-photon ionization in dielectrics due to collisions", *Appl.Phys.B*63, 617-621(1996).
- 3.19. A. Akella, T.Honda, A.Y.Liu, L. Hesselink, "Two-photon holographic recording in alumosilicate glass containing silver particles", *Opt. Lett.* 22, p.967(1997).
- 3.20. U. Busolt, E. Cottancin, H. Röhr, L. Socaciu, T. Leisner, L. Wöste, "Two photon photoemission of deposited silver clusters", *Eur. Phys.J D9*, p523-527(1999).
- 3.21. M. Fierz, K. Siegmann, M. Scharte, M. Aeschlimann, "Time resolved 2-photon photoionization on metallic nanoparticles", *Appl. Phys. B* 68, p.415-418(1999).
- 3.22. K. Ertel, U. Kohl, J. Lehmann, M. Merschdorf, W. Pfeiffer, A. Thon, S. Voll, G. Gerber, "Time resolved two photon photoemission spectroscopy of HOPG and Ag nanoparticles on HOPG", *Appl. Phys. B* 68, pp.439-445(1999).
- 3.23. L.Köller, M. Schumacher, J. Köhn, S. Teuber, J. Tiggesbäumker, K.H. Meiwes-Broer, "Plasmon enhanced multi ionization of small metal clusters in strong femtosecond laser fields", *Phys.Rev.Lett.*82, pp.3783-3786(1999).
- 3.24. T. Döppner, S. Teuber, M. Schumacher, J. Tiggesbäumker, K.H. Meiwes-Broer, "Charging dynamics of metal clusters in intense laser fields", *Appl. Phys. B* online 13 July 2000.
- 3.25. J. Lehmann, M. Merschdorf, W. Pfeiffer, A. Thon, S. Voll, G. Gerber, "Surface plasmon dynamics in silver nanoparticles studied by femtosecond time resolved photoemission", *Phys. Rev. Lett.* 85, pp.2921-2924(2000).
- 3.26. J. Lehmann, M. Merschdorf, W. Pfeiffer, A. Thon, S. Voll, G. Gerber, "Silver nanoparticles on graphite studied by femtosecond time resolved multiphoton photoemission", *J. Chem. Phys.* 112, pp.5428-5434(2000).
- 3.27. M. Merschdorf, W. Pfeiffer, A. Thon, S. Voll, G. Gerber, "Photoemission from multiply excited surface plasmons in Ag nanoparticles", *Appl. Phys. A* 71, pp.547-552(2000).
- 3.28. C. Kennerknecht, H. Hövel, M. Merschdorf, S. Voll, W. Pfeiffer, "Surface plasmon assisted photoemission from Au nanoparticles on graphite", *Appl. Phys. B*, online 10 October 2001.

## References

---

- 3.29. W. Pfeifer, C. Kennerknecht, M. Merschdorf, "Electron dynamics in supported metal nanoparticles: relaxation and charge transfer studied by time resolved photoemission", *Appl. Phys. A* online 21 January 2004.
- 3.30. O.M.Efimov, A.M.Mekryukov, "Investigation of energy structure of lead silicate glasses by non-linear absorption spectroscopy technique", *Journal of Non-Crystalline Solids* 191, p.94-100(1995).
- 3.31. O.M. Efimov, K.Gabel, S.V.Garnov, L.B. Glebov, S.Grantham, M.Richardson, M.J.Soileau, "Color-center generation in silicate glass exposed to infrared femtosecond pulses", *JOSAB*15, p.193(1998).
- 3.32. O.M. Efimov, L.B. Glebov, S.Grantham, M.Richardson, "Photoionization of silicate glasses exposed to IR femtosecond pulses" *J.Non-Crystalline Solids*253, p.58-67(1999).
- 3.33. J.R.Shulman, W.D.Compton, *Color centers in solids*, Pergamon Press, New York, 1962.
- 3.34. A.V.Dotsenko, L.B.Glebov, V.A.Tsekhomsky, "Physics and Chemistry of Photochromic Glasses", CRC Press, New York, 1998.
- 3.35. V.I.Arbutov, M.N.Tolstoy, "Phototransition of electron in doped glasses", *Fiz. I chim. Stekla* (in russian), 1, p.3 (1988).
- 3.36. S.Munekuni, T.Yamanaka, Y.Shimogaichi, R.Tohmon, Y.Ohki, K.Nagasawa, Y.Hama, "Various types of nonbridging oxygen hole center in high-purity silica glass", *J.Appl.Phys.*68(3), p.1212(1990).
- 3.37. L.B. Glebov, V.G. Dokuchaev, M.A. Petrov, G.T. Petrovskii, "Optical orientation of hole color centers in sodium silicate glass", *Sov. J. Glass Phys. Chem.*, 15, 259 (1989).
- 3.38. V.I.Arbutov, I.K. Vitol, V.J. Grabovskis, Yu.P. Nikolaev, U.T. Rogulis, M.N. Tolstoy, M.A.Elerts, "Degeneracy of activator energy levels with glassy matrix intrinsic states", *Phys.Stat.Sol. (a)*, 91, 199, 1985.
- 3.39. V.I.Arbutov, Yu.P. Nikolaev, M.N. Tolstoy, "Effect of composition of a glass on the relative arrangement of the energy levels of the activator and the intrinsic states of the matrix", *Sov.J.Glass Phys. Chem.*, 16, 91, 1990.
- 3.40. M.A. Villegas, J.M. Fernandez Navarro, S.E. Paje, J. Llopis, *Phys. Chem. Glasses* 37 (1996) 248.
- 3.41. E.Borsella, G. Battaglin, M.A. Garcia, F. Gonella, P. Mazzoldi, R. Polloni, A.Quartana, *Appl. Phys. A* 71 (2000) 125-132.
- 3.42. S.Munekuni, T.Yamanaka, Y.Shimogaichi, K.Nagasawa, Y.Hama "Various types of nonbridging oxygen hole centers in high-purity silica glass" *J. Appl. Phys.* 68 (1990) 1212.
- 3.43. W.Harbich, S.Fedrigo, Mayer, D.M. Lindsay, J.Lingnieres, J.C.Rivoal, D.Kreisle "Deposition of mass selected silver clusters in rare gas matrices" *J.Chem.Phys.* 93(1990)8535.
- 3.44. E. Borsella, E.Cattaruzza, G.De Marchi, F. Gonella, G. Mattei, P. Mazzodi, A. Quaranta, G. Battaglin, R. Polloni "Synthesis of silver clusters in silics-based glasses for optoelectronics applications" *J. Non-Cryst. Solids* 245 (1999) 122-128.
- 3.45. T.Tokizaki, A. Nakamura, S. Kaneko, K. Uchida, S. Omi, H. Tanji, Y. Asahara, *Appl. Phys. Lett.*, 65, 1994, p. 941.
- 3.46. J.Y.Bigot, J.-C. Merle, O. Cregut, A. Daunois, *Phys.Rev.Lett.*, 75, 1995, p. 4702.

## References

---

- 3.47. T.S.Ahmadi, S.L.Logunov, M.A. El-Sayed, *J.Phys.Chem.*, 100, 1996, p.8053.
- 3.48. M.Perner, P.Bost, U.Lemmer, G. von Plessen, J. Feldmann, U. Becker, M. Menning, M. Schmitt, H. Schmidt, *Phys.Rev.Lett.*, 78, 1997, p.2192.
- 3.49. G.V. Hartland, J.H. Hodak, I.Martini, *Phys.Rev.Lett.*, 83, 1998, p.3188.
- 3.50. P.V. Kamat, M. Flumiani, G.V. hartland, *J.Phys.Chem.B*, 102, 1998, p.3123.
- 3.51. G.Seifert, M.Kaempfe, K.J. Berg, H.Graener, *Appl.Phys.B*, 71, 2000, p.795.
- 3.52. N. Del Fatti, F. Vallee, *Appl.Phys. B*, 73, 2001, p.383.
- 3.53. C.Voisin, D.Christofilos, N. del Fatti, F. Vallee, B. Prevel, E. Cottancin, J. Lerme, M. Pellarin, M. Broer, "Size-dependent electron-electron interactions in metal nanoparticles", *Phys Rev Lett.*, 85, 2000, p. 2200.
- 3.54. J.Y.Bigot, V.Halte, J.-C. Merle, A.Daunois, *Chem Phys.*, 251, 2000, p. 181.
- 3.55. K. L. Kelly, E. Coronado, L. L. Zhao, G. C. Schatz, "The Optical Properties of Metal Nanoparticles: The Influence of Size, Shape, and Dielectric Environment", *J. Phys. Chem. B* 2003, 107, 668-677.
- 3.56. A.Melikyan, H.Minassian, "On surface plasmon damping in metallic nanoparticles", *Appl.Phys.B* online February 2004.
- 3.57. J.D.Jackson, "Klassische Elektrodynamik", Walter de Gruyter, Berlin; N.Y., 1982.
- 3.58. A.Yariv, "Quantum Electronics", 3<sup>rd</sup> edd. J.Wiley&Sons, p.163 (1989).
  
- 4.1.U. Kreibig, M.Vollmer, "Optical Properties of Metal Clusters" , Springer Series in Materials Science, Vol 25, 1995.
- 4.2.V. M. Shalaev, "Optical properties of nanostructured random media", Springer Verlag, 2001.
- 4.3.H. Xu, J. Aizpurua, M.Kall, P. Apell, "Electromagnetic contributions to single-molecule sensitivity in surface-enhanced Raman scattering", *Phys.Rev.E* 62, p.4318 (2000).
- 4.4.H.Xu, M.Käll, "Surface-Plasmon-Enhanced optical forces in silver nanoaggregates", *Phys.Rev.Lett* 89, p.246802(2002).
- 4.5.A.A. Lalayan, K.S. Bagdasaryan, P.G. Petrosyan, Kh.V. Nerkararyan, J.B. Ketterson, "Anomalous field enhancement from the superfocusing of surface plasmons at contacting silver surfaces", *J. Appl. Phys.* 91, p.2965(2002).
- 4.6.A.J. Babadjanyan, N.L. Margaryan, Kh.V. Nerkararyan, "Superfocusing of surface polaritons in the conical structure", *J. Appl.Phys.* 87, p.3785(2000).
- 4.7.M.I. Stockman, L.N. Pandey, L.S. Muratov, T.F. George, "Optical absorption and localization of eigenmodes in disordered clusters", *Phys.Rev.B* 51, p.185(1995).
- 4.8.M.Quinten, "The color of finely dispersed nanoparticles", *Appl.Phys.B*, on-line October (2001).
- 4.9.M.Quinten, "Local fields close to the surface of nanoparticles and aggregates of nanoparticles", *Appl.Phys.B*, on-line September (2001).
- 4.10. E. Yablonovitch, "Inhibited spontaneous emission in solid-state physics and electronics", *Phys.Rev.Lett.* 58, p.2059(1987).
- 4.11. E. Yablonovitch, "Photonic band-gap structures", *JOSA B* 10, p.283 (1993).
- 4.12. J.D. Joannopoulos, "Photonic crystals: molding the flow of light", Princeton University Press, 1995.

## References

---

- 4.13. A.Moroz, "Three-dimensional complete photonic-band-gap structures in the visible", *Phys.Rev.Lett.*83, p.5274(1999).
- 4.14. W.Y.Zhang, X.Y.Lei, Z.L.Wang, D.G.Zheng, W.Y.Tam, C.T.Chan, P.Sheng, "Robust photonic band gap from tunable scatterers" *Phys.Rev.Lett.* 84, p.2853(2000).
- 4.15. A. Moroz, "Metallo-dielectric diamond and zinc-blende photonic crystals", *Phys.Rev.B* 66, p.115109(2002).
- 4.16. E.Lidorikis, M.M.Sigalas, E.N.Economou, C.M.Soukoulis, "Tight-Binding parametrization for photonic band gap materials", *Phys.Rev.Lett.* 81, p.1405(1998).
- 4.17. E.Lidorikis, M.M.Sigalas, E.N.Economou, C.M.Soukoulis, "Gap deformation and classical wave localization in disordered two-dimensional photonic-band-gap materials", *Phys.Rev. B* 61, p.13458(2000).
- 4.18. C.Jin, X.Meng, B.Cheng, Z.Li, D.Zhang, "Photonic gap in amorphous photonic materials", *Phys.Rev.B* 63, p.195107(2001).
- 4.19. K.Velikov, W.L.Vos, A.Moroz, A. van Blaaderen, "Reflectivity of metalodielectric photonic glasses", *Phys.Rev. B* 69, p.75108(2004).
- 4.20. A. Abdolvand, A.Podlipensky, G.Seifert, O.Deparis, P.Kazansky, H.Graener, "DC electric field assisted modification of optical properties of glass with silver nanoparticles", *Opt.Express*, to be published.
- 4.21. A. Podlipensky, A. Abdolvand, G. Seifert, H. Graener, O. Deparis, P. G. Kazansky, "Dissolution of Silver Nanoparticles in Glass through an Intense DC Electric Field", *J. Phys Chem B* 108, p.17699(2004).
- 4.22. O. Deparis, P. G. Kazansky, A. Abdolvand, A. Podlipensky, G. Seifert, H. Graener, "Poling-assisted bleaching of metal-doped nanocomposite glass", *Applied Phys. Lett.* 85, 872 (2004).
- 4.23. M.Birnbaum, "Semiconductor surface damage produced by ruby lasers", *J. Appl. Phys.*, vol.36, p.3688(1965).
- 4.24. D.C.Emmony, N.J.Phyllips, J.H.Toyer, L.J.Willis, "The topography of laser-irradiated germanium", *J.Phys.D.8*, p.1472(1975).
- 4.25. G.N. Maracas, G.L. Harris, C.A. Lee, R.A. McFarlane, "On the origin of periodic surface structure of laser-annealed semiconductors", *Appl.Phys.Lett.*33, p.453(1978).
- 4.26. Z.Gousheng, P.M.Fauchet, A.E.Siegman, "Growth of spontaneous periodic surface structures on solids during laser illumination", *Phys.Rev.B*26, p.5366(1982).
- 4.27. S.R.J. Brueck, D.J.Ehrlich, "Stimulated Surface-Plasma-Wave scattering and growth of a periodic structure in laser-photodeposited metal films", *Phys.Rev.Lett.*48, p.1678(1982).
- 4.28. H.M. van Driel, J.P.Sipe, J.F.Young, "Laser-induced periodic surface structure on solids: a universal phenomenon", *Phys.Rev.Lett.*49, p.1955(1982).
- 4.29. F.Keilmann, "Laser-driven corrugation instability of liquid metal surface", *Phys.Rev.Lett.*51, p.2097(1983).
- 4.30. J.E.Sipe, J.F.Young, J.S.Preston, H.M. van Driel, "Laser-induced periodic surface structure. I. Theory", *Phys.Rev.B.* 27, p.1141(1983).
- 4.31. J.F. Young, J.S. Preston, H.M. van Driel, J.E.Sipe, "Laser-induced periodic surface structure. II. Experiments on Ge, Si, Al, and brass", *Phys.Rev.B*27, p.1155(1983).

## References

---

- 4.32. A.E.Siegman, P.M.Fauchet, "Stimulated Wood's anomalies on laser-illuminated surfaces", IEEE J. Quant.Electr.22, p.1384(1986).
- 4.33. V.N.Anisimov, V.Yu.baranov, O.N.Derkach, A.M.Dykhne, D.D.Malyuta, V.D. Pismennyi, B.P.Rysev, A.Yu.Sebrant, "Resonant phenomena in laser excitation of surface waves on solids", IEEE J.Quant.Electr. 24, p.675(1988).
- 4.34. J.Reif, F.Costache, M.Henyk, S.V.Pandelov, "Ripples revisited: non-classical morphology at the bottom of femtosecond laser ablation craters in transparent dielectrics", Appl.Surf.Sci.197-198, p.891(2002).
- 4.35. F.Costache, M.Henyk, J.Reif, Appl.Surf.Sci. 208-209, p.486(2003).
- 4.36. S.A.Akhmanov, V.I.Emel'yanov, N.I.Koroteev, "Interaction of strong laser radiation with solids and nonlinear optical diagnostics of surfaces", Teubner-texte zur Physik, Band 24, p.204(1990).
- 4.37. D.Bäuerle, "Laser processing and chemistry", 3<sup>rd</sup> ed. Springer-Verlag Berlin, 2000.
  
- 5.1. U. Kreibig, M.Vollmer, "Optical Properties of Metal Clusters" , Springer Series in Materials Science, Vol 25, 1995.
- 5.2. V. M. Shalaev, Optical properties of nanostructured random media, Springer Verlag, 2001.
- 5.3. C.F. Bohren, D.R. Huffman, „Absorption and scattering of light by small particles“, Wiley Science Paperback Series, 1998
- 5.4. J.P. Marton, J.R. Lemon, Phys.Rev.B4, 271 (1971).
- 5.5. G.Xu, M. Tazawa, P. Jin, S. Nakao, "Surface plasmon resonance of sputtered Ag films: substrate and mass thickness dependence", Appl.Phys.A (2004).
- 5.6. M.Kaempfe, "Laserinduzierte deformation metalischer Nanopartikel in Glaeser", Dissertation, Martin-Luther University Halle-Wittenberg, 2000.
- 5.7. J. Tominaga, D.P. Tsai "The Manipulation of Surface and Local Plasmons", Topics in Applied Physics, Springer, 2003.
- 5.8. H. Ditlbacher, J. R. Krenn, B. Lamprecht, A. Leitner, and F. R. Aussenegg, "Spectrally coded optical data storage by metal nanoparticles", Opt.Lett.25, p.563 (2000).
- 5.9. K. Baba, R. Yamada, S. Nakao and M. Miyagi, "Three-dimensional optical disks using metallic island films: A proposal," Elec. Lett. 28, 676(1992).
- 5.10. J. R. Wullert II and P. J. Delfyett, "Multiwavelength, multilevel optical storage using dielectric mirrors," IEEE Photonics Tech. Lett. 6(9), 1133(1994).
- 5.11. S. Homan and A. E. Willner, "High-capacity optical storage using multiple wavelengths, multiple layers and volume holograms," Elec. Lett. 31, 621(1995).
- 5.12. Philipp Hergert, The Data Storage System Center, Carnegie Mellon University, ECE Department Pittsburgh, USA, [http://www.ece.cmu.edu/research/dssc/news\\_events/seminars/lunch04/optical/9-9-04\\_Optical\\_Overview.pdf](http://www.ece.cmu.edu/research/dssc/news_events/seminars/lunch04/optical/9-9-04_Optical_Overview.pdf)
- 5.13. F.Korte, J.Serbin, J.Koch, A.Egbert, C.Fallnich, A.Ostendorf, B.N.Chichkov, "Towards nanostructuring with femtosecond laser pulses", Appl.Phys.A 77, p.229-235(2003).
- 5.14. J.C. Knight, T.A. Birks, P.St.J. Russell, D.M.Atkin, "All-silica single-mode optical fiber with photonic crystal cladding", Opt. Lett. 21, p.1547(1996).

## *References*

---

- 5.15. J.K. Ranke, R.S. Windeler, A.J. Stentz, „Visible continuum generation in air-silica microstructure optical fibers with anomalous dispersion at 800 nm“, *Opt. Lett.* 25, p.1415(2000).
- 5.16. A.B.Fedotov, A.N. Naumov, A.M. Zheltikov, I. Bugar, D. Chorvat, Jr., D. Chorvat, A.P. Tarasevitch, D. von der Linde, “Frequency-tunable supercontinuum generation in photonic-crystal fibers by femtosecond pulses of an optical parametric amplifier”, *JOSA B* 19, p.2156(2002).

# Acknowledgements

In this page, I would like to thank many friends and colleagues who helped me in the work described in this thesis.

First, I would like to thank my supervisor, Professor Heinrich Graener, owing to whom I got the possibility to conduct the research presented here. I very much appreciate his constant support in the scientific work, fruitful discussions and nice ideas as well as help in solving of ordinary bureaucratic problems.

I must also thank everyone in the group optic, where I have been fortunate to be as a PhD student. Particularly I have to thank PD Dr. Gerhard Seifert for support of ideas and fruitful discussions and Dr. Jens Lange for invaluable assistance in automation of the experimental set-up.

I would like to express my especial gratefulness to Frau Ingrid Otton for indispensable help in sample preparation and characterization.

Many thanks to Dr. G. Heine and Mr. A. Volke from CODIXX AG, Dr. K.J.Berg from MLU Halle for providing samples with Ag nanoparticles for the experiments.

I am very grateful to Dr. H. Hofmeister (Max-Planck-Institute of Microstructure Physics, Halle) and Mr. F. Syrovotka (IWZ Materialwissenschaft, MLU Halle) for assistance in electron microscopy studies.

Certainly, I greatly appreciate substantial moral support from my wife Anna and my daughters Julia and Xenia.

I owe my thanks to my friend Amin Abdolvand, whom I know for almost eight years and with whom I have a pleasure to work again.